2009

Design, optimization and evaluation of a free-fall biomass fast pyrolysis reactor and its products

Cody James Ellens
Iowa State University

Design, optimization and evaluation of a free-fall biomass fast pyrolysis reactor and its products

by

Cody James Ellens

A thesis submitted to the graduate faculty
in partial fulfillment of the requirements for the degree of
MASTER OF SCIENCE

Co-majors: Mechanical Engineering; Biorenewable Resources and Technology

Program of Study Committee:
Robert C. Brown, Major Professor
Terrence Meyer
Raj D. Raman

Iowa State University
Ames, Iowa
2009

Table of Contents

List of Figures

List of Tables

Acknowledgements

Creator of all,
source of all light and wisdom,
you made everything.
Let a ray of your light
penetrate the darkness of my mind.
Take from me all darkness of sin or ignorance.
Give me a keen understanding,
a good memory,
and the ability to grasp things
correctly and completely.
Help me to be exact in my explanations
and to express myself thoroughly and clearly.
Show me how to begin my work,
Direct my progress, and help me complete it.
I ask this through Christ, our Lord. Amen.
Thomas Aquinas

I would like to thank my major professor, Dr. Robert Brown for his guidance and instruction during the course of my research at Iowa State University. I also acknowledge Dr. Terry Meyer and Dr. Raj Raman for serving on my committee.

Many thanks are given to ConocoPhillips Co. for their financial support and helpful feedback.

Lastly, I would like to thank my wife, Katie, for her patient support and enduring kindness especially while we were dating and engaged to be married. Though my time in the laboratory easily outweighed my time spent with you, every moment we shared together was cherished and a source of encouragement.

Abstract

The focus of this work is a radiatively heated, free-fall, fast pyrolysis reactor. The reactor was designed and constructed for the production of bio-oil from the fast pyrolysis of biomass. A central composite design of experiments was performed to evaluate the novel reactor by varying four operating conditions: reactor temperature, biomass particle size, carrier gas flow rate and biomass feed rate. Maximum bio-oil yields of 72 wt % were achieved at a heater set point temperature of 600 °C, using particle sizes of 300 micron, carrier gas flow rates of 4 sL/min and Red oak biomass feed rates of 1.75 kg/hr. Optimal operating conditions were identified for maximum bio-oil yields at a heater set point temperature of 572 ˚C, feeding 240 micron sized Red oak biomass particles at 2 kg/hr. Carrier gas flow rates were not found to be significant over the 1 – 5 sL/min range tested.

CHAPTER 1: Introduction

The goal of this work is to develop a new biomass fast pyrolysis reactor that improves upon inefficiencies in traditional reactors while maintaining high bio-oil yields. Biomass is an abundant organic material composed of cellulose, hemicellulose and lignin. Biomass may be converted into useful products to offset petroleum based products. Fast pyrolysis of biomass is a thermochemical conversion process that produces a liquid bio-oil, a solid char and non-condensable gases. Bio-oil is a complex oxygenated liquid that has applications in heat and power, transportation fuels and specialty chemicals [1].

Many fast pyrolysis reactors exist but the most suitable reactor has not been identified [2]. Reactors like the bubbling fluid bed and circulating fluid bed require large amounts of carrier gas to mix a heat carrier with biomass while the spinning disk, rotating cone and auger reactors have many hot moving parts. These factors may increase the complexity of the reactor and make them expensive to operate or repair. More work is needed to investigate novel reactor types that overcome these disadvantages without compromising high bio-oil yield.

Additional motivation for studying the fast pyrolysis of biomass stems from a number of reasons. First, as stewards of Creation, humankind has the responsibility to effectively cultivate, develop and mold the resources at hand into beneficial products for the health and betterment of society and in so doing bring honor to the Creator. Second, advances and commercialization of biomass conversion technology producing renewable and sustainable bioproducts will ease reliance on imported fossil sources while simultaneously enhancing national security. Third, increased biomass usage will spur rural economic development. The thermochemical conversion of biomass can play an important role in making this transformation. Elaboration on the motivation for increased biorenewable resource usage are found in Reference [3].

A free-fall fast pyrolysis reactor was selected for this work because of its simple design and lack of moving parts. The reactor was optimized and evaluated for the production of bio-oil using a central composite design of experiments. Operating conditions including the reactor temperature, biomass particle size, carrier gas flow rate and biomass feed rate were varied.

CHAPTER 2: Background

2.1. Thermochemical Conversion of Biomass

A number of possibilities exist for thermochemical conversion of biomass including hydrothermal processing (HTP), combustion, gasification and pyrolysis. The thermochemical pathways are described in Table 1.

Table 1. Thermochemical process, products and applications

Oxidation	Process	Primary products	Application
None	Hydrothermal Processing →	Bio-crude, aqueous organics, H_2O, CO_2	Fuels, fertilizers
Complete	Combustion →	H_2O, CO_2, ash	Heat, power
Partial	Gasification →	CO, H_2 (synthesis gas), bio-char	Heat, power, synthesis into fuels
None	Pyrolysis →	Bio-oil, char, non-condensable gas	Heat, power, upgrading into fuels, chemicals and products

Hydrothermal processing of biomass occurs at high pressure (5-40 MPa) and moderate to high temperature (200-600 °C) in an aqueous environment. A liquid bio-crude is the primary product. Peterson et al. have written extensively about hydrothermal processing [4]. Combustion of biomass occurs predominantly under atmospheric conditions. Provided an ample amount of oxygen is present, the reaction will completely oxidize the carbon source and produce water (H_2O) and carbon dioxide (CO_2) leaving only inorganic ash behind. Biomass may be fed into a boiler or other combustor for heat and power generation. Gasification of biomass may be performed at atmospheric or pressurized conditions with less than stoichiometric amounts of oxygen present. The primary reaction products are a combustible mixture of carbon monoxide (CO) and hydrogen (H_2) gas and char. With sufficient cleaning, the gas can be combusted for power generation or process heat. Alternatively, synthesis gas combined in the correct CO:H_2 ratio may be fed into a catalytic reactor to create Fischer Tropsch fuels or an enzymatic fermentor for ethanol or renewable

plastic production. Of particular interest for this research is pyrolysis. Pyrolysis occurs at atmospheric conditions in the absence of oxygen. Three main types of pyrolysis exist: fast, intermediate and slow pyrolysis. Table 2 describes the three modes.

Table 2. Pyrolysis mode, conditions and products (dry basis)[a]

Mode	Conditions	Liquid (wt %)	Solid (wt %)	Gas (wt %)
Fast	-fast heating rate (1000 °C/s) -short vapor residence time (<2 s) -small particle sizes (<2 mm) -moderate temperature (450 °C - 500 °C)	75	12	13
Intermediate	-moderate temperature (500 °C) -moderate vapor residence time (10 - 20 s)	50	20	30
Slow	-slow heating rate -long solids residence time (hrs) -large particle sizes -low temperature (400 °C)	30	35	35

[a] Adapted from Bridgwater [5]

Operating conditions and modes for pyrolysis are selected according to the desired product distribution. Fast pyrolysis primarily produces a liquid product while slow pyrolysis will produce nearly equal amounts of liquid, solid and gaseous product.

2.2. Fast Pyrolysis of Biomass

Pyrolysis is an ancient technology dating back to the time of the Egyptians where tars and embalming agents were made. In the 1980's major efforts were put forth in the development of fast pyrolysis for the production of its liquid product [6-8]. Fast pyrolysis is the rapid thermal decomposition of a feedstock at moderate temperatures and atmospheric pressures in the absence of oxygen [9]. Products include a dark brown liquid called bio-oil, a solid charcoal like material named char or bio-char and a non-condensable gas. Traditional fast pyrolysis requires that a number of parameters be satisfied including:

- rapid heating rate of the biomass particle on the order of 1000 °C/s
- vapor temperatures between 450 °C and 500 °C

- particle sizes less than 2 mm in critical dimension
- vapor residence times less than 2 s
- rapid cooling of the pyrolysis vapors into bio-oil
- feedstock moisture content less than 10 wt %

Rapid heating of small particles vaporizes the feedstock into vapors and aerosols as well as char. Quickly removing the vapors from the hot reaction vessel and quenching them minimizes secondary reactions producing gas and char (further decomposition of the vapors) and optimizes bio-oil liquid yield [10]. Adding a sweep or carrier gas and increasing the feed rate will decrease the vapor residence time. A low feedstock moisture content will minimize the amount of water resulting in the bio-oil [9].

Fast pyrolysis product yields are typically reported between 60 –75 wt % bio-oil, 15 – 25 wt % bio-char and 10 – 20 wt % non-condensable gases[11]. Product yields and distribution are strongly determined by process operating conditions but are also influenced by biomass feedstock and its inherent ash content as indicated in Table 3 below.

Table 3. Biomass type and product yield[a]

Feedstock	Ash (mf wt %)[b]	Liquid (mf wt %)	Char (mf wt %)	Gas (mf wt %)	Closure (%)
Willow	1.34	68.9	20.9	9.3	99.0
Switch grass	4.3	63.8	24.7	7.9	96.5
Reed canary grass	5.1	60.2	22.0	11.1	93.4
Straw	6.3	50.5	31.9	15.6	98.3

[a] Adapted from Fahmi [12]
[b] Moisture free weight percent

Biomass with low ash content, such as woody biomass increase quantities of bio-oil. Ash present in the biomass largely remains within the char during pyrolysis [9, 13] and is known to catalyze char forming reactions [14]. Successful removal of the char from the product stream will therefore decrease catalytic and secondary reactions which shift towards char and non-condensable gas production [2, 15, 16]. Simultaneously, the removal of char provides increased bio-oil stability and quality [13]. This is essential for long term storage. Although char is generally removed from the bio-oil, in some instances char is mixed back

into the bio-oil to increase its heating value and specific gravity for use as a boiler fuel or pressurized gasification feedstock [17, 18].

Fast pyrolysis is feedstock-flexible and can produce biorenewable products from non-food sources. Unlike other biorenewable energy platforms, it does not require expensive catalysts or enzymes but rather uses heat to break down lignocellulosic biomass. An advantage of fast pyrolysis over other renewable energy platforms (wind and solar for example) is the fact that a liquid energy carrier is produced.

2.3. Bio-oil Characteristics

Bio-oil produced from fast pyrolysis is a complex mixture which may contain over 400 organic compounds. Species including acids, alcohols, aldehydes, esters, ketones, and aromatic compounds have been identified [19]. Pyrolysis oils are a direct result of the thermal decomposition of biomass and therefore the elemental composition closely resembles that of biomass rather than fossil based oils as shown in Table 4 [1].

Table 4. Typical properties of Pine, wood pyrolysis bio-oil and heavy fuel oil[a]

Physical Property	Ponderosa Pine[b]	Bio-oil	Heavy Fuel Oil
moisture content, wt %	-	15 - 30	0.1
pH	-	2.5	-
specific gravity	-	1.2	0.94
elemental composition, wt %			
C	49	54 - 58	85
H	6	5.5 - 7.0	11
O	44	35 - 40	1
N	0.06	0 - 0.2	0.3
ash	0.3	0 - 0.2	0.1
Higher heating value, MJ/kg	20	16 - 19	40
viscosity (at 50 °C), cP	-	40 - 100	180
solids, wt %	-	0.2 - 1	1
distillation residue, wt %	-	up to 50	1

[a] Adapted from Czernik [1]
[b] From Brown [3]

It is noteworthy that a number of other differences exist between bio-oil and heavy fuel oil specifically the moisture content, pH, oxygen content, higher heating value and

distillation residue. The high moisture and oxygen content within bio-oil contributes to a lower energy content compared to petroleum. On a mass basis, bio-oil contains roughly 42% of the energy of fuel oil, but since the density of bio-oil is much greater than fuel oil on a volumetric basis it improves to 61% [9]. Additionally, the low pH, high distillation residue and oxygen content make bio-oil is immiscible with petroleum derived fuels and prevent it from being co-processed with petroleum. Not shown in Table 4 is the difference in sulfur content between bio-oil and heavy fuel oil. Since very little sulfur is present in biomass, bio-oil has only trace amounts of sulfur while heavy fuel oil may have up to 3% by weight [6]. Thus bio-oil combustion releases little to no SOx emissions. Further exploration of these differences are addressed by Czernik and Bridgwater[1].

2.4. Bio-oil Applications

The dissimilarity between bio-oil and mineral oils is well known and its properties realistically limit the widespread use of bio-oil in standard petroleum based applications. Nonetheless, bio-oil is produced from a renewable carbon source and much research and demonstration has been performed in an effort to offset and in some cases replace fossil fuel usage. Bio-oil being an energy densified, liquid form of biomass allows for easy transportation, storage and handling. Many applications take advantage of bio-oil for these reasons.

2.4.1. Bio-oil Combustion

Bio-oil combustion for heat and power applications is a predominant and obvious end use for bio-oil. Bio-oil combustion may be considered carbon neutral and emits very low sulfur emissions compared to fossil fuels [1]. Direct combustion in boilers, engines and turbines has been tested with various results. Due to its heterogeneity, viscosity and corrosive nature, most equipment requires some modification in order to efficiently process bio-oil including a preheating section [10]. Red Arrow Products, a company producing liquid smoke food flavorings in Wisconsin, is likely the most reliable commercial scale facility that uses bio-oil combustion to heat the plant. A 5 MW_{th} swirl burner combusts a bio-oil mixture from a stainless steel, air atomized nozzle to provide heat to the facility [1].

Bio-oil combustion emissions are consistently lower than that of fuel oil, but particulate in the flue gas is higher. Mullany et al. [6] performed a technical, environmental and economic study determining the practicality of substituting bio-oil for home heating oil. He concludes that if home heating oil is sold for $0.90/gal it is not economical to use bio-oil as a substitute. At the same time, if taxes are imposed on nitrogen oxides (NO_x), sulphur oxides (SO_x) and CO_2 emissions, bio-oil may become feasible.

2.4.2. Bio-oil for Upgrading to Transportation Fuels

Though bio-oil is immiscible with fossil fuels, efforts have been made to upgrade bio-oil into transportation fuels [19]. As discussed earlier, the low heating value of bio-oil due to its high water and oxygen content as well the low pH prevent bio-oil from being used directly as a liquid fuel. A number of pathways exist for catalytic upgrading of bio-oil. Two approaches are 1) hydrodeoxygenation via hydrotreating catalysts and, 2) Zeolite upgrading. Hydrodeoxygenation of bio-oil is similar to hydrotreating of crude oil. It is a hydrogenation process that removes oxygen by combining a hydrogen stream with the bio-oil in the presence of a catalyst thereby producing water. Temperatures between 300 – 600 °C and high pressures (14 MPa) of hydrogen are required [19]. A two-staged process may be performed, the first to stabilize the bio-oil and preventing further decomposition, followed by a second more severe form of hydrotreating. Elliott et al. report hydrocarbon yields of 0.4 L/L bio-oil containing less than 1 % oxygen [20]. Typical catalysts include sulphided cobalt-molybdenum (CoMo) or nickel-molybdenum (NiMo) supported on alumina [9].

Upgrading via Zeolite catalysts involves passing the bio-oil through a microporous structure at moderate temperatures (450 °C). The advantage of Zeolite upgrading is that high pressure hydrogen is not required and it is often used in the petroleum industry [19]. Catalyst deactivation remains a concern and low carbon conversion efficiencies are seen since oxygen is rejected as CO_2 rather than water [9].

Additional non-catalytic methods have been suggested including bio-oil gasification to produce liquid fuels. This approach and others are discussed in more depth elsewhere [1, 11, 19].

2.4.3. Bio-oil for Chemicals

The production of renewable chemicals via biomass fast pyrolysis is another application of bio-oil. A number of chemicals that have been produced from fast pyrolysis are listed in Table 5 below.

Table 5. Chemicals from fast pyrolysis[a]

Acetic acid	Calcium enriched bio-oil
Hydrogen	Levoglucosan
Preservatives	Slow release fertilizers
Adhesives	Food flavorings
Hydroxyacealdehyde	Levoglucosenone
Resins	Sugars

[a] Adapted from Bridgwater [21]

While a large number of naturally occurring compounds have been identified in bio-oil, the relative concentration of each is small and separation processes are complex making some separation efforts uneconomical. For this reason, simple fractionation of bio-oil by water addition creating a water soluble and a water insoluble fraction is advantageous [1]. The water soluble fraction contains low molecular weight aldehydes and phenolic compounds. These compounds are being used commercially as meat browning agents and food flavorings. Specifically, Red Arrow Products in Wisconsin produces liquid smoke from bio-oil. This aqueous fraction also can be used in the production of calcium salts to be used as road de-icers [1]. The water insoluble fraction, often called pyrolytic lignin in literature, may best be applied as a resin or adhesive [8, 11, 22]. Other commodity chemicals and specialty products are being used and tested including BioLime™ for capturing SO_x emissions and a bio-binder for use as an asphalt binder. These and other applications are described in more depth elsewhere [1, 6, 22].

2.5. Reactor Technology

The reactor is the central component when considering an entire fast pyrolysis system. Since it is the key component many reactors have been developed in order to improve upon old methods and create proprietary technology.

The oldest and most well-understood is the bubbling fluidized bed or simply the fluid bed reactor as shown in Figure 1 [9]. The bed media is often sand supported by a perforated distributor plate within a cylinder. An inert fluidizing gas is forced through the plate causing the bed media to fluidize. The high gas flow rate also shortens the vapor residence time and allows for efficient char/vapor separation by means of a cyclone. The fluid bed has high heat transfer rates and is simple to construct and operate [11]. Bio-oil yields between 70 –75 wt % are often achieved with woody biomass. Scaling up the fluidized bed is well understood. Heat transfer limitations due to low bed height-to-diameter ratios cause temperature gradients and prevent scale-up past a point. Low thermal efficiencies in the fluid bed reactor are due to the cooling and reheating of the re-circulated gas stream [23]. Canadian based Dynamotive, Inc. uses this technology on a commercial scale for the production of bio-oil [2].

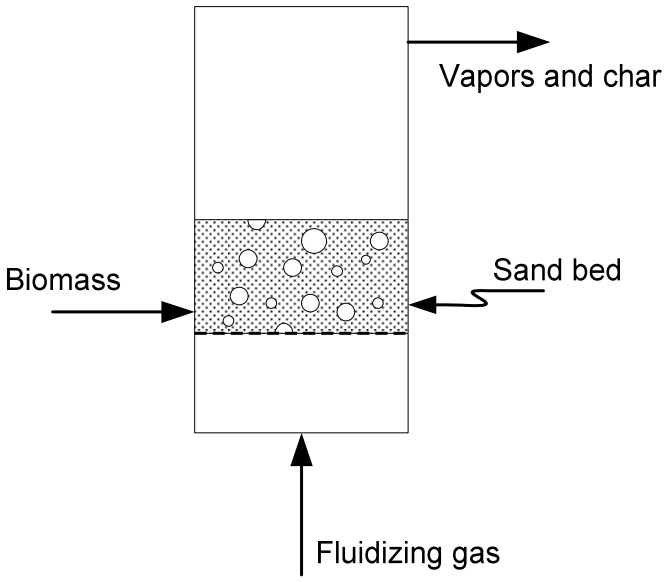

Figure 1. Fluidized bed reactor

The circulating fluidized bed reactor is closely related to the fluidized bed reactor. Higher gas flow rates are used to entrain the bed material and char out of the reactor into a cyclone separator. The sand and char mixture is combusted to heat the sand which is then re-circulated into the reactor as shown in Figure 2. The vapors exit the cyclone and enter a condenser system. Bio-oil yields comparable to the fluidized bed have been reported [11].

The circulating fluid bed though complex is capable of large biomass throughputs and has been commercially developed by another Canadian company, Ensyn, Inc. [2, 9].

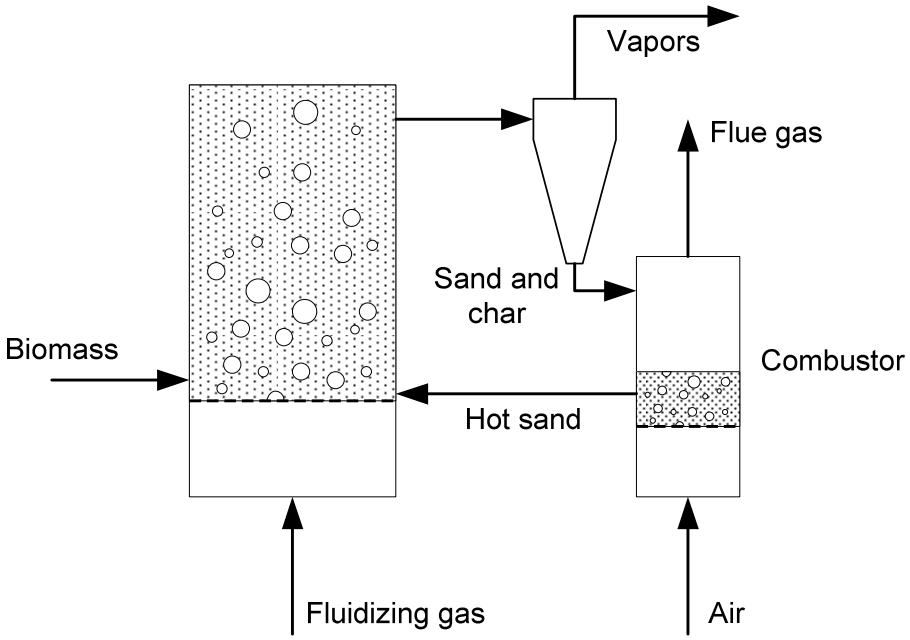

Figure 2. Circulating fluidized bed reactor

Another method is known as ablative fast pyrolysis. The premise is based on forcing biomass particles against a heated plate or wall to perform pyrolysis as Figure 3 indicates. A few reactors have been developed using this principle. The National Renewable Energy Laboratory's (NREL) Vortex reactor uses high gas flow rates to force small biomass particles into a heated cylindrical wall. The particles enter tangentially and travel at speeds over 200 m/s. Larger particles are re-circulated until completely pyrolyzed [24, 25]. Bio-oil yields up to 72 wt % are reported [26]. Another ablative reactor, the cyclone reactor was developed by Léde in France. Like the Vortex reactor, biomass enters the heated cyclone reactor tangentially. Bio-oil yields less than 20 wt % were reported for this bench scale reactor [27]. Short particle residence times lead to incomplete conversion of the particles and may require a re-circulating loop [23]. Aston University has developed an ablative technique whereby biomass particles are scraped along a heated plate by rotating blades. Yields between 70 –75 wt % have been reported. PyTec, a German company, hydraulically feeds wood particles into a heated spinning disk as shown in Figure 3a providing the advantage of using larger

biomass particles [8, 9]. This reactor involves moving parts operating at high temperatures [23].

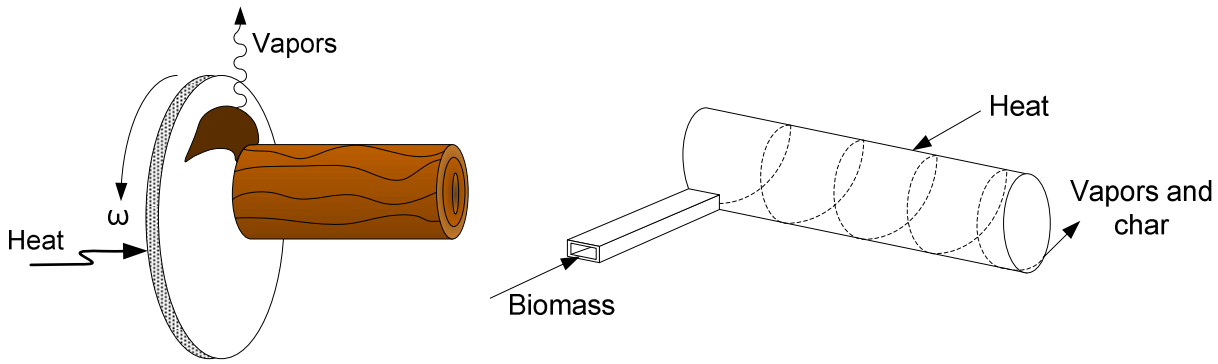

Figure 3. Ablative reactor types a) spinning disk and b) vortex reactor

The rotating cone reactor is a relatively new approach to fast pyrolysis. The concept was developed by Prins and Wagenaar at the University of Twente, The Netherlands [8]. The reactor is being commercialized by the Biomass Technology Group –Biomass to Liquid (BTG-BTL) [28]. Biomass and hot sand are fed into the bottom of a rotating cone. The centrifugal force pushes the hot sand and char out over top of the cone as shown in Figure 4. The mixture is combusted and the sand is re-circulated. No carrier gas is needed preventing product dilution [11, 29]. Liquid yields between 60 –70 wt % are reported. A 50 tpd reactor was built and operated in Malaysia [9, 30].

A continuous screw reactor was developed at the University of Tübingen, Germany for the conversion of sewage sludge into chemicals. Lower temperatures and longer residence times than traditional fast pyrolysis yield bio-oil between 18 –27 wt % and char from 50 –60 wt %. The liquid product reportedly has less than 5 wt % oxygen [2]. A twin-screw auger reactor developed by the Forschungszentrum Karlsruhe GmbH (FZK) research institute in Germany was designed for 10 kg/hr of biomass throughput. The char is mixed back into the bio-oil forming a pumpable slurry which is later gasified in a pressurized entrained flow reactor. Up to 50 wt % bio-oil yields have been achieved [31].

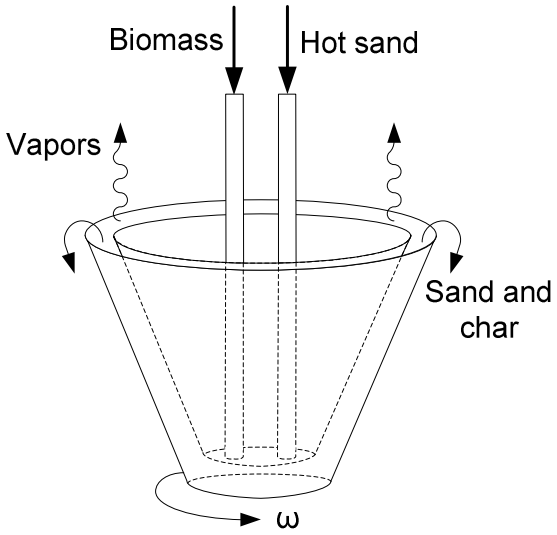

Figure 4. Rotating cone reactor

A 1 kg/hr externally heated auger reactor developed at the Mississippi State University does not use carrier gas or heat carrier to perform fast pyrolysis. Bio-oil yields up to 56 wt % are reported for oak wood [32]. Renewable Oil International, a company located in Alabama seeks to produce small and portable reactors for the localized production of bio-oil using an auger type reactor [33]. Similarly, Advanced BioRefinery, Inc. (ABRI) out of Canada has developed a skid mounted auger reactor. The reactor unit is self-contained and combusts some of the char for feedstock drying and process heat [34].

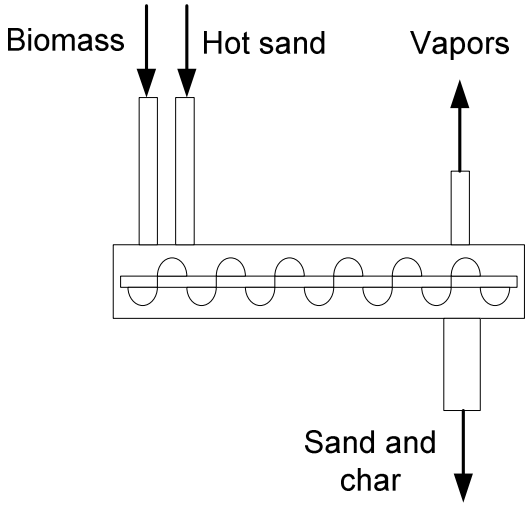

Figure 5. Auger reactor

2.6. Free-fall Reactors

Free-fall reactors are also referred to as a drop-tube reactors. Free-fall reactors have been used for many applications including gasification of coal [35-38], the pyrolysis of polystyrene and polyethelyne [39, 40], kinetic studies [41, 42] as well as various biomass pyrolysis studies [43-47]. A few studies performed the fast pyrolysis of biomass in a free-fall reactor and report notable bio-oil yields though bio-oil production was not necessarily the purpose of study [48, 49]. Typically, very little carrier gas is required for free-fall reactors as the feedstock is fed from the top of the reactor. Heating rates between 500 – 1000 °C/s have been reported for free-fall reactors but are still a degree of magnitude lower than some reported heating rates of 10,000 °C/s [11, 41, 47, 50].

A pilot scale entrained flow reactor, known as the Georgia Tech Entrained Flow Pyrolysis Process, is the largest free-fall reactor related system to be used for the production of bio-oil. The reactor was a bottom fed with roughly 1.5 ton/day hardwood biomass and achieved bio-oil yields up to 60 wt % on a dry basis. Georgia Tech Research Institute operated the reactor from 1982 until 1989 [51]. Even though entrained flow reactors may be fed from the bottom which requires large amounts of carrier gas to entrain the feedstock, the reactor shares a tubular shape and may be heated in a similar fashion as a free-fall reactor [43]. Most of the free-fall, drop-tube or entrained flow reactors reported are constructed for lab scale experimentation.

Zhang et al. used a free-fall reactor to determine if any synergetic relationships existed in the pyrolysis of coal and biomass, particularly Dayan lignite coal and legume straw biomass. The reactor, a 0.02 m inner diameter and 1.8 m long heated tube is shown in Figure 6. Three electrical heaters were used to heat the process and two screw feeders located on top fed each feedstock. A churn dasher or plunger mechanisim was used to promote uniform falling of the biomass. A nitrogen flow rate of 35 mL/min, particle sizes between 0.3 and 0.45 mm and temperatures of 500 °C, 600 °C and 700 °C were the parameters tested. The particles were first dried at 105 °C for 2 hours. Zhang proposed that the temperature of the falling particle depends on its adsoptivity. He suggested that coal and biomass will decompose simultaneously thus creating synergetic effects. Increasing liquid yields and decreasing char yields were observed below 600 °C at mixing ratios of 73 wt % legume

straw when compared to individually pyrolyzed feedstock's suggesting a synergetic relationship [46].

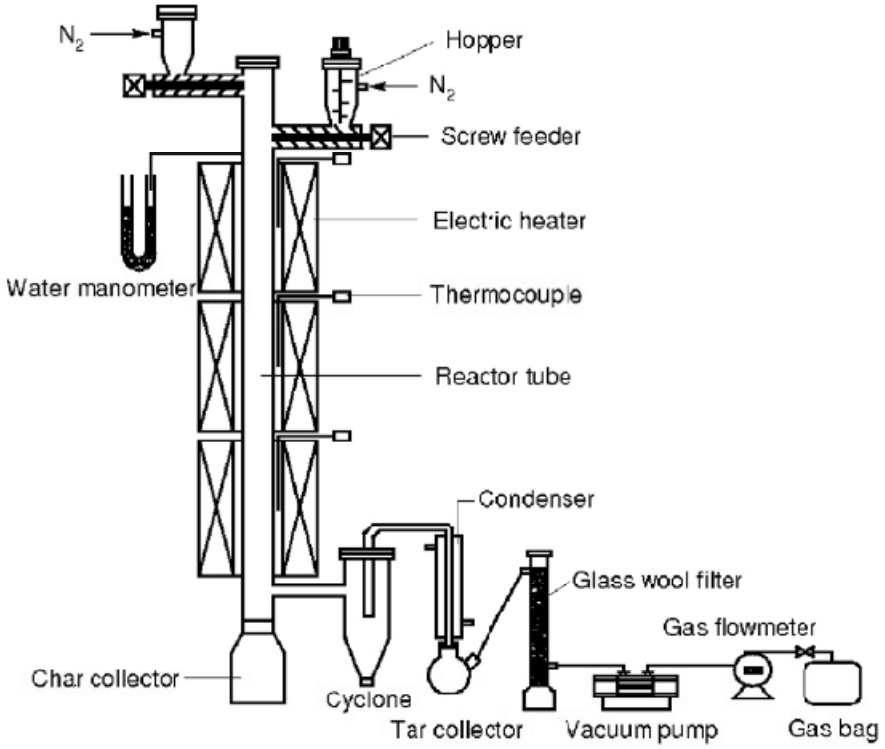

Figure 6. Schematic of free-fall reactor; used with permission from Zhang [46]

Li et al. experimented with two types of biomass for the production of hydrogen gas. The reactor is the same as described by Zhang et al. except it only one feeder was used. Three separately controlled heaters were used to heat the reactor. Legume straw and apricot stone were fed using a screw feeder on top of the reactor. Nitrogen carrier gas was pulled through the system by a vacuum pump downstream. A char collector was located at the bottom of the reactor. The vapors exited above the char catch and passed through a metallic filter or cyclone where solids were separated and then were condensed in ice-cooled condensers. The aerosols were removed with a glass wool filter. Decreasing the particle size from 0.90-2.00 mm to 0.20-0.30 mm lowered bio-oil production from 48.3% to 17.8%, but increased gas production at 800 °C. Using legume straw particles between 0.45-0.90 mm, liquid yields decreased above 500 °C. Liquid yields reached a maximum of 66 wt % at 600 °C for the same sized apricot stone particles [49].

Lee et al. experimented with coal gasification using a drop tube reactor. Pulverized coal ranging from 11 to 20 μm was fed via screw feeder at a rate between 18 and 60 g/min using 1-2 L/min of Argon carrier gas. A reactor with a diameter of 0.05 m and 1 m long was used at the Korea Advanced Institute of Science and Technology. Four silicon carbide (SiC) heaters capable of temperatures up to 1550 °C heated the reactor tube. The coal particles attained terminal velocities of 0.17 m/s in 5-10 ms and the residences time was calculated by dividing the reactor length of the average particle velocity. Hydrogen and carbon monoxide production increased with higher reaction temperature [35].

Xu et al. performed high pressure hydropyrolysis of coal in a free-fall reactor at Tohoku University, Japan. The 1 cm inner diameter reactor was selectively heated between 0.3, 0.7 and 1.0 m in length. Coal was fed with a screw feeder positioned on top of the stainless steel reactor a rate of 6 –9 g/hr. A char collector located at the bottom was maintained at 400 °C to prevent premature condensation. Two dry ice cooled condensers in series were used to collect the liquid product. The gaseous products were analyzed using a gas chromatograph. Higher temperatures and pressures led to increased coal conversion. For a pressure of 1 MPa and temperature of 600 °C, 50, 26 and 15 C% is found in the char, tar and gas, respectively [38].

Zanzi et al. focused on the production and reactivity of char obtained in pyrolysis of biomass using a free-fall reactor. The authors found the reactivity of char increased when higher heating rates and smaller particles are used. The 0.04 m inner diameter reactor was selectively heated up to 2.9 m in length. Eight independently controlled heaters were used to heat the reactor. The carrier gas was preheated. The reactor can operate at a maximum pressure and temperature of 5.0 MPa and 1100 °C, respectively. Birch wood, white quebracho wood, straw pellets, bagasse and sugar cane agricultural residue (SCAR) biomasses were tested. A 1 kg/hr screw feeder metered the biomass into the top of the reactor as illustrated in Figure 7. Particle sizes were pneumatically classified and ranged from 0.5 mm to 1.0 mm. The heated length was selected so that the residence time was long enough for complete pyrolysis. The volatiles passed through a heated metallic filter after which they were condensed in a water cooled condenser. The minimum reactor temperature reported in the study is 750 °C. Bio-oil yields less than 5 wt % are reported [45].

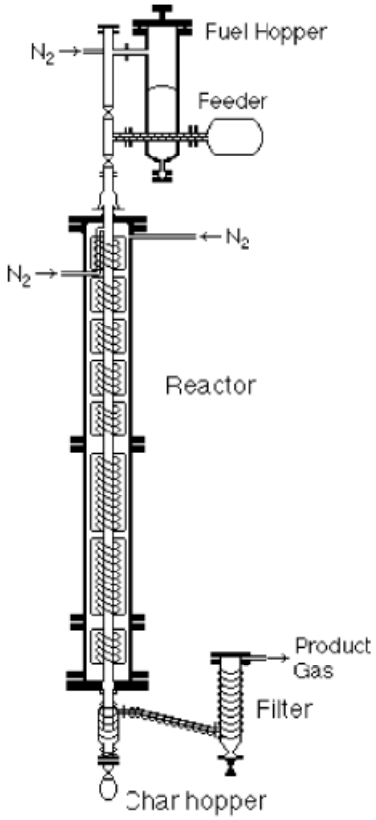

Figure 7. Schematic of free-fall reactor; used with permission from Zanzi [50]

Yu et al. performed pyrolysis of birch wood in a free-fall reactor to determine the effect of temperature on tar production. Bio-oil was defined as volatiles, other than water, which condense at room temperature. The reactor used is previously described by Zanzi et al. [45]. The wood was sieved and classified between 0.5 –0.75 mm and fed using a 1 kg/hr screw feeder. Experiments were performed at temperatures of 700, 800 and 900 °C. Maximum bio-oil yields of 8 wt % were produced at 700 °C. Temperature was found to have a significant effect on bio-oil production [52].

Onay and Kockar used a free fall reactor for the production of bio-oil from rapeseed. Experiments were performed to determine the effects of varying temperature, particle size and sweep gas flow rate. Particle sizes between 0.224 mm and 1.8 mm in size and were fed at 120 g/hr. The temperature range tested was between 400 °C to 700 °C and the nitrogen purge rate was varied between 50 and 400 cm^3/min.

The 1.2 cm in diameter, 70 cm long electrically heated reactor is shown in Figure 8. To prevent the feedstock from pyrolyzing prior to the reactor entry cool, water was pumped through a cooling jacket around the feeder inlet. Two main experiment groups were carried out; the first measuring yields while changing the particle size and temperature, and the second examining the sweep gas velocity on oil yields. The first group revealed that maximum bio-oil yields of 75 wt % are possible feeding particles smaller than 0.224 mm while operating at 600 °C. Bio-oil yields between 68-75 wt % were recorded for particles greater than 1.8 mm down to 0.224 mm and temperatures from 500 °C and 600 °C. The first group of experiments was performed using a 100 mL/min nitrogen flow rates. The second group used particles between 0.425 mm and 0.6 mm and an operating temperature of 600 °C while testing the effects of varying flow rates. Onay and Kockar showed relatively little gain in bio-oil yields for sweep gas flow rates greater than 50 mL/min. For adequate sweeping to occur, the minimum flow rate must be over 100 mL/min.

Bio-oil with 13 wt % oxygen content compared to the 25 wt % of the feedstock was reported. Bio-oil and diesel are compared as transportation fuels. Bio-oil was found to have a pH of 3.2 due to the high amounts of acetic and formic acids present. Both bio-oil and diesel were said to have less than 0.05 wt % water content. The higher heating value was reported to be 37.9 MJ/kg compared to 45.5 MJ/kg in diesel. Both the density and viscosity of the bio-oil were higher than that of diesel [48].

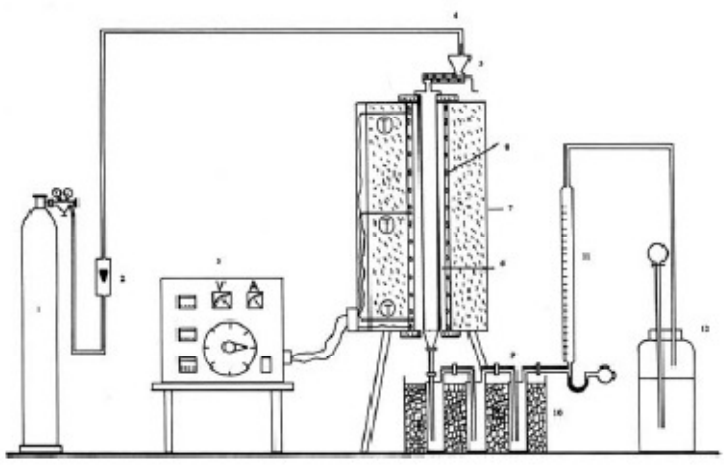

Figure 8. Schematic of free-fall reactor; used with permission from Onay [48]

Karaduman et al. performed flash pyrolysis in a free-fall reactor at Ankara University, Turkey. Interest focused on the pyrolysis of plastics in an effort to reduce plastic waste and recover valuable products. A char collector was located at the bottom of the free-fall reactor. Two salt-ice bath condensers collected liquid products further downstream. A jacketed furnace heated the 50 mm diameter, 1.2 m long quartz reactor. A funnel located at the bottom of the feeder prevented the feedstock from sticking to the walls. The vapors were pulled out of the reactor using a vacuum pump. The temperature along the heated portion of the reactor varied as much as 300 °C due to uneven heating. The solid, liquid and gas yields at 750 °C are 47 wt %, 32 wt % and 21 wt % respectively [39].

Yorgun et al. performed flash pyrolysis of sun flower oil cake using a tubular reactor to determine the effect of temperature, particle size and gas flow rate. A 60 cm long, 3.5 cm diameter reactor was electrically heated. Two set of experiments were performed. The first varied the reactor temperature between 450, 550 and 700 °C, while keeping gas flow rate at 100 mL/min and feeding 0.224 –0.425 mm particles at 120 g/hr. The second set of experiments maintained a 550 °C temperature and varied the particle size from <0.224, 0.224 –0.425 and 0.425 –0.850 mm and gas flow rates from 25, 100, 300 and 600 mL/min. The maximum liquid yield was 45 wt % occurring at 550 °C using 0.425 –0.850 mm particles and a nitrogen flow rate of 300 mL/min [53].

Shuangning et al. used a plasma heated laminar entrained flow reactor at China Agricultural University to study and characterize the volatilization of biomass particles. The reactor employs a plasma torch to heat the biomass providing heating rates on the order of 10^4 °C/s. Particles of cornstalk and wheat straw between 117-173 μm were used for each experiment. Carrier gas flow rates were varied between 0.5 and 1.5 L/min. Volatile material yields for corn stalk and wheat straw are reportedly 69 wt % and 75 wt % respectively. Difficulties in providing a consistent feed rate caused the particles feed in clumps resulting in a mass too large to undergo complete pyrolysis [43].

Bohn and Benham reported on research examining important variables pertaining to an entrained-flow reactor. The reactor was fed at the bottom while a carrier gas lifted the feedstock up its 4.9 m length. Its purpose was to produce charcoal. Another reactor was operated at 500 °C, atmospheric pressure and fed wood waste at 2 kg/hr. The respective

yields for oil, char, gas and water are 40, 20, 27 and 13 wt %. Another reactor injected carrier gas from either top or bottom to control the particle residence time. Bohn and Benham commented that the entrained flow reactor is *the optimum reactor configuration for maximizing gas yield*.

Two main reactor tube types were used during experimentation, one a straight tube either 60 or 120 cm long the other a helical tube 645 cm long. The tubes were oriented horizontally and steam was used as a carrier gas to enable particle entrainment. Pyrolysis gas volumetric flow rate was converted into a mass flow based on the gas composition; any purge gas was subtracted off. Wheat straw was the feedstock of choice because of an interest in liquid hydrocarbon production.

It was observed that gas yields did not vary significantly due to the Reynolds number suggesting that the primary method of heat transfer is due to radiation. For high steam-to-biomass ratios the view factor is near one but larger feedstock flow rates reduce the view factor. Bohn and Benham go on to say that since particle conversion is independent from convection as shown by the Reynolds number, the reaction is not significantly tied to the fluid mechanics unlike a fluidized bed. The authors conclude that the primary method to increase total conversion is to increase the reactor temperature [54].

Matsuoka et al. performed experiments that simulate pyrolysis at the early stages in gasification using a drop tube reactor. The goal was to determine the reliability of the data and compare it with similar research particularly examining weight loss data. Coal particles between 75 and 150 μm were fed into the drop tube furnace at a rate of 0.1 g/min. Helium is used as the carrier gas flowing at a rate of 3.5 sL/min. The operating pressure in the reactor was varied between 0.3, 1.0 and 3.0 MPa. The 0.76 cm inner diameter, 1.83 m long reactor was heated using three furnaces. Experiments were performed at 600, 700, 800 and 850 °C. Typical yields for char, tar, gas and liquid are 58, 22, 17 and 5 wt % (daf) respectively [37].

Probstein and Hicks performed occidental flash pyrolysis of coal. Essentially this is the pyrolysis of coal using the hot char produced to provide heat for the reactor. An entrained flow reactor was used through which pulverized coal particles (<250 μm) were fed. At the entrance of the reactor, the top, the particles were mixed with preheated and recycled char to temperatures between 650 °C and 980 °C. The hot char heated the coal between 510

°C and 730 °C. One to three second residence times were reported. The vapors exited the reactor to a cyclone. Up to 35 wt % tar yields were achieved with feed rates of 1.7 ton/day and reactor temperatures ranging from 590-650 °C [55].

Though free-fall type reactors have been used for many applications very few have been used for the pyrolysis of biomass to produce bio-oil. Two studies that have reported significant bio-oil yields examined the effects of temperature, particle size and carrier gas flow rate [48, 49]. Both performed parametric studies using lab scale reactors with small biomass feed rates (2 – 6 g/min) to determine conditions favoring maximum product yield; not necessarily bio-oil. There has been little research examining the effect of biomass feed rate on bio-oil yields and no research examining interaction effects between parameters or optimizing bio-oil yields.

The development of a 1 kg/hr (16 g/min) free-fall reactor for the production of bio-oil provides an opportunity to examine key areas of research that have not been studied. Optimization of the free-fall reactor for the production of bio-oil using a central composite design of experiments enables the analysis of interaction effects and generation of quadratic models describing the system. The results of the study will provide new depth to the field of fast pyrolysis and specifically the use of free-fall reactors.

CHAPTER 3: Reactor Design

Various configurations and sized free-fall reactors have been used in a wide range of applications. The free-fall reactor has no moving parts and is simple to construct, operate and maintain. Even so, very few free-fall reactors have been constructed for the production of bio-oil via fast pyrolysis of biomass. Designing the free-fall reactor required a multidisciplinary approach. The only restriction on the design was a specified biomass feed rate of 1 kg/hr.

3.1. Design Principles

A number of calculations and assumptions were made during the design phase of this project. Two basic principles were combined in the design of the free-fall reactor. The first principle dealt with the particle heating rate and the second involved the particle's free-fall velocity. After integrating both of these concepts, one can determine both the required wall temperature of the reactor as well as its length for complete conversion.

3.1.1. Particle Heating Rate

It is often reported that the optimum operating temperature for fast pyrolysis is in the range of 475 –525 °C [9, 23, 56]. By assuming that complete pyrolysis has taken place once the center of a spherical biomass particle reaches 500 °C, only the time needed to be calculated for the particle to reach this temperature. Ignoring all effects due to shrinking and changing particle density, a lumped capacitance method was used to solve for the transient heating time. The lumped capacitance approach assumes a uniform temperature distribution throughout the body. Since this can only be the case if the conductive resistance within a solid body is zero, lumped capacitance is assumed accurate for small ratios of convection at the surface of the body over conduction within the body. This ratio is non-dimensionalized and generally represented by the Biot number, *Bi* given in Equation 1:

$$Bi = \frac{hL_c}{k} \qquad \textbf{Equation 1.}$$

where, h is the convective heat transfer coefficient at the surface of the body and k is the conductive heat transfer coefficient within the body. The characteristic length, L_c is defined as the ratio of an objects volume, V to its surface area, A_s as given in Equation 2:

$$L_c = \frac{V}{A_s} \qquad \textbf{Equation 2.}$$

In general, the lumped capacitance method is applicable if Equation 3 is satisfied[57].

$$Bi \leq 0.1 \qquad \textbf{Equation 3.}$$

MathCad 13, a computational software package from Mathsoft was used to perform many of the following calculations. A more detailed version of the calculations may be found in the Appendix A. In order to find the Biot number so that lumped capacitance could be assumed, the convective and conductive heat transfer coefficients as well as the particle size must be defined. Since the biomass particles would be free-falling through a heated reactor tube, the only heat transfer to the particles is due to convection and radiation. According to Cengal, typical free convection heat transfer coefficients for gases range between 2 and 25 W/m^{2}K [57]. Likely the convective heat transfer coefficient is greater than 10 W/m^{2}K but by assuming a low value for free convection one could be assured that the system would be over designed. Bohn and Benham [54] conclude that radiation heat transfer is the primary means in which particles are heated within an entrained flow reactor. To account for this, a radiation heat transfer coefficient, h_{rad} was derived as shown in Equation 4:

$$h_{rad} = \frac{\sigma\left(T_p^2 + T_{wall}^2\right)\left(T_p + T_{wall}\right)}{\frac{1}{\varepsilon_p} - 1 + \frac{1}{F_{p\_wall}}} \qquad \textbf{Equation 4.}$$

where, σ is the Stefan-Boltzmann constant, T_p is the particle temperature, T_{wall} is the reactor wall temperature, ε_p is the emissivity of the particle and F_{p_wall} is the view factor from the particle to the reactor wall. In Appendix A, the radiative heat transfer coefficient is

calculated for various wall temperatures. Comparing this value to the assumed convective heat transfer coefficient reveals that it is about 4 to 10 times greater.

By defining the biomass particle as a cube the view factor can be estimated. Assuming the particle cannot *see* the reactor wall through the top and bottom faces of the cube due to the other particles falling before and after it, the view factor can be approximated to be somewhere between 4/6^{ths} (2/3^{rds}) and 1. By choosing a view factor of 0.7 and assuming that the biomass particle enters the reactor at room temperature and that the particle is a blackbody, only the wall temperature is undefined. Details concerning the view factor assumptions are in Appendix A.

Bailey [58] defines the thermal conductivity of softwood at 500 °C to be 0.09 W/mK. Using the thermal conductivity and selecting a range of temperatures between 850 K and 1250 K and a range of particle sizes between 50 and 1000 microns, one can find a number of solutions (wall temperatures and particle sizes) that satisfy the lumped capacitance requirements (Bi ≤ 0.1).

Again, assuming that complete pyrolysis occurs when the particle reaches 500 °C, the next step is to calculate the time required for a particle to reach that temperature. Using a lumped capacitance approach, Equation 5 can be solved for *t*, the time required to reach a specified temperature, *T(t)*:

$$\frac{T(t)-T_\infty}{T_i-T_\infty}=e^{-bt}$$ **Equation 5. [57]**

where, T_∞ is the fluid temperature, in this case assume the fluid temperature is equal to the wall temperature, T_i is the initial particle temperature and b is the time constant given in Equation 6.

$$b=\frac{hA_s}{\rho VC_p}$$ **Equation 6. [57]**

Replacing h in Equation 6 with the radiation heat transfer coefficient in Equation 4 while specifying a particle density, ρ a specific heat, C_p and a particle diameter, Equation 5 can be

solved for *t*, the time to reach *T(t)* or 500 °C. Note that only the radiation heat transfer coefficient is substituted to be conservative. Kanury and Blackshear [59] report the density of a number of wood types. The densities considered range from 450 kg/m^3 for char to 1350 kg/m^3 for coal with typical biomass densities falling somewhere in between. The results from Equation 5 confirm that particles with high densities require more time to reach 500 °C then those with lower densities at the same wall temperature. Similarly, larger particles require longer heating times than smaller particles. Refer to Appendix A for further detail. Figure 9 depicts the time required for a 600 kg/m^3 particle of various diameters to reach 500 °C. Figure 10 depicts the time required for a 1350 kg/m^3 particle of various diameters to reach 500 °C.

It is also well reported that the vapor residence time for fast pyrolysis should be less than 1–2 s [8, 9, 11, 26]. By limiting the heating time to 2 s, a reasonable particle size of 300 microns and wall temperatures between 780 °C and 880 °C were selected as the basic operating parameters. The energy required to pyrolyze 1 kg/hr of biomass, was computed based on the enthalpy of pyrolysis, 1.53 MJ/kg as reported by Daugaard [60]. Plugging the total heat required into a simple, steady state, thermal resistance network, the thermal resistance between the heater surface and the center of the reactor pipe was calculated. The temperature drop across the thermal network was found to be around 150 °C if the center of the reactor was to be maintained at 500 °C. As a result of these calculations, a set of Watlow ceramic radiative heaters were selected with ample wattage and set-points capable of reaching over 1000 °C.

3.1.2. Particle Free-fall Velocity

Knowing the restrictions on particle size set by rapid heating to 500 °C in 2 s or less the length of the reactor was determined. To be conservative, all effects due to particle heating, such as changing density and loss of mass were ignored. A 300 micron diameter, with a 1350 kg/m^3 density biomass particle was assumed for the following calculations. The forces on a particle in free-fall yields the force balance shown in Figure 11.

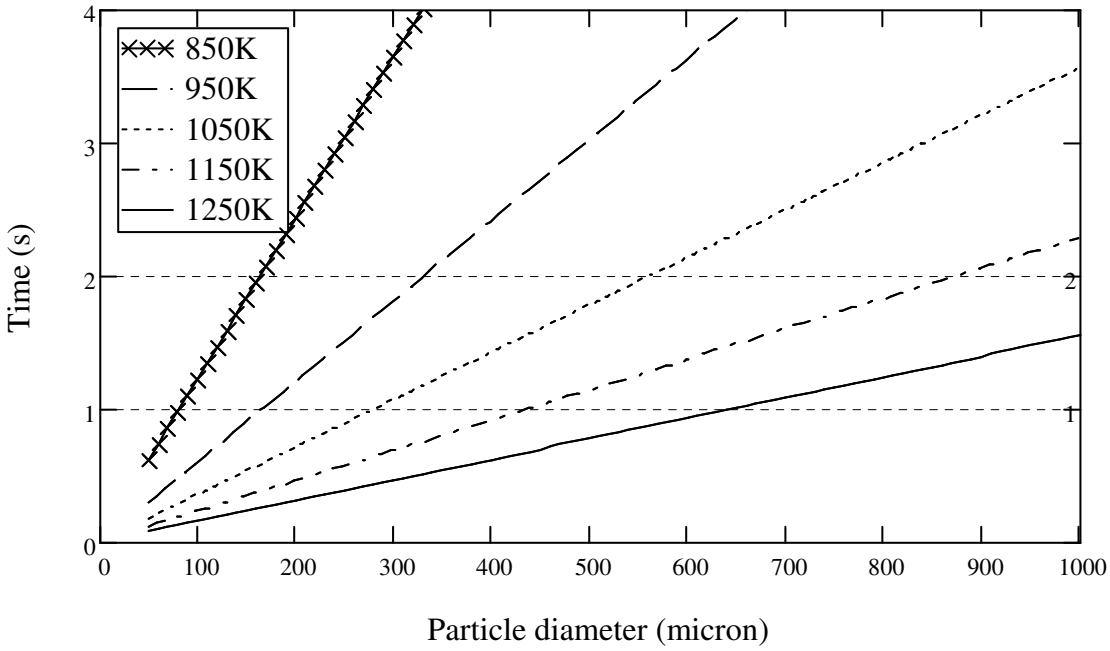

Figure 9. Time required for 600 kg/m^3 particle to reach 500 °C at given wall temperatures

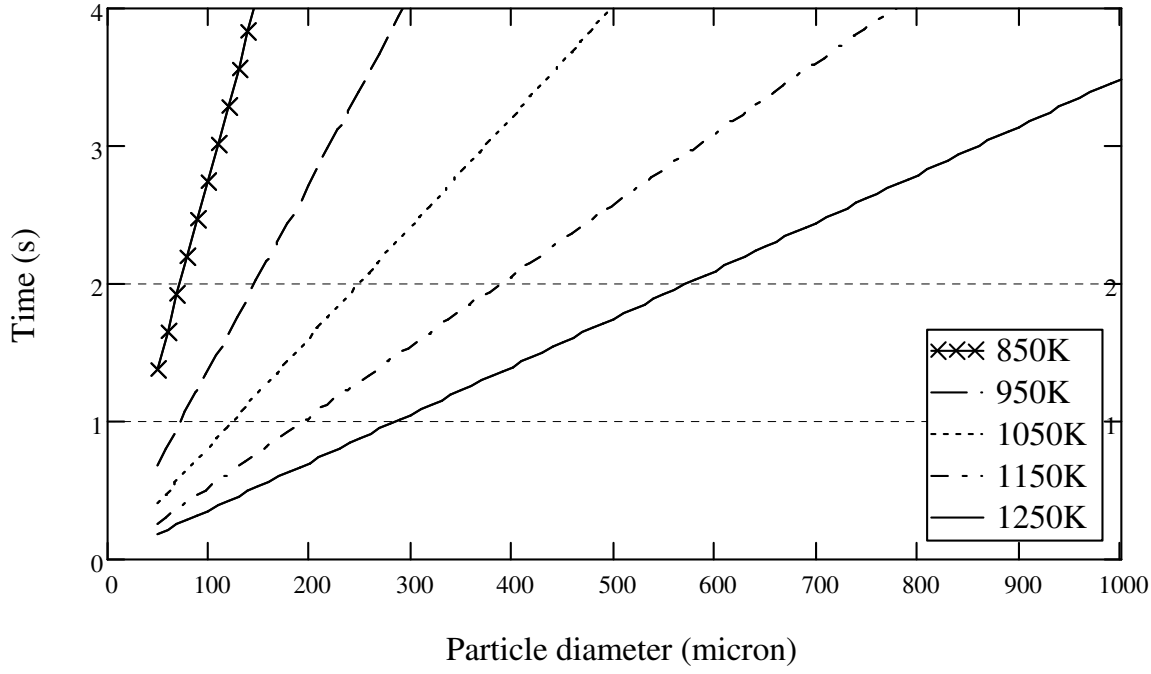

Figure 10. Time required for 1350 kg/m^3 particle to reach 500 °C at given wall temperatures

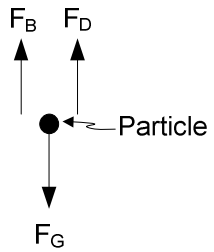

Figure 11. Biomass particle free body diagram

The buoyant force, F_B and drag force, F_D oppose the force due to gravity, F_G. Summing the forces around the particle yields the following in Equation 7:

$$\sum F = m \cdot a = m\frac{dv}{dt} = F_B + F_D - F_G \qquad \textbf{Equation 7.}$$

or written another way,

$$\frac{dv}{dt} = \frac{\rho_f g V_p}{m} + \frac{C_D \rho_f A_c}{2m} v^2 - g \qquad \textbf{Equation 8.}$$

where dv/dt is the change in the particles velocity, ρ_f is the fluid density, g is gravity, V_p is the particles volume, m is the particles mass, C_D is the drag coefficient and A_c is the particles cross sectional area. The drag coefficient is a function of the Reynolds number which is defined in Equation 9,

$$\mathrm{Re} = \frac{\rho_f D_p v}{\mu} \qquad \textbf{Equation 9.}$$

where D_p is the particle diameter and is μ the fluid viscosity. An iterative approach must be used to solve for the velocity since it is a function of the drag coefficient which is a function of the Reynolds number, which in turn is a function of the velocity. Once the velocity has been found, the corresponding drag coefficient can be used in Equation 8. Solving the Equation 8 using Euler's method with the initial condition of $dv/dt=0$ at $t=0$, the particle's

velocity at time *t* can be found. For a 300 micron particle falling for 1.5 s from rest, it will be travelling near 1.32 m/s and will have fallen 1.9 m. This is the length required for the reactor to heat that same particle to 500 °C.

The diameter of the reactor was selected based on the volumetric flow rate of pyrolysis vapors produced. Applying the Ideal Gas Law as a rough estimate, the volumetric flow rate of the pyrolysis vapors leaving the reactor at 500 °C and 1 atm is approximately 9.3 sL/min. To find the velocity of the vapors leaving the reactor, the volumetric flow rate was divided by select pipe diameters. For a standard Schedule 40, stainless steel pipe, the inner diameter is 2.1 cm. At this diameter the vapors will exit the reactor at 0.45 m/s. Accordingly, in 2 s, the vapors travel 0.9 m –about half of the reactor length. This pipe diameter was justified for several reasons. One, it was assumed that most of the vapors would be formed in the lower half of the reactor. Two, moving to a smaller diameter may jeopardize the structural integrity of the reactor. Three, a smaller diameter would increase the likelihood of biomass becoming lodged inside. Four, since the vapors at the exit would be travelling less than half as fast as the biomass particles, it is relatively safe to assume that addition of nitrogen carrier gas to decrease the vapor residence time would not significantly affect the particle velocity. Addition of 5 sL/min of nitrogen carrier gas would effectively double the pyrolysis vapor velocity to 1 m/s which is under that of the particle velocity. This corresponds to a vapor residence time of about 1.9 s.

For versatility, the reactor was designed to have four sections. The bottom three sections were equipped with vapor ports spaced at 0.3 m intervals from the bottom. This allows for the pyrolysis vapors to be pulled off earlier if the residence time was found to be too long. Additional provisions were made by placing a nitrogen purge line on top of the reactor. The purge line served a dual purpose. It both removed the oxygen from the system and also permitted a degree of control over the flow rate of the vapors. While increasing the nitrogen flow rate increases the vapor flow rate it also can potentially increase the particle velocity if set greater than 5 sL/min.

3.1.3. Char Removal Technique

Another important design consideration that was taken into account was removing char from the vapor stream. As the synonym name of the reactor suggests, char is entrained in the vapor stream exiting the reactor. The particulate is entrained when sufficiently high fluid velocities creating a low pressure region pick up the fine particulate. It is important to remove char from the vapor stream as it acts as a catalyst for secondary reactions [2]. As previously mentioned, this has implications for both bio-oil yield and stability [13]. Traditional char separation techniques include cyclone particulate filters and more recently hot gas filtration. Hot vapor filtration techniques may remove finer particulate matter, but at the cost of bio-oil yield [13, 25, 61].

Zhang et al. [46], Zanzi et al. [50] and Li et al. [49], all show a char catch located at the bottom of the free-fall reactor. A vapor port located above the char catch leads into a cyclone to remove fine char particulate. Expanding on this idea, a char catch and cyclone were incorporated in the free-fall reactor design. In an effort to remove any entrained char exiting the reactor a sudden expansion was designed into the top of the char catch. The expansion is similar to a settling chamber where an abrupt drop in the vapor velocity would allow particulate to fall out. In principle, if the velocity of the fluid is lower than the particles terminal velocity, the particle will disengage from the flow. The diameter changes from 2.1 cm in the reactor to 15 cm in diameter in the char catch. The superficial velocity calculated by dividing the volumetric flow rate by the cross-sectional area is reduced by a factor of 50. This corresponds to removing all particles greater than 40 microns. The char catch is 15 cm in diameter and 0.40 m in length. Refer to Appendix A for further details.

High efficiency cyclones may be up to 90 % effective at capturing particles as small as 5 microns in diameter[62]. A cyclone is designed in part on volumetric flow rate and superficial velocity of the fluid passing through it[63]. As the flow rate increases, generally the diameter of the cyclone increases and all other dimensions proportionally. A fluidized bed reactor has a consistently high fluidization velocity and a series of cyclones are often used to remove char. The free-fall reactor on the contrary does not require a high amount of carrier gas. This implies two things. One, the particulate loading is much greater per unit volume of vapor produced and secondly, a much smaller cyclone is needed. The flow rates

of the free-fall reactor are such that a properly sized cyclone would have an inner diameter just over 0.8 cm. Due to the expense and intricacy of fabricating a cyclone, a slightly larger cyclone from another system was experimented with and found adequate. A second cyclone similar in size was later designed to take the place of the original and allow the original to be returned to its normal use. On average less than 2 wt % char is collected in the cyclone largely depending on the feedstock particle size. The cyclone is heated to 475 °C using a 2.4 m (8 ft) Amptec 120 V heat tape to prevent vapor condensation and subsequent blockage.

3.1.4. Bio-oil Collection

Multiple methods have been tried including spray quenches, water, ice or dry-ice cooled condensers or impingers as well as electrostatic precipitators and glass wool or cotton filters [15, 23, 47, 49, 64, 65]. The focus of the project was focused on the design of the reactor, therefore an iterative approach based on experience and trial and error was followed for the development of the bio-oil collection system. Initially, glass impingers placed in a salt-ice mixture condensed the pyrolysis vapors. Glass wool placed in the final impinger served to capture the aerosols. The sudden temperature shift from a hot reactor to ice-cold impingers caused heavy coking at the transition. Additional difficulties in removing the bio-oil from the impingers as well as cleaning the glassware led to a change in bio-oil collection technique. A second and improved approach to bio-oil collection involved the transition to stainless steel quick clamp fittings. The fittings are commonly used in the dairy industry for transporting milk. A variety of shapes and diameters are available. Each section is held together by a clamp and sealed with a polytetrafluoroethylene (PTFE) gasket rated at 200 °C. The stainless steel fittings were arranged in a capital “H” shape and placed into an ice bath followed by an impinger with glass wool. This evolved into the final set of condensers using the “H” shape. The stainless steel fittings were eventually wrapped in copper tubing and cooled with water. The final impinger and glass wool were replaced with a high voltage electrostatic precipitator (ESP) to collect the aerosols. The bottom of the “H” condenser and ESP were fitted with Nalgene® bottles which were replaced after each test and used to store the bio-oil collected. A stainless steel coil and glass wool filter submerged in an ice bath serve to remove any vapor and moisture in the product stream. In all, four bio-oil fractions

are collected. The first two are captured in the "H" style condenser, a third in the ESP and a fourth in the ice bath as shown in Figure 12.

Figure 12. Bio-oil collection system

3.2. Reactor Description

The free-fall reactor converts raw, lignocellulosic biomass into bio-oil, char and non-condensable gas via fast pyrolysis. The process begins by climbing a ladder and placing biomass into the Tecweigh® 5 Series Flex-Feed Volumetric feeder located on top of the reactor frame. The feeder is sealed by clamping an acrylic lid to the rubber hopper preventing any oxygen from entering. The feed rate is set with a 3-digit potentiometer ranging from 000 to 999 depending on the calibration curve. An auger feeds 1 –2 kg/hr of biomass directly into the top of the reactor after the on/off button is pulled out to start the feeder. The reactor is a 2.1 cm (0.8 inch) inner diameter, schedule 40 stainless steel pipe. The entire height of the reactor is 2.1 m (82 inches). The pipe is bolted together with four flanged sections, the top two sections and bottom two sections are 24 and 12 inches long,

respectively. The total heated length is 1.8 m (72 inches). Each section is radiatively heated using two Watlow® Semi-cylindrical ceramic fiber heaters. The 0.6 and 0.3 m (24 and 12 inch) heaters can provide 1100 and 550 W, respectively for a total reactor power of 6600 W. A panel mounted control box and feedback loop is used to set the heater temperature between 450 and 650 °C.

An Alicat Scientific™ mass flow controller regulates a nitrogen purge line feeding into the top of the reactor and feeder. The carrier gas serves to remove all oxygen from the system before starting the feeder. K-type Omega® thermocouples are located in 0.30 m (12 inch) increments along the reactor. The seven thermocouples serve to monitor the temperature of the biomass particles as they fall through the reactor and are rapidly heated. On average, over 98 % of the char is collected in a 0.15 m (6 inch) diameter, 0.40 m (16 inch) tall stainless steel catch located at the bottom of the reactor. The char container is clamped to the reactor with a 0.15 m (6 inch) quick clamp using ceramic rope as a high temperature gasket material. It is heated by a 0.15 m (6 inch) diameter barrel heater to prevent condensation of vapors from occurring inside.

The vapors and non-condensable gas that are produced from the high-temperature reaction exit the reactor and enter a heated cyclone particulate filter to remove any entrained char. Vapors leaving the cyclone enter a four fraction bio-oil collection system. The first two bio-oil fractions are collected in a water cooled condenser. The water flow rates are controlled using rotometers. There are two water loops. The first passes through a heater and is maintained around 100 °C at the condenser inlet. The second loop is cooled in a chiller. The inlet temperature is kept near 15 °C. The third bio-oil fraction is an electrostatic precipitator or ESP. Rather than condensing the vapors, the ESP collects aerosols or tiny liquid droplets by inducing a negative charge on them using a Glassman ER series 30 kV DC power supply. The charged aerosols then collect on the ESP wall and flow down the sides. The fourth and final fraction condenses any remaining vapors. A circular stainless steel coil is submerged in an ice bath reducing the temperature of the vapors to nearly 0 °C. Only the non-condensable gas exits the bio-oil collection system after passing through a glass wool filter.

The reactor is maintained at a gage pressure of 12 cm (5 inches) of water by a vacuum pump. The pump pulls the non-condensable gases out of the system and through a Drierite® filter before they are analyzed. A slip stream of gas is characterized online by a Varian 4900 Micro Gas Chromatograph every three minutes. The main constituents are carbon monoxide, carbon dioxide, methane and hydrogen. The gases subsequently pass through an Excel diaphragm fuel gas meter to determine the volume produced and are then vented into a fume hood.

National Instruments LabVIEW software and hardware are used to collect and record reactor temperatures and pressures as well as control flow rates. A schematic and photograph of the reactor and bio-oil collection system is shown in Figure 13 and Figure 14.

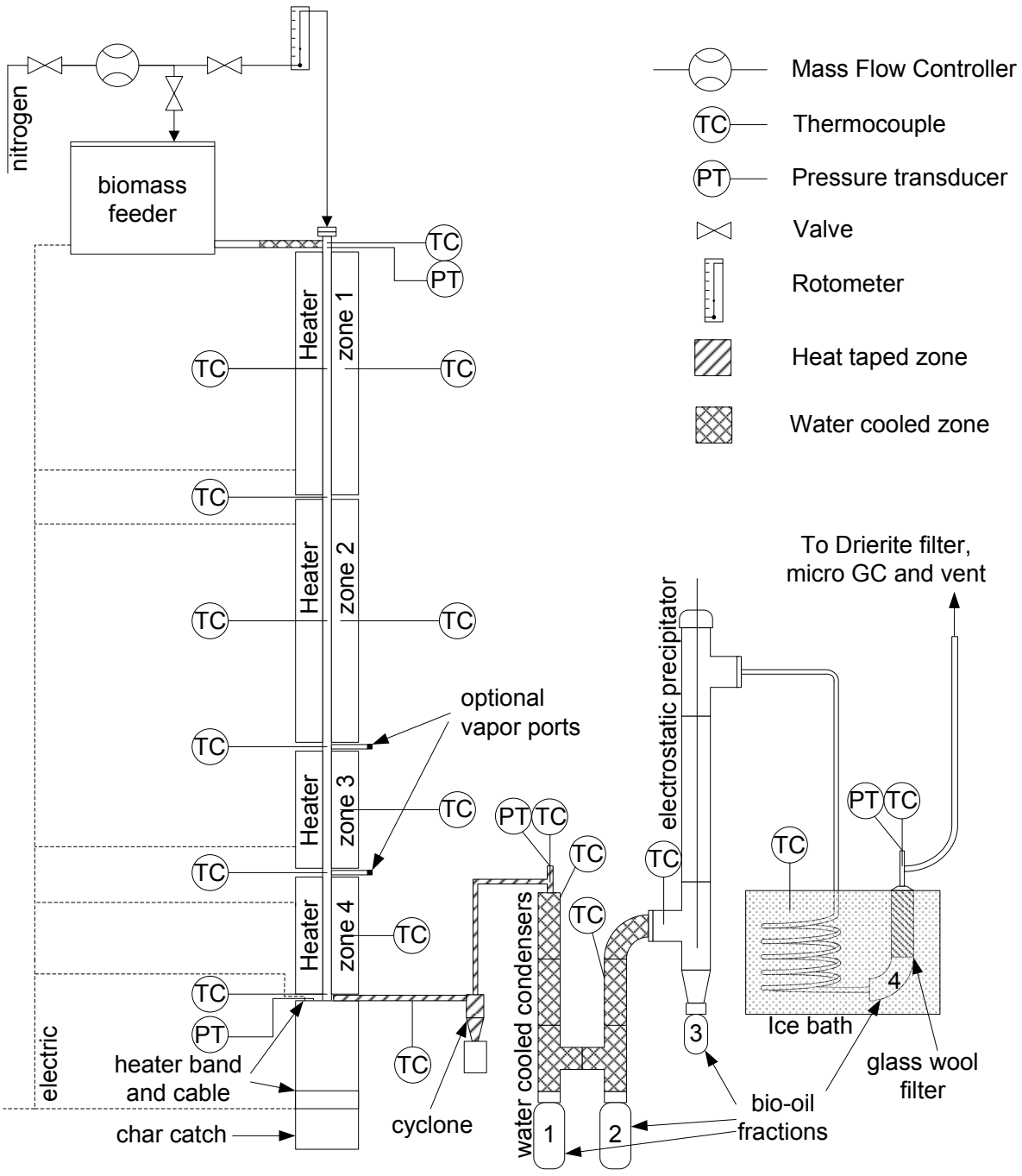

Figure 13. Free-fall reactor schematic used in experimentation (not drawn to scale)

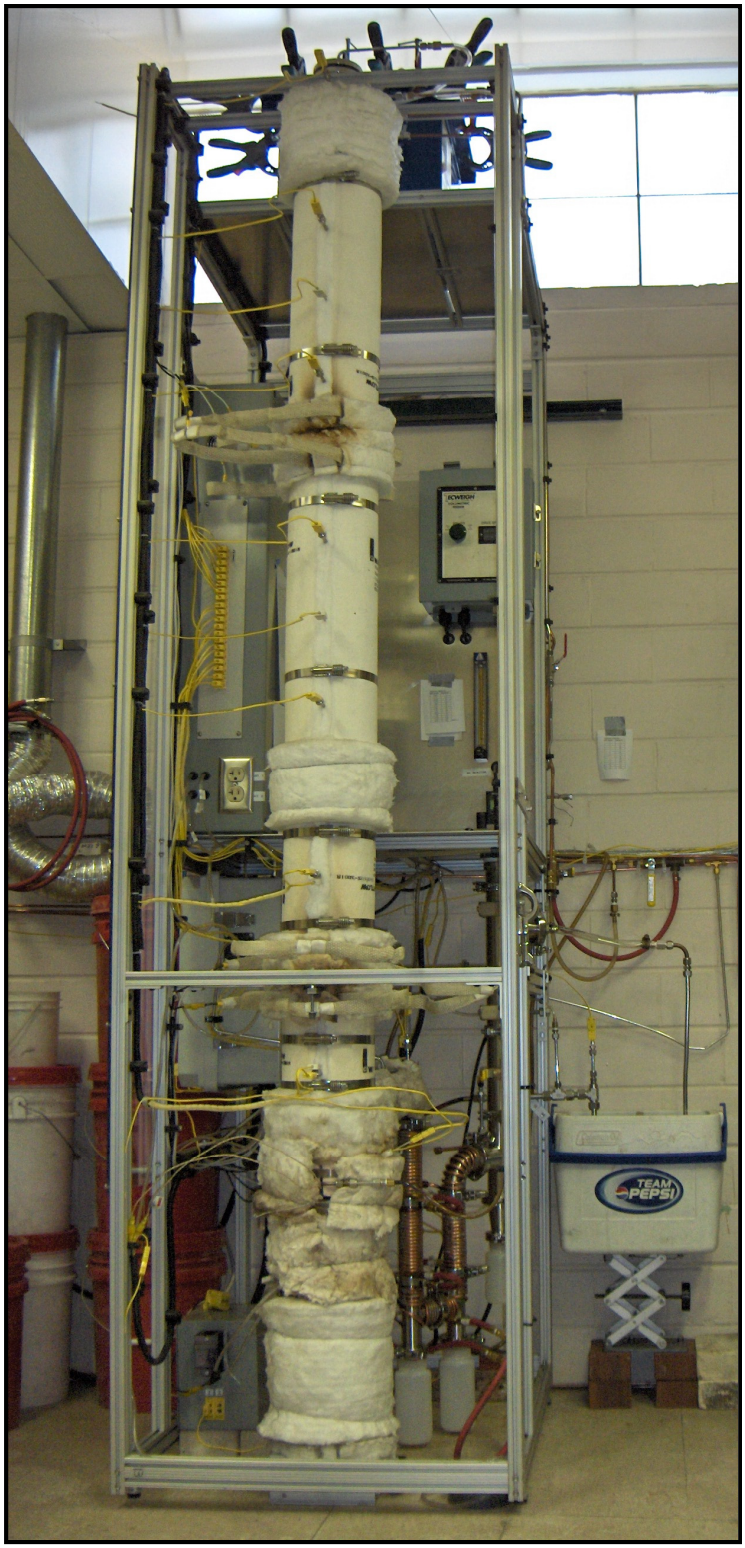

Figure 14. Actual free-fall reactor and bio-oil collection system

CHAPTER 4: Experimental Methodology

4.1. Shakedown Trials

The purpose of the shakedown trials was two-fold. The first was to identify areas in need of improvement. In-depth knowledge of fast pyrolysis and the free-fall reactor were gained through this process. Trial and error, instrumentation and data analysis as well as gut-level instinct played important roles in solving reoccurring problems and fixing new ones.

Two major difficulties were encountered during the initial shakedown trials. The first was the repeated plugging of the system causing a large pressure buildup. The plugging primarily resulted from bio-oil vapors condensing prematurely on cool surfaces before the entering the condensers. The moment the vapors began to condense, char and more vapors would coalesce together and quickly plug the system. This problem was alleviated only after all surfaces were adequately heated to prevent bio-oil vapor condensation. The second problem relates to particulate removal. The low amounts of carrier gas comparable to the fluid bed reactor prohibit the use of traditional filtration devices, specifically a properly sized cyclone. The majority of the heavy particulate settles at the bottom of the reactor in a char catch. After filling a 3-L char catch within a 1 hour experiment, a larger 7-L char catch was fabricated. The larger catch was shown to decrease the bio-oil yield slightly and increase the char yield presumably due to a longer vapor residence time. Fine char entrained in the vapors passed through an oversized cyclone. The cyclone removed the majority of the fine particulate but is not entirely effective especially at low biomass feed rates and small particle sizes as particulate is visible in the bio-oil. The cyclone may plug with char at the bottom where it would normally enter the cyclone catch. This is a concern for processing un-sieved biomass.

The second role of the shakedown trials was to determine the extreme operating conditions of the reactor. This knowledge was crucial in setting the levels for each factor in the future design of experiments. Combinations of high and low biomass feed rates, particles sizes, carrier gas flow rates, and reactor temperatures were tested.

The shakedown trials proved that the free-fall reactor was capable of handling particle sizes much larger than the 300 microns as well as feed rates double the 1 kg/hr design parameters. In fact, particle sizes as large as 1 mm were tested and feed rates as high as 2

kg/hr performed well. Heater temperatures between 400 °C and 800 °C were also tested. Nitrogen flow rates between 1 and 5 standard liters per minute (sL/min) were arbitrarily selected –primarily to purge any oxygen in the system.

Visual observation of the bio-oil and char displayed how well the trial went. Careful attention to the system temperature and pressure through the duration of an experiment also provided a gauge to the quality of the experiment. Only after all multiple trial runs of the free-fall reactor at various operating conditions and configuration could a design of experiments be performed.

4.2. Design of Experiments

A statistically designed set of experiments were performed as a means through which the free-fall reactor could be evaluated. The four factor central composite design minimized the number of tests to be run with the reactor while simultaneously maximizing the amount of data generated. Central composite designs are efficient in determining main effects, two-factor interaction effects and the quadratic effects [66]. Figure 15 symbolizes a three factor central composite design. Each dot represents a different set of conditions at which one experiment is performed. The central point, (0,0,0), is repeated to establish the variance within the system. This variance is then applied to each of the other points since they are only performed once.

The purpose of the 30 experiments was to determine the optimal operating conditions for maximum production of bio-oil as prescribed by the second order response surface. The four factors tested include biomass feed rate, particle size, heater temperature and carrier gas flow rate. Each factor contains five levels. Table 6 displays the levels for each factor.

Table 6. Design of experiment factors and levels

Variable	Factor	Coded level and actual level				
		-2	-1	0	1	2
x_1	Reactor temperature (°C)	450	500	550	600	650
x_2	Biomass particle size (μm)	200	300	400	500	600
x_3	Carrier gas flow rate (sL/min)	1	2	3	4	5
x_4	Biomass feed rate (kg/hr)	1	1.25	1.5	1.75	2

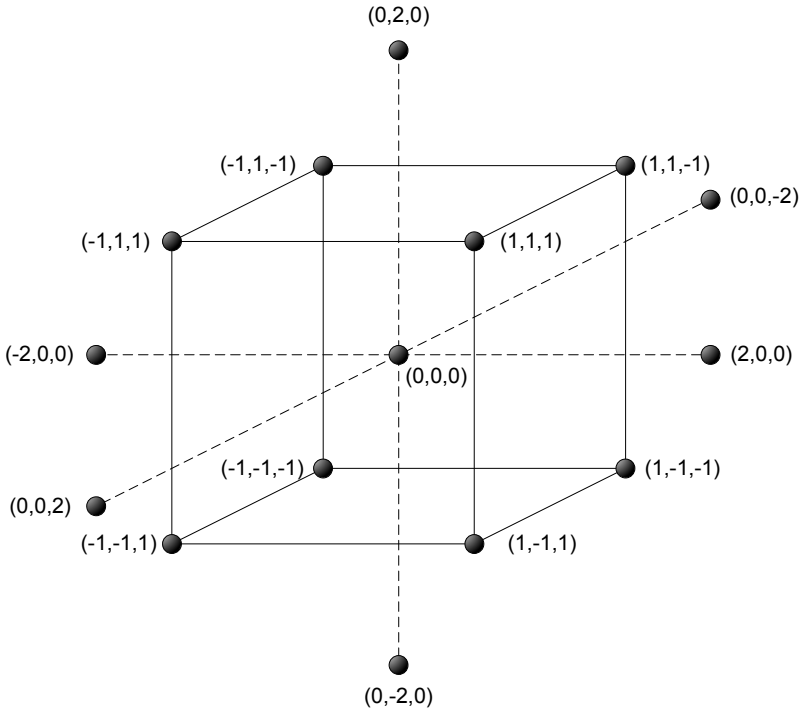

Figure 15. Three factor central composite design

In all, 30 experiments were run, 6 identical center points, 8 axial experiments and 16 factorial experiments. Table 7 lists the conditions for each experiment.

Using the outcome of the design of experiments, models were created in section 5, to show how the operating conditions affect product yield and composition. SAS Institute's JMP 6.0 statistical software package was used to perform statistical calculations and model the central composite design results. Full quadratic models for the product yield and other parameters were fit using all 30 experiments. Each model can be simplified into the following second-order polynomial:

$$Y_i = \beta_0 + \sum_i \beta_i x_i + \sum_{ij} \beta_{ij} x_i x_j + \sum_{ii} \beta_{ii} x_i^2 \qquad \textbf{Equation 10.}$$

where, Y_i is the model response, β_0 is a constant, β_{ii} and β_{ij} are model coefficients, x_i, $x_i x_j$ and x_i^2 are single terms, interaction terms and quadratic terms, respectively.

JMP 6.0 represents the levels for each factor as coded variables. These values linearly correspond to the actual levels as shown in Table 6. For example entering -1 into a model for x_1 would correspond to the temperature 500 °C.

A good model will have a P-value less than 0.05 and a lack of fit P-value greater than 0.05. A model P-value less than 0.05 indicates that the model is significant. A P-value greater than 0.05 for the lack of fit test indicates that the lack of fit is not significant. A significant lack of fit indicates that another model (possibly linear) may fit the data better. A model can be significant and have a significant lack of fit.

Some models in section 5 have been reduced. Reducing the models eliminates many of the insignificant terms making the model easier to understand and more manageable. Not all models are reduced leaving only significant terms. A number of terms that were on the borderline of being significant were kept with the reduced models. Reduced models often become more significant than the full models they are based upon. The Root Mean Square Error (RMSE) often decreases with the reduced model making it a better predictive model. The R^2 value will decrease once the model is reduced. All models that were produced can be found in Appendix D.

The experiments were performed in random order to minimize and distribute any effects due to changes within the reactor setup. It is important to note that the results of the statistically designed set of experiments are specific first of all to the free-fall reactor and secondly to the factors tested. One should not extrapolate the results to other feedstocks, reactors and situations, and though the results may correlate, the statistics and models hold only for the specific conditions utilized during the set of experiments. Therefore using the resulting models to accurately predicting the outcomes will depend on the similarity of the conditions used to create the model.

Any models reported herein are created using values either directly from the experiments or as a result of the product analysis. The models report 95% confidence intervals which are calculated based upon the data from the six replicate tests or center points.

Table 7. Central composite design list of experiments

Type	Run	Factor			
		Temperature (°C)	Particle size (μm)	Flow rate (sL/min)	Feed rate (kg/hr)
Center point	1	550	400	3	1.5
	2	550	400	3	1.5
	3	550	400	3	1.5
	4	550	400	3	1.5
	5	550	400	3	1.5
	6	550	400	3	1.5
Axial experiments	7	550	400	3	2
	8	550	400	3	1
	9	550	400	5	1.5
	10	550	400	1	1.5
	11	550	600	3	1.5
	12	550	200	3	1.5
	13	650	400	3	1.5
	14	450	400	3	1.5
Factorial experiments	15	600	500	4	1.75
	16	600	500	4	1.25
	17	600	500	2	1.75
	18	600	500	2	1.25
	19	600	300	4	1.75
	20	600	300	4	1.25
	21	600	300	2	1.75
	22	600	300	2	1.25
	23	500	500	4	1.75
	24	500	500	4	1.25
	25	500	500	2	1.75
	26	500	500	2	1.25
	27	500	300	4	1.75
	28	500	300	4	1.25
	29	500	300	2	1.75
	30	500	300	2	1.25

4.3. Feedstock Preparation

Many biomass types were tested including corn stover, corn fiber and Red oak during shakedown trials. As previously mentioned, the ash content of a biomass influences the product distribution. The shakedown trials confirmed this when biomass with higher ash contents such as corn stover resulted in lower bio-oil yields. Red oak biomass was selected as the feedstock of choice for design of experiments. This decision was made in part because of the higher bio-oil yields achieved during shakedown trials but also due to the homogeneity and low moisture content of the biomass. Since the goal of the design of experiments was to optimize the reactor operating conditions this ideal feedstock was chosen. The Red oak properties are listed in Table 8.

Table 8. Red oak properties

Constituent (wt %)		Ultimate Analysis (wt %)			Proximate Analysis (wt %)		
Hemicellulose	20	Carbon	48.70	± 3.56	Moisture	3.86	± 1.25
Cellulose	29.8	Hydrogen	6.80	± 0.40	Volatiles	81.90	± 0.45
Lignin	43.3	Nitrogen	0.072	± 0.012	Fixed Carbon	12.56	± 0.51
Extractives	3.3	Oxygen[a]	44.03	± 3.87	Ash	0.39	± 0.18
Ash	0.3	Sulfur	0.002	± 0.001	Other	1.28	-
Other	3.3	Ash	0.39	± 0.18			
Total	100		100			100	

[a] calculated by difference

The Red oak chips are produced by Glen Oak Lumber and Milling out of Montello, Wisconsin. A subsidiary named Wood Residual Solutions distributes the wood chips and shavings produced by the mill. The wood is kiln dried to 8 wt % moisture at the lumber mill and passes through a 2 cm grinder screen before packaging. The Red oak has a higher heating value of 18.05 ± 0.98 MJ/kg.

The biomass particle size is important for the free-fall reactor. A particle that is too large will not be able to heat up quickly and the bio-oil yields will decrease while char and gas production will increase. For this reason, it was critical to determine the effect of particle size on the reactor performance.

Upon arrival, the wood chips were put through an Art's Way 60 hp hammer mill with a 0.6 cm screen. Further grinding was performed using both a Retsch® SM2000 cutting mill and a Schutte Buffalo hammer mill. The ground material was then classified using a Gilson Test Master® TM-3 sieve shaker. Sieve trays with screens sizes ranging from 200 micron to 700 microns in 100 micron increments were placed in the shaker. The Red oak was loaded into the top and the shaker was turned on until the sieve trays were full. The trays were emptied into containers according to particle size. This process was performed until between 20 and 40 kg of each was collected depending on the number of tests with that particle size. The sieved Red oak particles are shown in Figure 16.

Figure 16. Sieved Red oak particles

The density of the particles is also an important factor in determining the particle heating rate as well as its free-fall velocity as discussed in sections 3.1.1 and 3.1.2. A Pentapycnometer was used to determine the particle density. The pycnometer uses a series of differential volumes and the ideal gas law to calculate the particle density. The instrument

was purchased after the reactor was constructed and therefore the particle density was evaluated as a means to compare the design assumptions. In both the particle heating rate and the particle free-fall velocity calculations a particle density of 1350 kg/m^3 was assumed. This is slightly under the densities reported in Table 9.

Table 9. Red oak particle density

Particle size (micron)	Density (kg/m^3)	Error (kg/m^3)
200	1427.6	±1.2
300	1432.3	±1.3
400	1400.4	±4.3
500	1387.4	±5.4
600	1376.1	±5.6

A feeder calibration curve was made for each particle size. About 3 kg of Red oak was placed into the feeder. An acrylic lid was clamped down on top of the feeder to prevent oxygen from entering. A 1 gallon Ziploc® bag was placed on the end of the feeder auger. The initial mass was recorded. The 3-digit potentiometer was set to 100. After 5 minutes, the bag was weighed and the mass recorded. The potentiometer was increased by 100 and the process was repeated until a full calibration was made.

The biomass was stored in sealed 5 gallon pails within the laboratory. Before each experiment, the Red oak moisture content was determined by an Omnimark Instrument, Co. Mark 2 Standard moisture analyzer. The Red oak moisture content was consistently 5.2 ± 0.25 wt % throughout the 30 experiments. The feeder was filled with nearly 3 kg of Red oak before each experiment.

4.4. Product Analyses

The bio-oil, char and non-condensable gas from each of the 30 experiments were analyzed. The non-condensable gas was analyzed for gas composition throughout the duration of the experiments. The bio-oil and char were stored and analyzed much more thoroughly. To cut down on the number of samples, especially for the analysis that requires many hours to be completed, the following approach was taken. Each bio-oil sample of the

six center points was analyzed in triplicate. From these, an average value was calculated for each center point. Since the center point products were all performed at the same conditions the averages values were expected to be quite similar. Any deviation then can likely be attributed to experimental error due to the sample preparation technique or equipment error. The error due to the instrumental analysis was assumed to be small enough to be ignored.

The average error (95% confidence interval) of the six center points was then applied to the remaining 24 experimental values whose analysis was performed only once. This methodology was applied for the water insoluble content, solid content, ultimate and proximate analysis, and GC/MS analysis for bio-oil analysis as well as the ultimate analysis for char. Only the moisture analysis was performed in triplicate for all bio-oil samples. The remaining bio-oil analysis tests namely, higher heating value, total acid number and viscosity were only conducted on the six center point samples. The confidence intervals are reported for tabulated values. All models use confidence intervals derived from the six centerpoints.

Since four bio-oil fractions were produced, all resulting analysis was mathematically recombined according to the bio-oil fraction mass and reported as a single bio-oil fraction value. The fourth fraction of bio-oil made up 1.9 wt % of the total bio-oil on average. This amount was often not enough to perform a complete analysis on and therefore the sample was not analyzed completely in some cases. The average values of the center points were thus adopted in place. The procedures and types of product analyses are given.

Mass Balance: All unfed biomass was removed from the feeder by a vacuum and weighed after each experiment. The amount of biomass fed was calculated by the difference in initial and final biomass weights.

At the beginning and end of each experiment, the condenser, ESP and ice bath coil are weighed individually to determine the bio-oil yield. The four fractions of bio-oil are removed, capped and placed in a refrigerator. The refrigerator temperature cools the bio-oil to prevent polymerization or aging.

The reactor char catch and cyclone char catch were cooled to room temperature before being removed from the system. The difference between the final and initial char catch weights were used to determine the char yield.

The total volume of non-condensable gas was calculated by the difference of the final and initial volume meter reading. An average molecular weight was determined over the steady state region of the gas chromatogram. Modeling the non-condensable gases as an ideal gas, the mass produced was calculated at the average pressure and temperature of the volume meter over steady state.

Bio-oil Sample Preparation: At the time of analysis, the bio-oil containers were taken out of the refrigerator and allowed to reach room temperature. Bio-oil fractions 1, 2 and 3 were somewhat viscous and may have undergone some separation while in the refrigerator. To ensure that a representative sample was taken a homogenized mixture was created. To do so, the bottle was shaken by hand for one minute and then stirred with an impeller for another minute. Once this procedure was performed, a sample was ready to be prepared for bio-oil analysis.

Moisture Content: Moisture content of the bio-oil fractions was measured by a Karl Fischer titrator. ASTM E203 standard test method was used to determine moisture content. Before use the titrator accuracy was verified using a 100 % water standard. Hydranal Composite 5K was the reagent while Hydranal Working Medium K was used as a solvent.

Water Insolubles Content: Water insolubles found in bio-oil are also known in literature as pyrolytic lignin since it traced from the lignin portion of the biomass. It is the fraction of bio-oil that when water is added the insolubles are precipitated [3]. The water insoluble method was developed in house and can be found in Appendix B.

Solids Content: The solids found in bio-oil are predominantly fine char particles that pass through the cyclone. The percentage of solids is determined by pouring a bio-oil/methanol mixture onto a filter paper and finding the difference in weight before and after. The solids content method was developed in house and can be found in Appendix B.

Higher Heating Value: The higher heating value was determined on the center point experiment bio-oil samples, the Red oak biomass and a number of char samples. ASTM D240 test methodology was followed to determine the higher heating values using a Parr oxygen bomb calorimeter model 1341EB.

Proximate Analysis: The moisture, volatiles, fixed carbon and ash of the bio-oil and char were determined by way of a thermogravimetric analyzer. A Mettler Toledo TGA/DSC1 STAR^{e} system using ASTM D5142 standard test method was followed.

Ultimate Analysis: The carbon, hydrogen, nitrogen and sulfur and contents of the bio-oil and char were found using a LECO® TruSpec CHN, and a TruSpec S analyzer. ASTM D5291 standard test method was used to determine bio-oil carbon, hydrogen and nitrogen contents. ASTM D1552 standard test method was used to determine the bio-oil sulfur content. ASTM D5373 standard test method was used to determine carbon, hydrogen and nitrogen content of char, while ASTM D4239 standard test method was used for sulfur. For both bio-oil and char, oxygen was calculated by difference.

In all analysis, the instrument ranges for carbon, hydrogen and nitrogen and sulfur are 0.005 %, 0.02 %, 0.008 % and 0.001 %, respectively. The ash content was determined by thermogravimetric analysis.

GC/MS: A Varian Saturn 2200 gas chromatograph/mass spectrometer (GC/MS) with a CP-Sil 19CB (CP 8722) column was used to find the chemical composition of the bio-oil. Over 32 compounds have been calibrated for and were used to find the concentrations within the bio-oil.

Total Acid Number: The total acid number (TAN) is a measure of the acidity of the bio-oil. A Metrohm 798 MPT Titrino analyzer was used to determine the bio-oil acid number using ASTM D664 standard test methodology. It is reported on a mg KOH/g bio-oil basis; that is the amount of potassium hydroxide required to neutralize the acids within one gram of bio-oil.

Viscosity: The kinematic viscosity of the center point bio-oil fractions was determined with a Cannon-Fenske Opaque viscometer. Standard testing methodology found in ASTM D445 and ASTM D446 was applied. The viscosity was measured at 40 °C for all bio-oil fractions. The viscosity of the bio-oil is determined by the duration of time it takes for the bio-oil to pass through a set of bulbs from a capillary tube. An appropriate capillary size was chosen for each bio-oil viscosity range. The kinematic viscosity is reported in centi-Stokes (cSt).

Micro-gas Chromatography: The non-condensable gases produced during the fast pyrolysis experiment are analyzed on-line using a Varian 4900 Micro Gas Chromatograph. Two columns are used to determine the gas composition. The Varian Molsieve 5A detects hydrogen, oxygen, nitrogen, carbon monoxide and methane gases. The Varian Pora Plot Q detects carbon dioxide, ethylene, acetylene and ethane. The data is plotted and an average molecular weight is computed based on the steady state region.

CHAPTER 5: Results and Discussion

5.1. Mass Balance Distribution

Product yield is influenced by both feedstock type and operating conditions. In addition, the reactor type may influence the product distribution. For this reason the products were examined. Figure 17 provides a summary of the product yields for each of the 30 experiments. The bio-oil yields are broken down into organic liquid, reaction water and carried water. The sum of these three is the bio-oil yield reported on a wet basis. The carried water is the amount of moisture carried over from the biomass and assumed to be entirely retained in the bio-oil. This amount is on average 5.2 ± 0.25 wt %. The reaction water is the amount of moisture produced during the pyrolysis reaction and retained in the bio-oil. To calculate the amount of reaction water one must subtract the amount of carried water from the total bio-oil moisture content. Knowing the bio-oil moisture content, Equation 11 can be used to calculate the bio-oil yield on a *dry* basis.

$$Y_{bio-oil\ yield,db} = m_{bio-oil\ yield,wb} - \%_{bio-oil\ moisture} \times m_{bio-oil\ yield,wb} \qquad \textbf{Equation 11.}$$

Bio-oil yields are reported on a wet basis (includes reaction and carried water) unless otherwise stated. A complete list of experimental conditions and product yield may be found in Appendix C. The experiments were performed in random order and are therefore listed chronologically.

Table 10 summarizes the design of experiment product yield and mass balance closure for all experiments and the center points. The mass balance closures were always above 97 %. This can largely be attributed to the size of the system. Since the char container and condensers were small enough to weigh on a scale, it was not necessary to dismantle each piece and weigh individually. By weighing the components as a whole (rather than piecewise) prevented compounding of errors. Since it is more difficult to weigh or calculate the mass of the non-condensable gases compared to the solid and liquid products, experiments with high gas yields typically have lower mass balance closures.

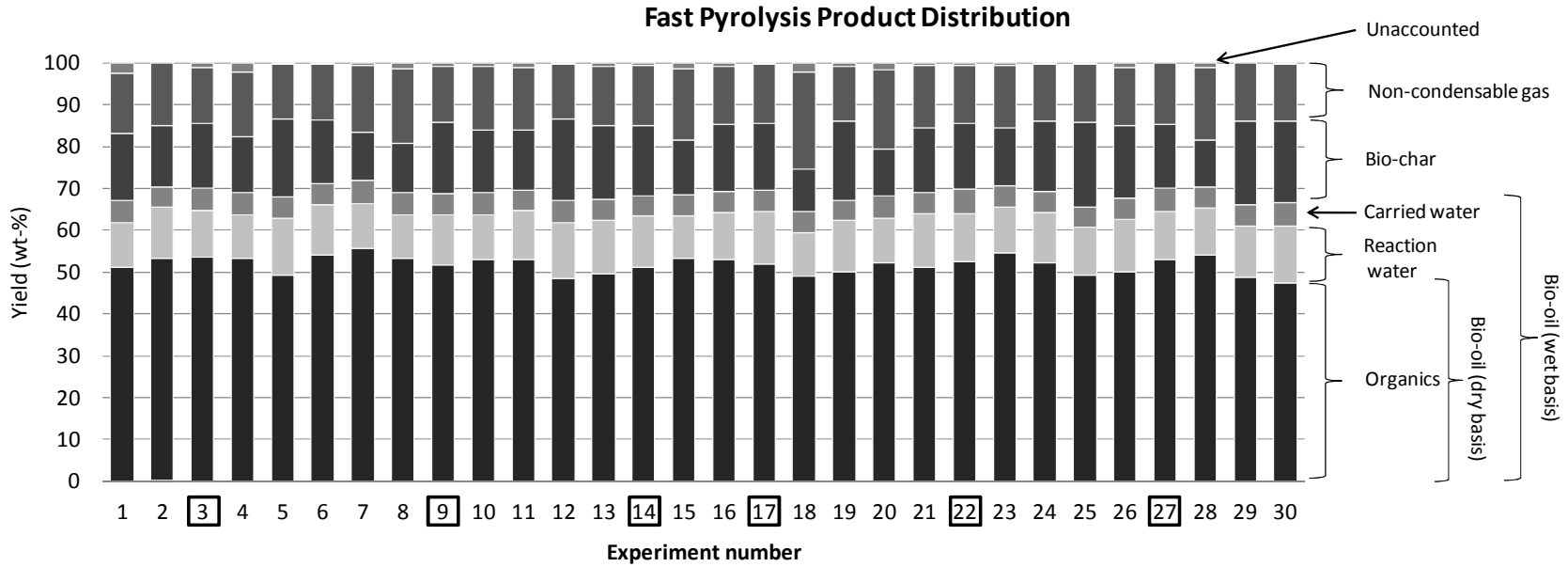

Boxed experiment numbers represent the center point experiments.
Center point experiments operated at temperatures of 500 °C, particle sizes equal to 400 micron, flow rates of 4 sL/min and feed rates of 1.5 kg/hr.

Figure 17. Product yield distribution

Table 10. Experimental summary of product yield and mass balance closure

Product Yield	Organic liquid (wt %)[a]	Water (wt %)		Char (wt %)	NCG[b] (wt %)	Closure[c] (%)
		Reaction	Carried			
All experiments						
Minimum	47.5	10.3	4.8	10.3	13.0	97.7
Maximum	55.7	13.6	5.8	20.1	23.3	100.1
Average	51.8	11.7	5.2	15.6	15.0	99.3
Center point experiments						
Minimum	51.1	11.1	4.9	15.2	13.5	99.1
Maximum	53.6	12.6	5.8	17.0	14.7	100.0
Average	52.3	11.8	5.4	16.0	14.0	99.5
St Dev[d]	0.9	0.5	0.3	0.8	0.4	0.3
± 95 % CI	0.7	0.4	0.3	0.62	0.36	0.3

[a] The sum of the organic liquid and reaction water is the bio-oil yield on a dry basis
[b] Non-condensable gas
[c] Closure is not the sum of each row rather it is for an individual experiment
[d] Standard deviation

Though the 6 center points were operated at the same conditions each experiment resulted in slightly different product yields. The differences within these 6 experiments can be attributed to experimental error. This is the natural variation that occurs within any system. The confidence intervals calculated from these 6 points are the basis for the experimental error for each other experiment since all other experiments were only performed once. For the organic liquid, the 95 % confidence interval is ± 0.7 wt %.

The narrow confidence intervals for the center point experiments listen in Table 10 are an indication that the error inherent within the system (experimental error) is quite small for the production of bio-oil, char and non-condensable gas. Larger confidence intervals are indicative of an unreliable system.

The organic liquid, char and non-condensable gas from Figure 17 are plotted only as a function of temperature in Figure 18. The variation in product yield due to biomass particle size, biomass feed rate and carrier gas flow rate can be seen by the multiple data points at the different temperatures. It is evident that the largest variation in product yield is predominantly due to the reactor temperature. The curve in the organic liquid data indicates

that a maximum yield exists between the temperature range tested. The maximum organic liquid yield occurs around 600 °C and is 55.7 wt % as shown in Table 10. No clear maximum or minimum is shown for the char and non-condensable gas yield as these products decrease and increase with temperature, respectively. Models of the product yields as a function of all variables are presented.

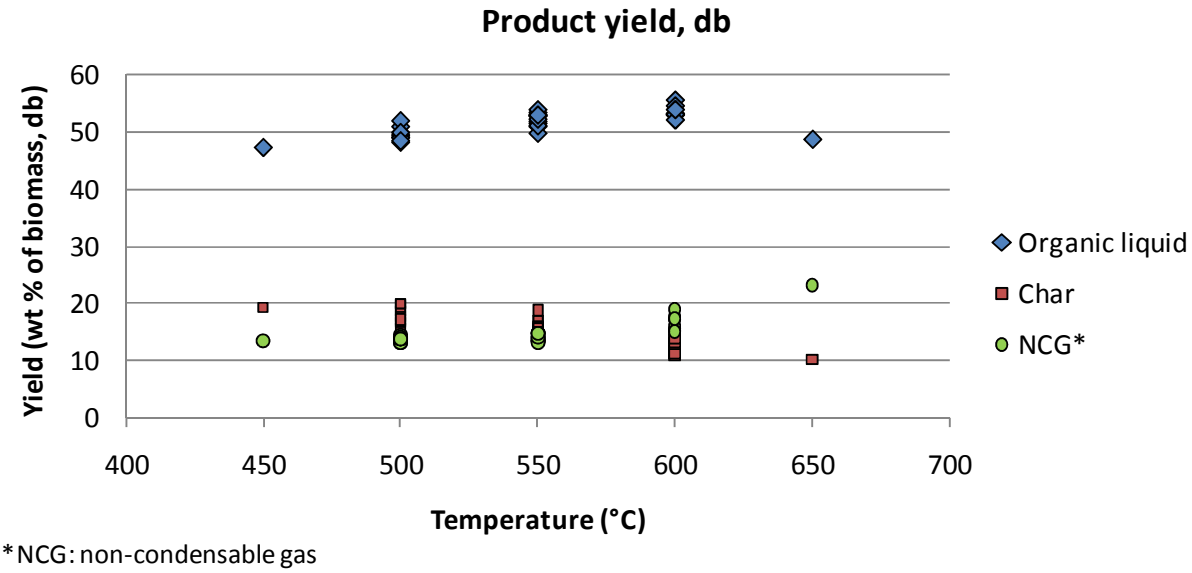

Figure 18. Product yield as a function of temperature on a dry basis

5.2. Bio-oil Yield Model

Plotting the actual bio-oil yield versus the predicted bio-oil yield from the model reveals that the model deviates the most when predicting at extreme low and high operating temperatures as outlined in Figure 19. For low temperatures, the model will under predict the yield and for high temperatures, the model will over predict the yield. Since only one experiment was performed at each high and low temperature (and feed rate, flow rate and particle size) the model will naturally have a larger confidence interval at these conditions. The solid diagonal line is the regression curve. It intersects the average yield of the six center point experiments. As the slope of the regression line decreases the less significant the model becomes. The horizontal line is the average response of the entire data set, in this case bio-oil yield. The inner most set of dashed lines represent the 95 % confidence interval for a set of tests. That is, if one were to perform multiple experiments at identical conditions, the average response of those experiments is expected to fall within the confidence interval 95 %

of the time. The outer most set of dashed lines represents the 95 % prediction interval. These lines are wider than the confidence interval as they provide a range in which one might see bio-oil yield from a single experiment rather than an average of multiple experiments. The models were created on a wet bio-oil basis. For all models, a P-value equal to or less than 0.05 indicates the significance of a term.

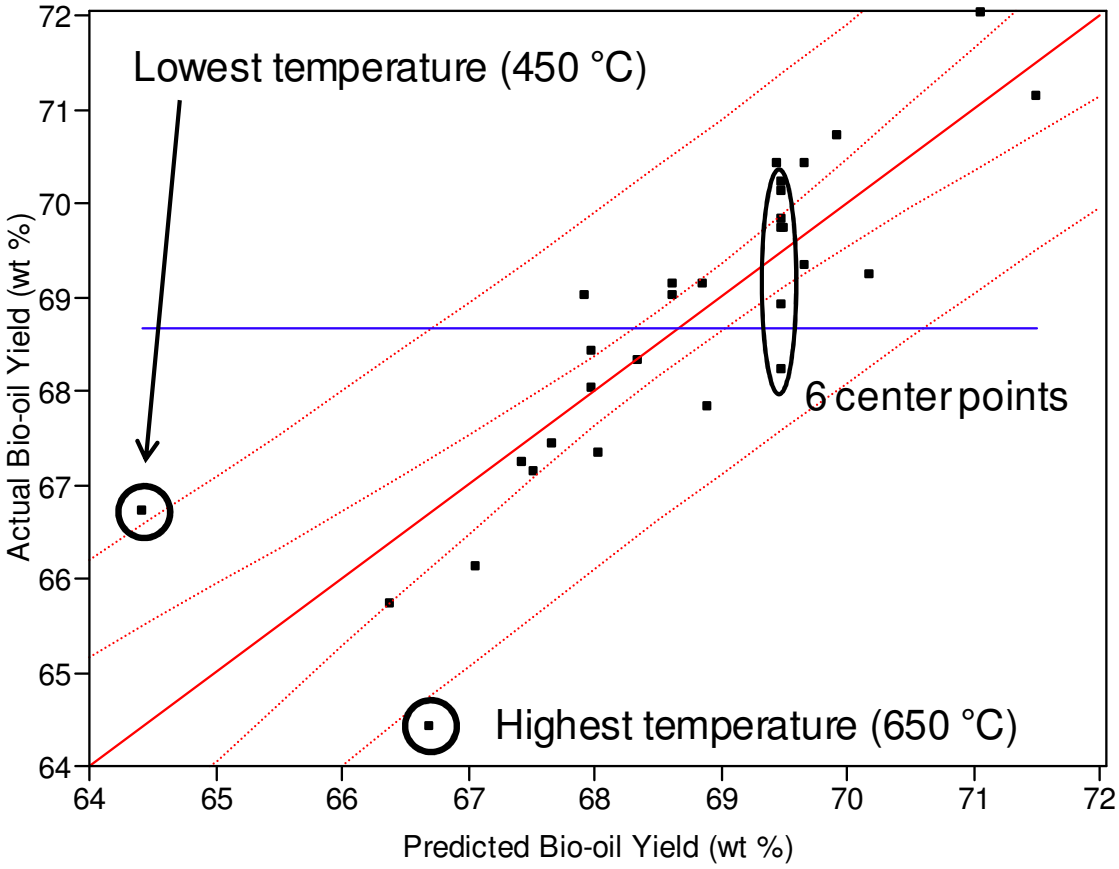

Figure 19. Actual bio-oil yield versus predicted bio-oil yield

Though the extreme high and low temperatures are outside of the model prediction interval, the model is still significant with a P-value of 0.0278 and an R^2 value of 0.72. The root mean square error (RMSE) indicates that the prediction value of the model is on average about ± 1.24 wt % of the actual bio-oil yield.

The analysis of variance (ANOVA) results in Table 11 were used to evaluate the full (unreduced) model and the factors. It is apparent that many factors are insignificant and thus

a reduced model was created to identify only the significant terms. Once the bio-oil model is reduced only four parameters are significant as shown in Table 12. Temperature, particles size, feed rate and the quadratic temperature term all have P-values less than 0.05.

Table 11. ANOVA results for full bio-oil yield model

Parameter	Variable	SS	MS	F ratio	Prob>F	Significance
Model	-	60.49	4.32	2.82	0.0278	Significant
Intercept	-	-	-	-	<0.0001	Significant
Temperature	x_1	7.82	7.82	5.10	0.0393	Significant
Particle size	x_2	6.51	6.51	4.25	0.0571	Not significant
Flow rate	x_3	0.77	0.77	0.50	0.4893	Not significant
Feed rate	x_4	12.47	12.47	8.13	0.0121	Significant
Temperature*Particle size	x_1*x_2	0.33	0.33	0.22	0.6491	Not significant
Temperature*Flow rate	x_1*x_3	0.39	0.39	0.25	0.6211	Not significant
Particle size*Flow rate	x_2*x_3	0.11	0.11	0.07	0.7966	Not significant
Temperature*Feed rate	x_1*x_4	0.18	0.18	0.12	0.7362	Not significant
Particle size*Feed rate	x_2*x_4	0.18	0.18	0.12	0.7362	Not significant
Flow rate*Feed rate	x_3*x_4	1.27	1.27	0.83	0.3780	Not significant
Temperature*Temperature	x_1^2	26.35	26.35	17.18	0.0009	Significant
Particle size*Particle size	x_2^2	1.79	1.79	1.16	0.2975	Not significant
Flow rate*Flow rate	x_3^2	0.19	0.19	0.12	0.7327	Not significant
Feed rate*Feed rate	x_4^2	0.58	0.58	0.37	0.5495	Not significant
Pure error	-	3.03	0.61	-	-	-
Lack of fit	-	19.98	2.00	3.30	0.1000	Not significant

Table 12. ANOVA results for reduced bio-oil yield model

Parameter	Variable	SS	MS	F ratio	Prob>F	Significance
Model	-	54.30	13.57	11.62	<0.0001	Significant
Intercept	-	-	-	-	<0.0001	Significant
Temperature	x_1	7.82	7.82	6.70	0.0159	Significant
Particle size	x_2	6.51	6.51	5.57	0.0263	Significant
Feed rate	x_4	12.47	12.47	10.68	0.0031	Significant
Temperature*Temperature	x_1^2	27.50	27.50	23.54	0.0001	Significant
Pure error	-	8.57	0.57	0.01	-	-
Lack of fit	-	20.62	2.06	3.61	0.0126	Significant

For each of the plots in Figure 20, all but one variable is fixed at the center point conditions as indicated. The plots were produced with the full bio-oil, char and non-condensable gas yield models. The char and non-condensable gas models may be found in section 5.3 and 5.4 respectively and the ANOVA results may be found in Appendix D.

A maximum bio-oil yield of 72 wt % was achieved at 600 °C, feeding 300 micron particle sizes at 1.75 kg/hr with 4 sL/min of nitrogen carrier gas. This yield is greater than the 66 wt % reported by Li et al. [49] at around 600 °C with apricot stone (pit) particle sizes between 450 and 900 microns. The bio-oil yield falls within than those reported by Onay et al. [48] which range between 68 and 75 wt % for rapeseed. For his maximum reported yield, the reactor was operated at 600 °C, feeding particles from 224 to 600 microns with a carrier gas flow rate of 0.1 sL/min and a feed rate of 0.12 kg/hr. Both performed fast pyrolysis experiments in free-fall reactors. Thus the bio-oil yields are quite comparable to those achieved in other free-fall reactors and even similar to the 65 – 70 wt % reported for wood feedstocks in a fluidized bed by Horne and Meier [8, 64].

Actual bio-oil, char and non-condensable gas yields are plotted in Figure 20 with the error bars listed in Table 10. Temperature has the greatest influence on the product yields in all cases as the slope and curvature are the most defined compared to particle size, flow rate and feed rate. The reduced bio-oil yield model can be written as shown in Equation 12:

$$Y_{bio-oil\ yield(wb)} = 69.46 + 0.57x_1 - 0.52x_2 + 0.72x_4 - 0.98x_1^2 \qquad \textbf{Equation 12.}$$

The trends in Figure 20a are similar to those reported by Bridgwater et al [16] for a fluidized bed reactor. As temperature is increase from 450 °C to about 550 °C the bio-oil yield increases about 5 wt % while the char yield decreases by the same amount from 20 wt %. The non-condensable gas yield is relatively static just under 15 wt %. Increasing the temperature to 650 °C yields an increase in non-condensable gas yield to 22 wt % at the expense of both bio-oil and char yield. As noted in Table 12 only temperature, feed rate and particle size are significant in modeling bio-oil yield. To provide a better understanding of these three conditions a series of surface contour plots were produced based on the full bio-oil yield model. The plots in Figure 21 were produced using Sigma Plot v.10.0 software from

Systat Software, Inc. The plots show how the parameters interact with each other. In all cases, the two variables not shown were held fixed at the center point conditions as noted. The plots on the left are surface plots and the plots on the right are the equivalent contour plots.

The bio-oil yield model does not have a single optimum operating condition for the production of maximum bio-oil over the conditions tested. Critical values of the model do exist however and are located on a saddle point. Some of the critical values exist outside of the range of the conditions tested and may be impossible to physically achieve as indicated in Table 13. These conditions represent the point at which the first derivative of the model is equal to zero. Examining Figure 21, one can see that the critical point is a maximum for temperature, particle size and feed rate while the carrier gas flow rate is a minimum. The predicted maximum occurring within the operating range as well as the center point conditions are also shown. Over the ranges tested, the full model predicts that maximum bio-oil yield will occur at conditions using small particle sizes, high carrier gas flow rates and high biomass feed rates as well as reactor temperatures around 575 °C.

Table 13. Predicted bio-oil yield occurring at the critical point, predicted maximum and center point

Parameter	Critical point	Maximum point	Center point
Temperature (°C)	548	572	550
Particle size (micron)	330	240	400
Flow rate (sL/min)	-1.95	5	3
Feed rate (kg/hr)	2.02	2	1.5
Predicted value (wt %)	69.96 ± 14.55	74.29 ± 5.24	69.48 ± 1.08

Temperature is a significant factor in the bio-oil yield model as indicated by the P-value in Table 12. It is also the only factor whose quadratic term is significant. Figure 20a confirms the significance of temperature as the bio-oil yield clearly varies with temperature. A clear optimum temperature condition is evident between 550 °C and 575 °C. These values appear larger than those reported in Table 2 (450 °C – 500 °C). Note that the temperatures reported are the heater set point values.

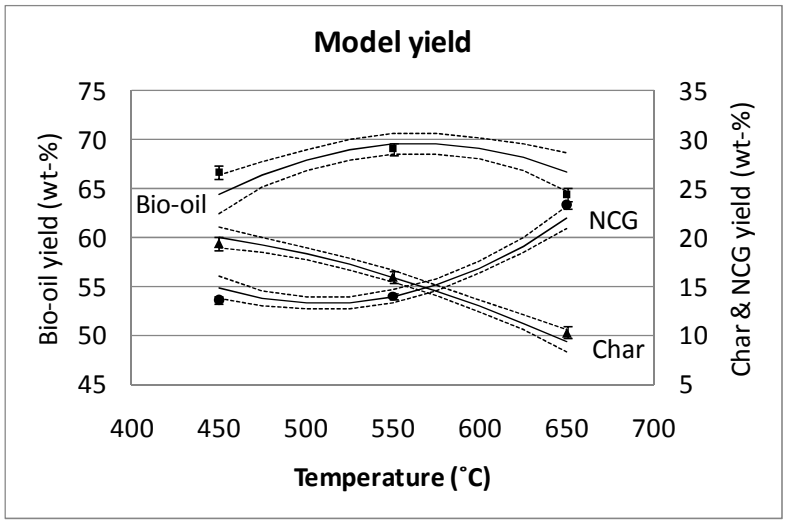

a) PS: 400 µm, FLR: 3 sL/min, FDR: 1.5 kg/hr

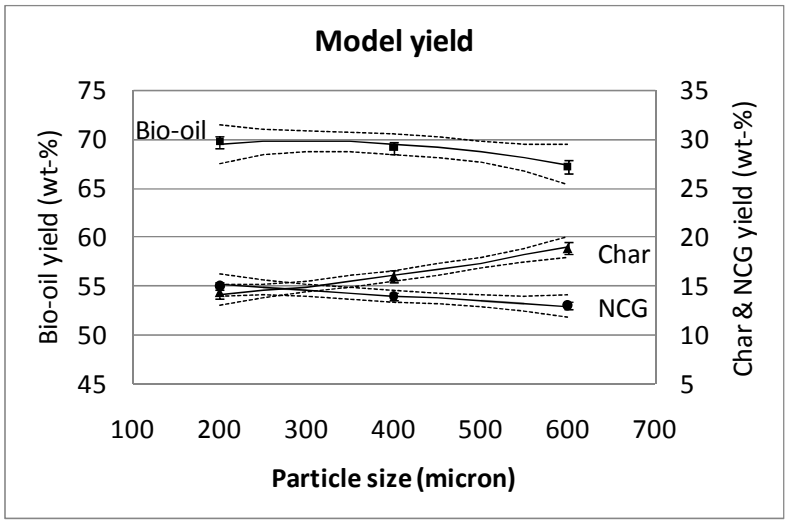

b) Temp: 550 °C, FLR: 3 sL/min, FDR: 1.5 kg/hr

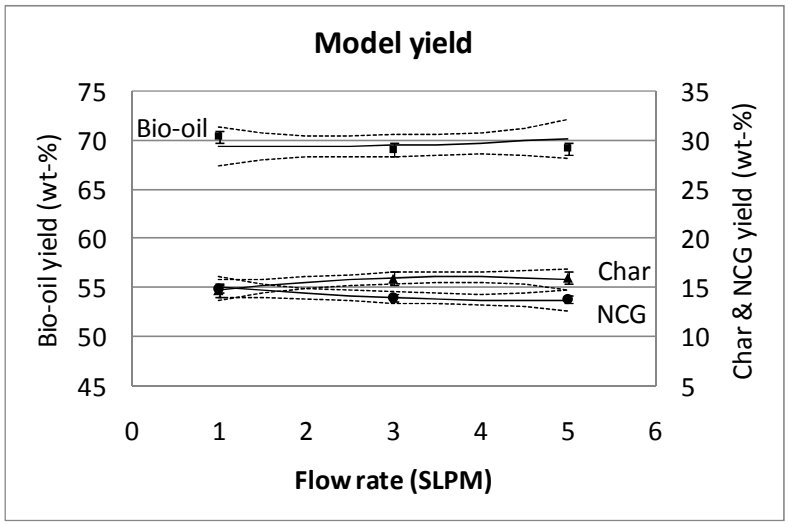

c) Temp: 550 °C, PS: 400 µm, FDR: 1.5 kg/hr

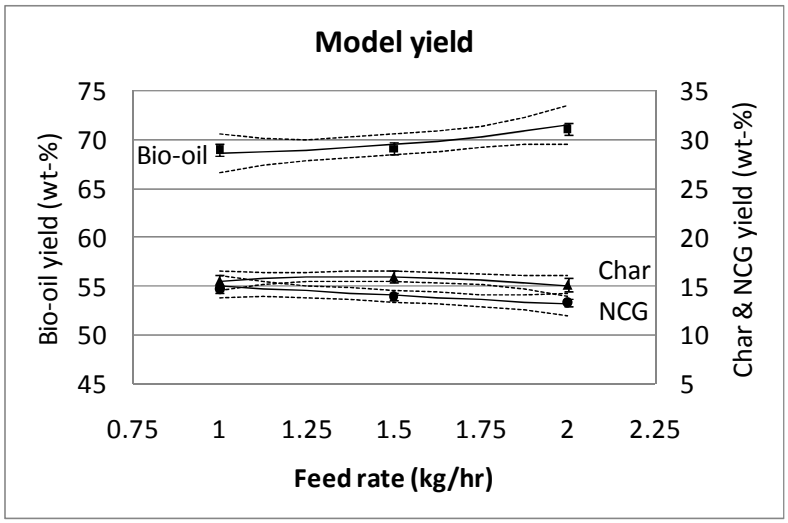

d) Temp: 550 °C, PS: 400 µm, FLR: 3 sL/min

Figure 20. Bio-oil, char and non-condensable gas yield models (solid line) and actual yield (symbol) versus a) temperature b) particle size c) flow rate and d) feed rate. Temp, PS, FLR and FDR indicate temperature, particle size, flow rate and feed rate, respectively.

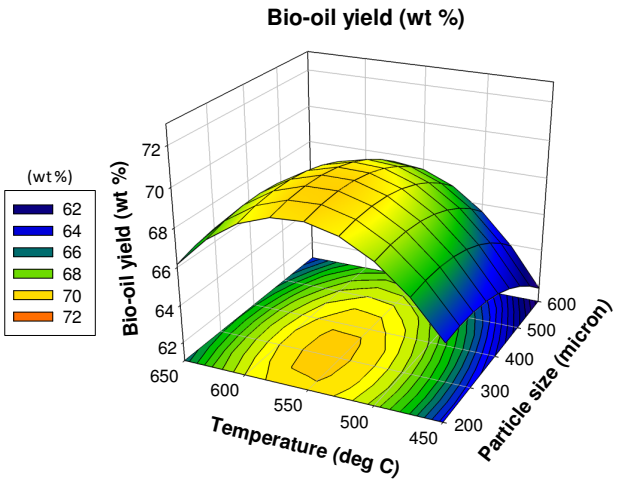

a) Feed rate: 1.5 kg/hr, Flow rate: 3 sL/min

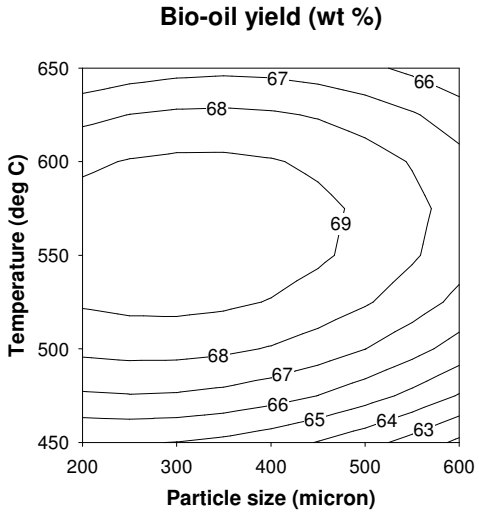

b) Feed rate: 1.5 kg/hr, Flow rate: 3 sL/min

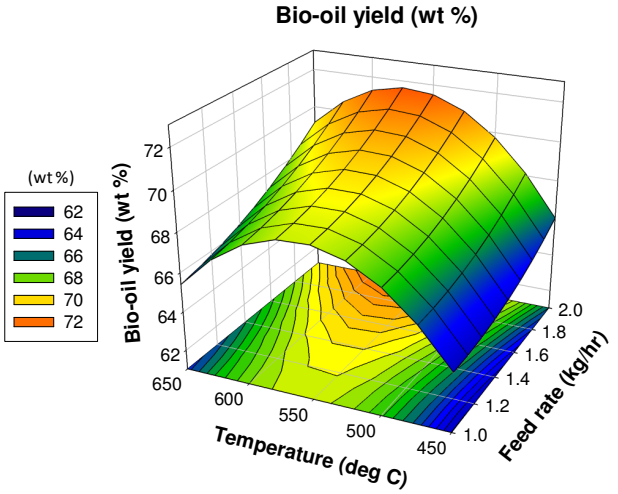

c) Particle size: 400 µm, Flow rate: 3 sL/min

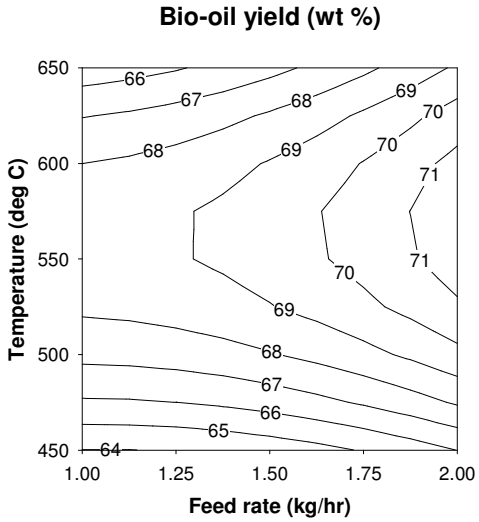

d) Particle size: 400 µm, Flow rate: 3 sL/min

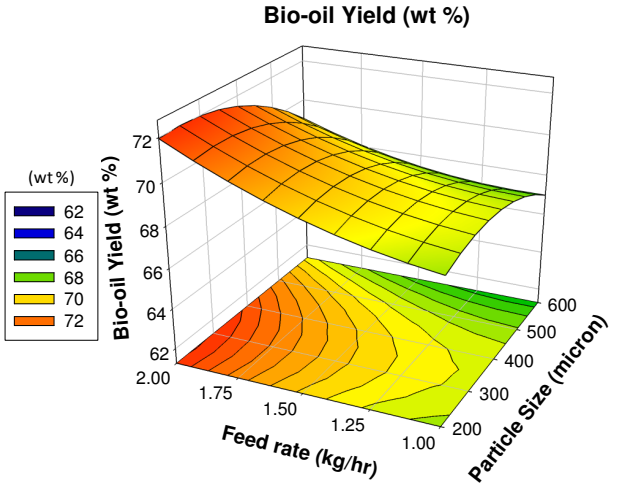

e) Temperature: 550 °C, Flow rate: 3 sL/min

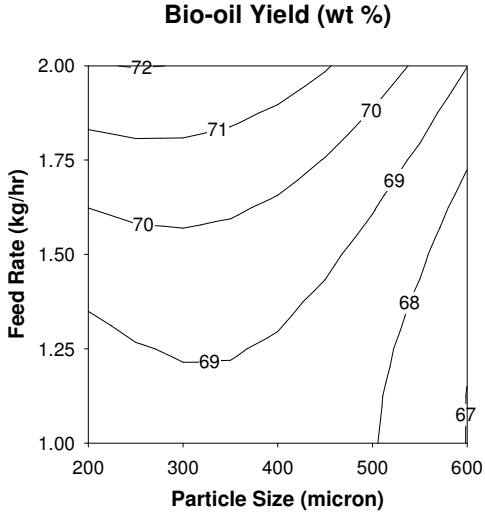

f) Temperature: 550 °C, Flow rate: 3 sL/min

Figure 21. Bio-oil yield model on surface and contour plots

The actual vapor temperature within the reactor varies along its length as shown in Figure 22. For the center point conditions the maximum temperature within the reactor was nearly 75 °C below the heater set point during steady state conditions. This corresponds to a maximum vapor temperature between 475 – 500 °C which is slightly lower than 500 – 520 °C temperatures for maximizing bio-oil yield from wood reported by Bridgwater [10]. The four reactor heating zones are outlined in Figure 22. The top zones are 60 cm long while the bottom two are 30 cm in length.

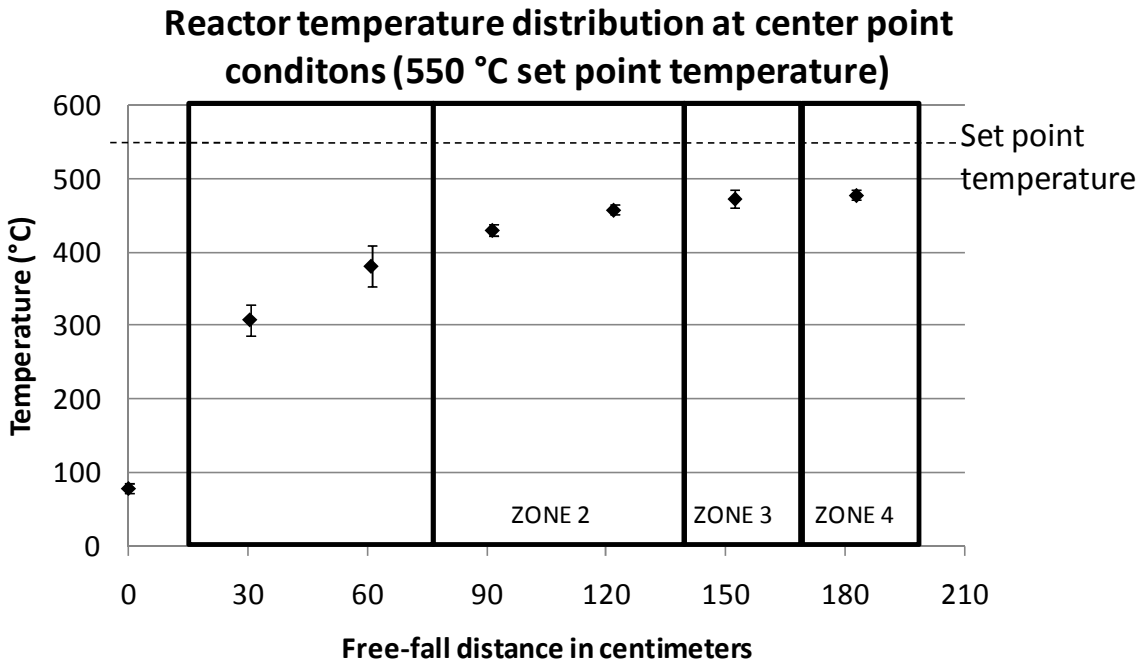

Note: All temperature measurements are roughly 12 inches apart from one another.

Figure 22. Internal free-fall reactor temperature distribution at steady state, center point conditions

Fitting a model to the maximum vapor temperature in the reactor confirms that the temperature is much lower than the set point. Figure 23 suggests that the temperature is about 75 °C lower than the 550 °C heater set point at the center point conditions. At the lowest set point, the vapor temperature is 35 °C lower meaning that bio-oil yields around 65 wt % were achieved at 415 °C. The model suggests that temperature is the primary significant factor in determining the actual vapor temperature. The reduced maximum vapor

temperature model in Equation 13 shows that both flow rate and feed rate are significant factors but each has a negative effect when increased.

$$Y_{\max\ vapor\ temperature} = 477.07 + 42.04x_1 - 4.89x_3 - 3.68x_4 + 5.58x_1^2 \qquad \textbf{Equation 13.}$$

As flow rate and feed rate are increased, one would expect that the maximum vapor temperature would decrease as the amount of time to heat the material is being reduced. Interestingly, particle size has little or no effect on the vapor temperature. This may imply that particles even larger than 600 microns may be successfully employed in the reactor.

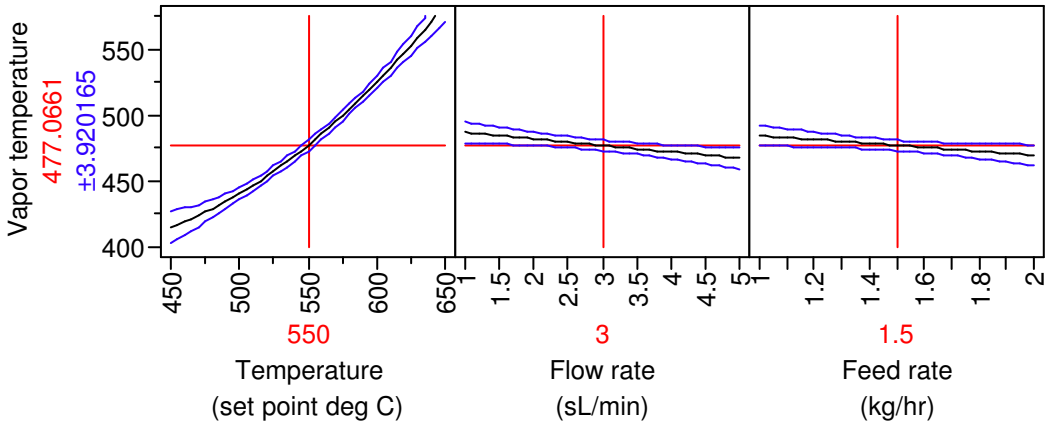

Note that particle size is not shown since it does not significantly affect the vapor temperature. All other set points are indicated on the figure.

Figure 23. Model summarizing the maximum vapor temperature in reactor over steady

The product yield models with respect to temperature can be explained by examining the literature. The high temperatures cause secondary reactions cracking the bio-oil vapors into gas [10]. This decreases the overall bio-oil yield while the non-condensable gases increase. At temperatures below 550 °C bio-oil yields also drop off and char yields increase. The low temperatures do not quickly or fully decompose the biomass particles and thus fewer vapors are produced resulting in decreased bio-oil yields. The remaining biomass particle is then left to turn into char.

Particle size also affects the bio-oil yield as indicated in Equation 12. With a P-value of 0.0263 as shown in Table 12, its effect on bio-oil yield is significant. Unlike temperature,

no clear maxima or minima exist with changing particle size hence the quadratic particle size term is not significant. As the biomass particle size increases the bio-oil and non-condensable gas yields drop off slightly. Increasing the particle size slows down the rate at which vapors are released providing more time for secondary reactions to take place. This cracks the vapors and builds upon the layers of char [67]. Thus the continual increase in char production with increasing particle size can be explained. Decreasing the particle size from 300 microns however, also results in slightly lower bio-oil yields. The smaller particles allow for increased biomass conversion, but this also increases the surface area. As the particles turn to char the increased surface area provides additional opportunity for the vapors to be cracked into gas decreasing the bio-oil yield slightly as noted in Figure 21a and 21b.

Since all tests were performed with biomass that had been sieved, very few particles less than 200 microns were pyrolyzed. It was noted that in experiments using particles less than 400 microns the appearance of the bio-oil visibly changed. It was determined that this change was due to the presence of char in the bio-oil. Smaller particle sizes are much more easily entrained and pass through the cyclone. When using bulk, un-sieved biomass the fine particles may end up in the bio-oil. There is a need to improve the particulate filtration of the system. Operating the reactor with un-sieved biomass will likely affect the performance of the reactor. In fact, the optimum conditions for maximum bio-oil yield may shift as the radiative method of heat transfer within the reactor will be changed as many small particles are introduced.

Nitrogen flow rates between 1 and 5 sL/min through the reactor did not significantly impact bio-oil yield as Table 12 shows. This result is unexpected as it is well documented that increased gas velocity corresponds to increased bio-oil yield. Higher flow rates decrease the vapor residence time and thus minimize secondary reactions and cracking due to the hot environment and presence of char so that the liquid yield is maximized[48, 67].

Since the 1 – 5 sL/min corresponds to 2.6 and 13.2 L/min of gas at 500°C it is difficult to justify that the nitrogen flow rates did not affect the vapor residence time. Rather, one might suggest that the pyrolysis vapors dominated the flow through the reactor and this had a much greater affect than the nitrogen flow. Thus, using carrier gas in the free-fall reactor may be only warranted to purge oxygen at start-up or flow rates greater than 5 sL/min

are needed to have a significant affect. This finding may imply an economical advantage over other reactors that require carrier gas for fluidization.

Biomass feed rate has a positive impact on bio-oil yield over the 1 – 2 kg/hr range tested. The 0.0031 P-value in Table 12 confirms the significance of the biomass feed rate as also indicated in Figure 20d and Figure 21c and 21d. In fact, the single feed rate term is more significant than the single temperature term. Bio-oil yields increase from 68.6 wt % to 71.5 wt % in the model while actual bio-oil yields increased from 69.0 wt % to 71.1 wt % over the 1 to 2 kg/hr range. Unlike temperature, particle size and carrier gas flow rate, the biomass feed rate is the most difficult to maintain at the set point. On average, the biomass feed rate was about 4 % higher than the set point, but as much as 16 % greater in one instance.

Since the reactor was designed around a 1 kg/hr biomass feed rate, it is unexpected to find that the bio-oil yield continues to increase with feed rates twice the magnitude. One might imagine that at higher feed rates it would be increasingly difficult to heat the biomass particles due to radiation blocking and increased mass flow rates, resulting in lower conversion to bio-oil, but this was not observed. The increased bio-oil yield with increased feed rate has a number of possible explanations. One, with increased biomass feed rates, the mass of volatiles increases. Although the nitrogen flow rates did not significantly affect bio-oil yield over the 1 – 5 sL/min tested, the volume of pyrolysis vapors generated from the decomposition of biomass is larger than that of the carrier gas flow. That is, the pyrolytic vapors dominate the flow and reduce the vapor residence time resulting in higher bio-oil yield. Since 1 kg/hr of biomass equates to a vapor flow rate of about 9.3 L/min as suggested in section 3.2.1. doubling the feed rate to 2 kg/hr will effectively double the vapor flow rate to over 18 L/min. The flow rate due to the decomposition of biomass may be even greater than 9.3 L/min at a 1 kg/hr feed rate if the molecular weight of the vapors is less than the 88 kg/kmol assumed in Appendix A. Additional evidence of the pyrolytic vapors dominating the carrier gas flow may be supported by the observation that the condenser inlet temperature was often much higher for experiments with high biomass feed rates. The higher feed rates resulted in an increased thermal mass and thermal load on the condenser. This was not noticed with the nitrogen carrier gas flow rates as the 1 – 5 sL/min flow rates correspond to

0.076 – 0.378 kg/hr. The 1 – 2 kg/hr increase of the biomass feed rate however was much more noticeable. Secondly, if in fact the primary means of heat transfer is due to radiation as Bohn and Benham [54] suggest, the increased number of particles may act as a shield to the vapors and prevent further cracking into char and non-condensable gas. Thus, increased carrier gas flow rate will affect residence time but will not influence the heat transfer mechanism as increased biomass feed rates do.

Temperature, particle size and feed rate are all significant factors in predicting the bio-oil yield. Over the ranges tested, the full model predicts that the maximum bio-oil yield will occur at a heater set point temperature of 572 ˚C, feeding 240 micron sized particles at 2 kg/hr. Carrier gas flow rates are not significant over the 1 – 5 sL/min range tested implying that inert carrier gas is only necessary to purge oxygen.

5.3. Char Yield Model

The reduced char yield model has an R^2 value of 0.95 and the P-value is less than 0.0001 indicating the model is a very significant fit. The char yield model is shown in Equation 14 where x_1, x_2 and x_3 are the coded temperature, particle size and flow rate terms, respectively. Increasing particle size demonstrates a significant positive effect on char yield while increasing temperature reduces the yield as shown in Figure 20a and 20b and Figure 24. Over the temperature range tested, the char yield decreased from nearly 20 wt % to 10 wt % as indicated by the 400 micron particle size line in Figure 24. The increasing temperature corresponds to increased particle heating rate. As a particle is heated more quickly it more quickly decomposes into vapors and char. The higher temperatures also decompose difficult to break down biomass components such as lignin, that may otherwise be turned into char [68]. Thus the char yield decreases with increasing temperature. The quadratic temperature term in the model is evident by the slight curvature in the same figure. Operating at optimal temperature conditions for maximum bio-oil yield would result in char yields around 15 wt %.

$$Y_{Char\ yield} = 15.82 - 2.65x_1 + 1.23x_2 + 0.28x_3 - 0.30x_1^2 \qquad \textbf{Equation 14.}$$

Figure 24 shows the char yield increasing by approximately 5 wt % as the particle size increases from 200 microns to 600 microns. Reasons for increasing char yield with increasing particle size are discussed in section 5.2. Flow rate, though not statistically significant is included in the char yield model since it has a P-value of 0.06. The char yield increases about 1 wt % from 15 wt % with nitrogen flow rates ranging from 1 – 5 sL/min. Feed rate is also not a significant factor.

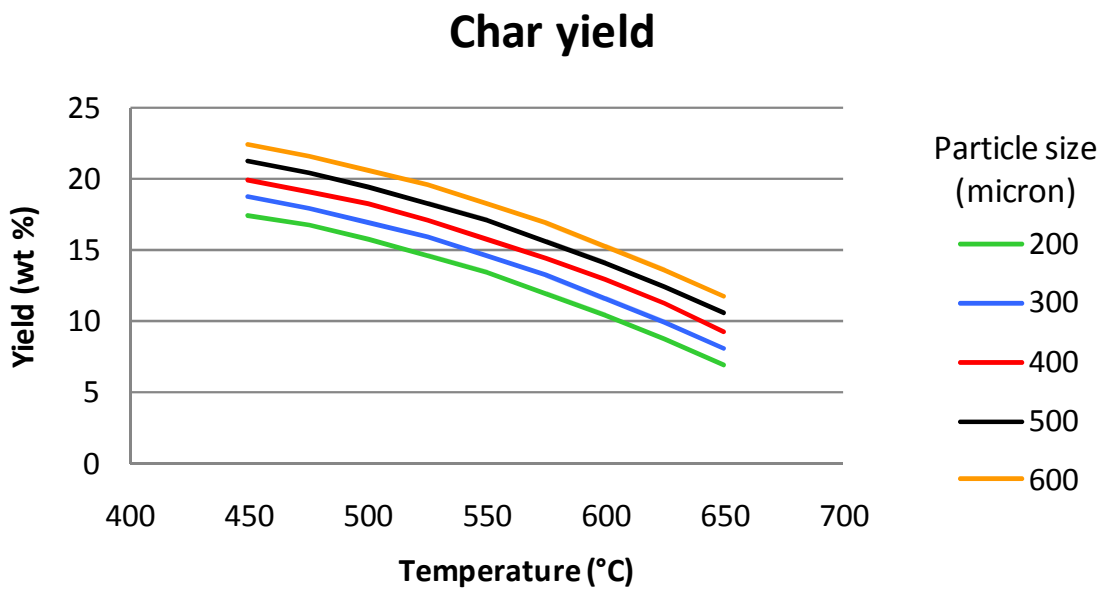

Figure 24. Char yield with respect to temperature and particle size

5.4. Non-condensable Gas Yield Model

The reduced non-condensable gas model has an R^2 value of 0.95 and the P-value is also less than 0.0001 indicating the model is a very significant fit. The non-condensable gas yield model is shown in Equation 15 where x_1, x_2, x_3 and x_4 are the coded temperature, particle size, flow rate and feed rate terms, respectively. The two temperature terms are the only positive terms in the model indicating that increasing temperature will yield increased non-condensable gas.

$$Y_{NCG\ yield} = 14.13 + 1.78x_1 - 0.55x_2 - 0.32x_3 - 0.45x_4 - 0.32x_1x_2 + 1.09x_1^2$$ **Equation 15.**

The temperature and particle interaction term has a P-value of 0.054 and is included as a significant interaction affect. The temperature and particle size interaction is demonstrated in Figure 25. While increasing temperature has a positive contribution to the non-condensable gas yield, increasing particle size, flow rate and feed rate negatively affect the yield as Figure 25 and Figure 26 suggest. The solid parallel lines in Figure 26 show that no interaction exists between flow rate and feed rate.

Non-condensable gas yield is minimized around 525 °C but increases with temperature thereafter. A P-value less than 0.0001 indicates that the single temperature term and the quadratic term affect non-condensable gas yield with convincing significance. At high temperatures the pyrolysis vapors are cracked into lower molecular weight species leading to an increase in non-condensable gas production [69].

The non-condensable gas yield is also significantly impacted by particle size with larger reducing the amount of non-condensable gases produced. Non-condensable gases decrease from 15 wt % to around 13 wt % with particle sizes ranging from 200 – 600 micron in Figure 20b.

While the carrier gas flow rate is not significant for bio-oil or char production, it is significant for non-condensable gas yield. The yield decreases about 1.5 wt % over the 1 –5 sL/min increase in nitrogen flow rate. Feed rates increasing from 1 –2 kg/hr significantly (P-value of 0.002) decrease non-condensable gas yield by about 1.5 wt %.

The bio-oil, char and non-condensable gas product yield models all contain significant single temperature and particle size terms as well as a significant quadratic temperature term. With temperatures increasing from 450 – 650 °C, bio-oil yield is maximized around 70 wt % at a reactor set point temperature near 575 °C corresponding to a vapor temperature around 500 °C. Over the same temperature range, char yields will continue to decrease the entire range and non-condensable gas will generally increase. For particle sizes increasing from 200 – 600 microns, bio-oil yields will peak using particles below 300 microns, char yields will increase about 5 wt % and non-condensable gas yields will decrease by about 5 wt %.

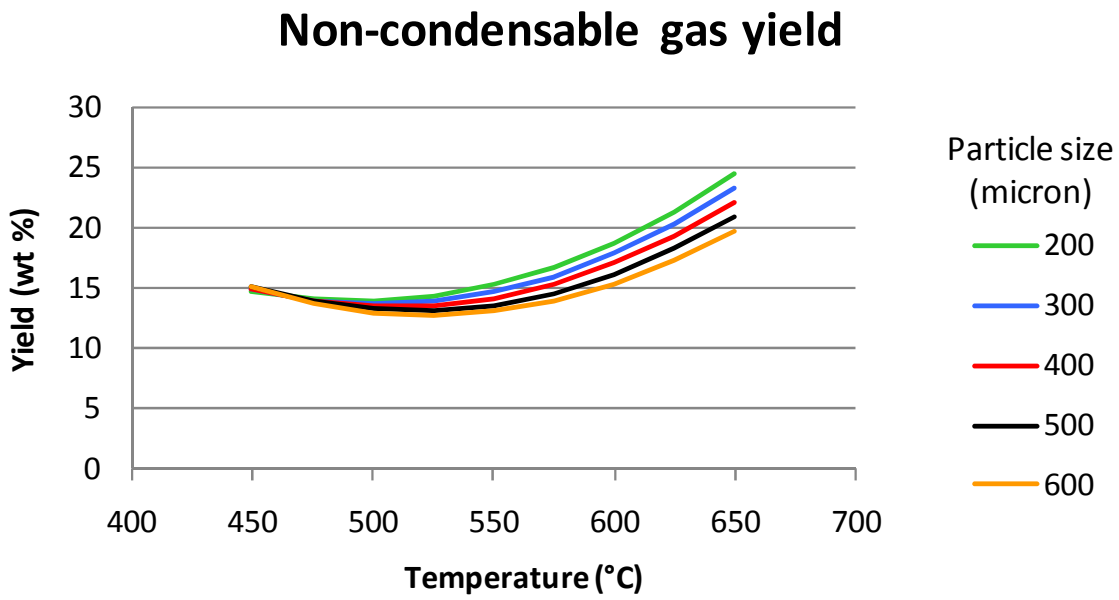

Fixed conditions: feed rate at 1.5 kg/hr, flow rate at 3 sL/min.

Figure 25. Non-condensable gas yield with respect to temperature and particle size

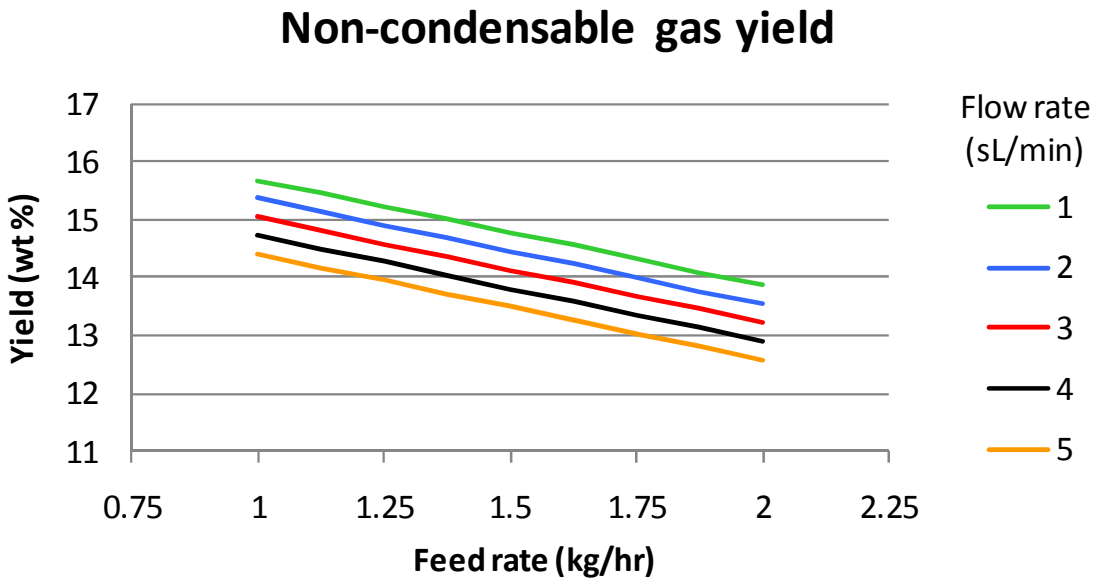

Fixed conditions: temperature at 550 °C, particle size at 400 micron.

Figure 26. Non-condensable gas yield with respect to feed rate and flow rate

5.5. Fast Pyrolysis Product Characterization

The bio-oil, char and non-condensable gas from the free-fall reactor were analyzed. The analysis allows for comparison of between reactors and is another means through which the free-fall reactor can be evaluated aside from product yield. Figure 27 provides the average mass balance composition for the 6 center point experiments as produced from 100 wt % Red oak biomass. The bio-oil yield is comparable to the yields reported by Fahmi et al. [12] for various biomasses from a fluidized bed reactor. The char values are lower than the roughly 20 wt % reported and the non-condensable gas yield higher that the 10 wt % reported in the same paper. The 17.2 wt % combined water content corresponds to an average bio-oil moisture content of 24.7 wt %. As discussed in section 5.1, the carried water is the portion that is carried over from the biomass. It is assumed that all of the water in the biomass remains in the bio-oil since the bio-oil vapors are passed through an ice bath to trap the moisture before leaving the condensers. The reaction water refers to the water that is produced during the thermochemical production of bio-oil. Czernik et al. [26] suggest that long vapor residence times (>2 s) at high temperatures cause vapor cracking and produce more undesired reaction water.

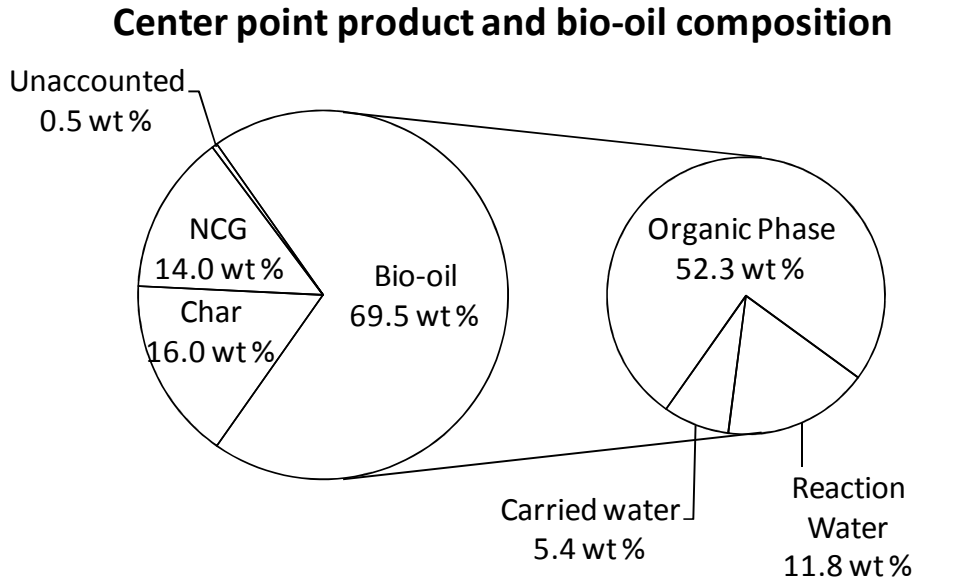

Figure 27. Average center point product and bio-oil composition

Each of the four bio-oil fractions shown in Figure 28 was analyzed individually and the results combined and reported on a whole bio-oil basis. As noted in section 4.4 all center point products (besides the non-condensable gas) were analyzed in triplicate. From these values a 95 % confidence interval was calculated and applied to the remaining product analysis which was performed only once.

As shown in Figure 20 temperature plays a primary role in product distribution. Similarly, many product characteristics are predominantly influenced by temperature. Subsequently, only those portions of a model demonstrating a high degree of significance will be discussed. The parameter estimates for the models can be found in Appendix D.

5.5.1. Bio-oil Characterization

Complete results summarizing a comprehensive center point bio-oil analysis may be found in Table 14. For the most part, the whole bio-oil matches quite well with that of typical bio-oil. The carbon content appears somewhat low while the oxygen content is high in comparison to typical bio-oils.

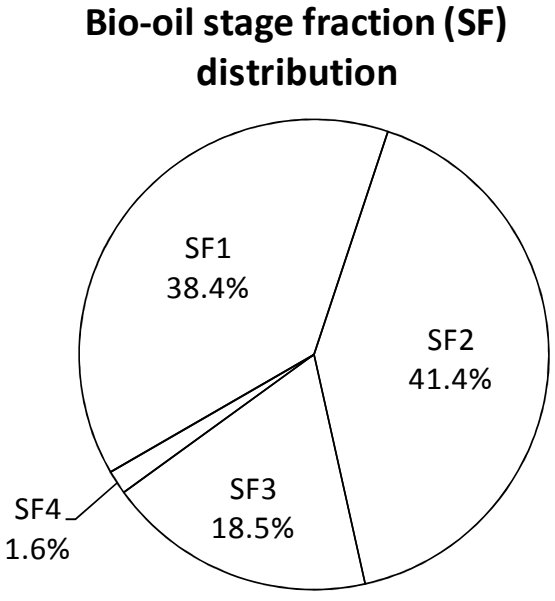

Figure 28. Bio-oil stage fraction distribution

Stage fractions 1 and 3 are quite similar except for water insolubles. The higher water insolubles content in stage fraction 3 is due to the bio-oil collection method. The third fraction is collected using an electrostatic precipitator and is designed to trap liquid aerosols. The understanding is that the aerosols are formed from the decomposition of lignin and thus water insolubles are often referred to as pyrolytic lignin [70, 71]. The similar carbon content for stage fractions 1 and 3 are also due to the bio-oil collection system and the amount of moisture in the bio-oil. The second stage fraction collected far more moisture than either the first or third fractions since it was operating at a cooler temperature. The cool temperature condensed the water before entering the third fraction and this decreased its relative carbon content.

As noted in section 2.3, the high moisture content of bio-oil negatively affects the heating value. The opposite effect can be seen in stage fraction 1 (SF1) and stage fraction 3 (SF3) both having low moisture contents at 9.9 and 12.7 wt % respectively, compared to typical bio-oil. This corresponds to a heating value of 20.4 MJ/kg compared to 12.3 MJ/kg for stage fraction 2 having an average moisture content of 42.1 wt %. Figure 30 shows a sample of stage fraction 1 being poured into a beaker.

The bio-oil can further be characterized according to its chemical composition. Figure 29 depicts the bio-oil chemical composition from GC/MS analysis (water soluble identified) as well as solids, moisture and water insoluble contents as indicated in Table 14.

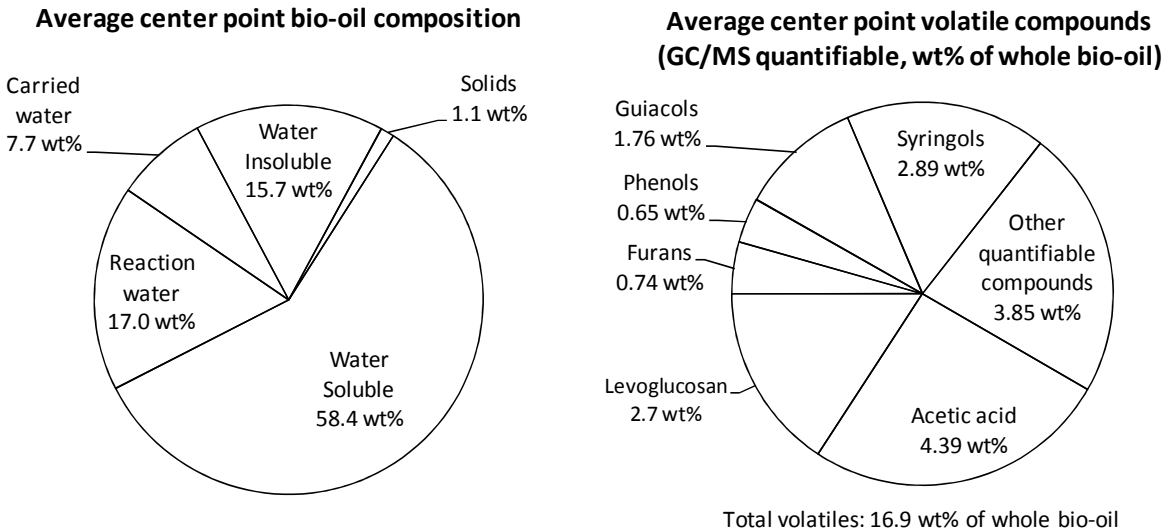

Figure 29. Average center point bio-oil composition

Figure 30. Bio-oil stage fraction 1 from experiment number 12

Table 14. Center point bio-oil characteristics compared to typical wood derived bio-oil

	SF1[a]	SF2	SF3	SF4	Whole	St Dev	95 % CI	Bio-oil[b]
Yield (wt %)	38.4	41.4	18.5	1.6	100	-	-	-
Moisture content (wt %)	9.9	42.1	12.7	64.2	24.7	0.6	0.5	15-30
Water Insolubles (wt %)	20.2	9.8	31.1	1.07	18.0	0.9	0.7	16.2, 20.6[c]
Solids (wt %)	1.3	1.1	0.9	0.8	1.1	0.3	0.2	1
Total Acid Number (mg KOH/g)	93	114	90	74	101	2	1	94[d]
HHV (MJ/kg)	20.4	12.3	20.4	7.0	16.8	0.1	0.1	16-19
Ultimate Analysis (wt %)								
Carbon	49.118	28.138	48.036	12.238	39.558	0.598	0.478	55-58
Hydrogen	6.74	8.28	6.92	7.62	7.42	0.13	0.11	5.5-7
Nitrogen	0.037	0.011	0.025	0.029	0.021	0.018	0.015	0-0.2
Oxygen[e]	44.05	63.47	44.97	80.03	52.93	0.69	0.55	35-40
Sulfur	0.001	0.008	0.001	0.006	0.003	0.004	0.004	-
Ash	0.054	0.093	0.052	0.077	0.066	0.033	0.027	0-0.2

[a] SF denotes stage fraction
[b] Values from wood derived bio-oil unless otherwise stated, Bridgwater [21]
[c] Values from poplar and white spruce respectively, Piskorz [72]
[d] TAN value from mixed hardwoods, Moens [73]
[e] Oxygen calculated by difference for all fractions

Figure 31 provides the moisture content, water insoluble content and Total Acid Number (TAN) for whole bio-oil produced at low, middle and high temperatures tested in the design of experiments. As the temperature increases from 450 ˚C to 650 ˚C, the bio-oil moisture content decreases by about 4 wt %. Bio-oil water insoluble content on the other hand, increases nearly 7 wt %. The Total Acid Number decreases by nearly 20 mg KOH/mg bio-oil over the same temperature increase. While low moisture content and TAN values are good properties in bio-oil these characteristics come at the expense of bio-oil yield. Operating temperatures 450 ˚C, 550 ˚C and 650 ˚C correspond to bio-oil yields of 66.7, 69.5 and 64.4 wt %, respectively. Thus operating conditions that correspond to optimal bio-oil properties do not necessarily equate to conditions producing maximum bio-oil yields.

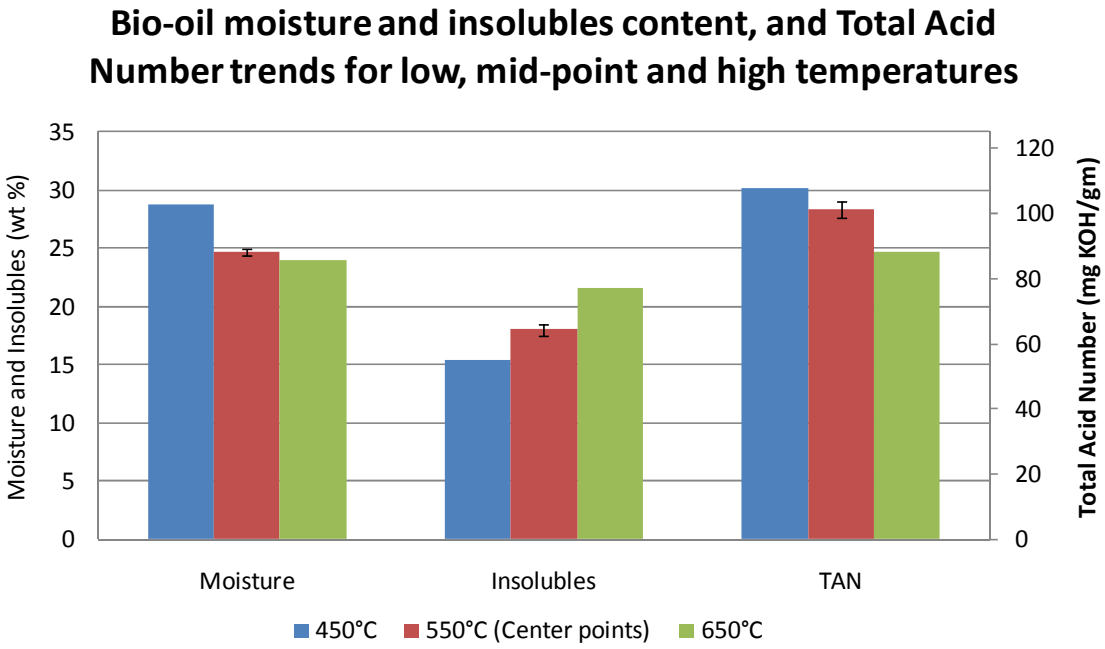

Operating conditions: Particle size at 400 micron, Feed rate at 1.5 kg/hr, Flow rate at 3 sL/min.
Mid-point temperature results and error bars calculated from the average of the center point values.
Bio-oil yields for the respective temperatures are: 66.7, 69.5 and 64.4 wt %, respectively.

Figure 31. Bio-oil moisture and insolubles content, and Total Acid Number trends for low, mid-point and high temperatures

5.5.1.1 Bio-oil Moisture Content

A bio-oil moisture content model was fit to the data. The reduced model is significant with a P-value less than 0.0001 and R^2 value of 0.78. Only temperature and

particle size are significant with P-values less than 0.05 as noted in Appendix D. Figure 32 below displays the changing moisture content with respect to temperature and particle size. For operating temperatures above 585˚C it is best to use larger particles to minimize the moisture in the bio-oil. For temperatures below 585˚C it is best to use smaller particle sizes even though the moisture content will generally be greater in the bio-oil compared to those produced at higher temperatures. As noted earlier, high temperature conditions may be favorable for low moisture content bio-oil but also results in lower bio-oil yields. Fortunately, the bio-oil yield model predicts that the maximum yield will occur at temperatures around 575 ˚C as shown in Table 13. At this temperature the particle size chosen makes little difference in the bio-oil moisture content. The bio-oil moisture content model is in Equation 16 where x_1 is temperature and x_2 is particle size.

$$Y_{bio-oil\ moisture\ content} = 23.34 - 1.46x_1 + 0.32x_2 - 0.43x_1x_2 + 0.38x_1^2 \qquad \textbf{Equation 16.}$$

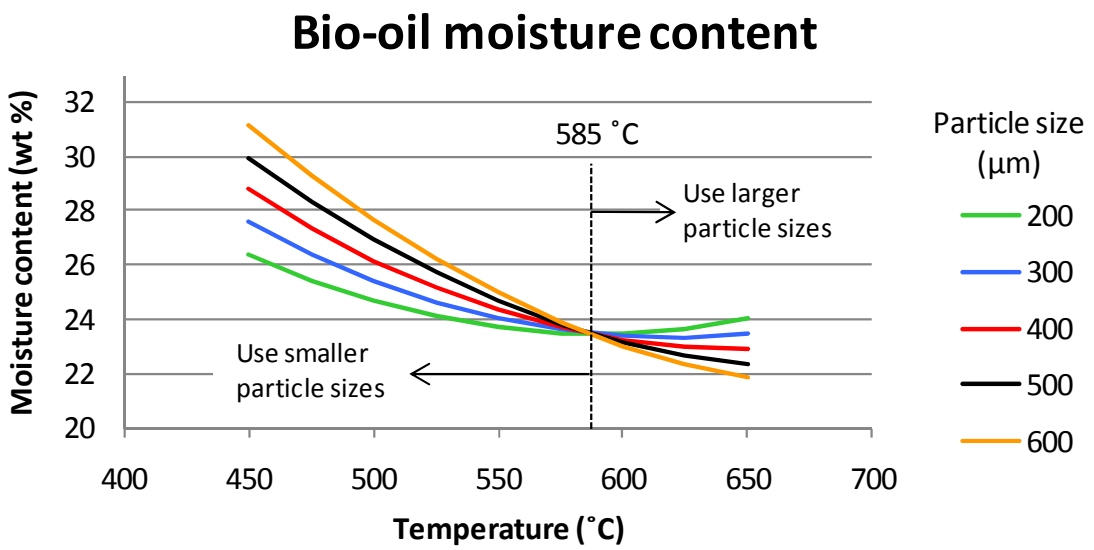

Fixed conditions: flow rate at 3 sL/min and feed rate at 1.5 kg/hr.

Figure 32. Bio-oil moisture content

5.5.1.2 Bio-oil Water Insoluble Content

Bio-oil water insoluble content was performed using the procedure in Appendix B. The water insoluble content is reported for whole bio-oil from combined fractions. The

water insoluble content for the fourth fraction of the bio-oil center points was 1.1 wt % on average. Since the mass of the fourth stage fraction was small this amount often contributes less than 0.05 wt % to the whole bio-oil water insolubles. For this reason the average center point water insoluble content of the fourth fraction was applied to all remaining experiments.

A model was fit to relate water insoluble content to the operating conditions as given in Equation 17. The reduced model can be found in Appendix D. With an R-squared value of 0.86 and a P-value less than 0.0001, the model is significant.

$$Y_{bio\text{-}oil\ water\ insoluble} = 18.01 - 2.01x_1 - 0.90x_2 + 0.50x_1x_2 \qquad \textbf{Equation 17.}$$

Figure 33 indicates how water insolubles are affected by the processing conditions. Temperature and particle size play a significant role each with P-values less than 0.05. Figure 33 can be understood when comparing it to the char yield model in Figure 24. Water insolubles are the large, lignin derived molecules within the bio-oil. These large molecules are difficult to break down and require high temperatures to do so. Yang et al. [68] showed that over 47 wt % of the original lignin mass remained and formed a solid residue after heating the sample to 900 °C. Looking at the effect of temperature on water insolubles and char yield it appears that at low temperatures fewer water insolubles are present in the bio-oil while the char yields remain high. With increasing temperature however, more water insolubles are present in the bio-oil and the char yield drops. At low temperatures the biomass particle is not quickly broken down or vaporized trapping the lignin that is converted to char. At high temperatures, the biomass particle is quickly vaporized and may even explode due to steam vaporization [19]. The cellulose and hemicellulose have fully degraded after 400 °C leaving primarily lignin [68, 74]. Thus more lignin derived insolubles are found in the bio-oil at high temperatures corresponding to low char yields.

A similar affect is noticed with particle size. Smaller particles allow for the heat to rapidly penetrate and decompose the biomass particle leaving little char. Larger particle sizes are not heated as quickly and therefore lock in the lignin component and increase the char yield as indicated in Figure 24 and Figure 33.

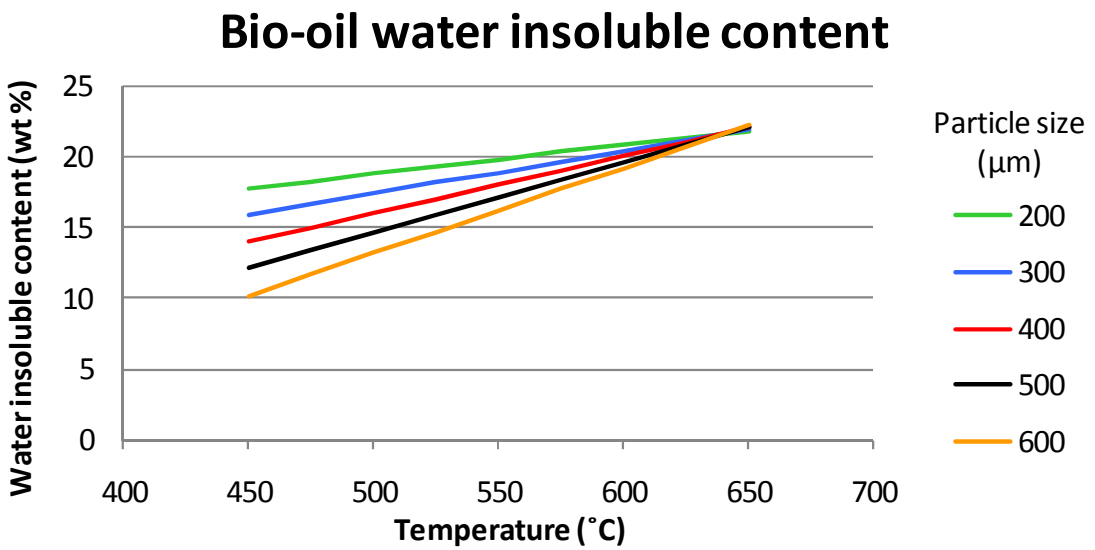

Fixed conditions: flow rate at 3 sL/min and feed rate at 1.5 kg/hr.

Figure 33. Bio-oil water insoluble content

As the bio-oil water insoluble content increases with temperature it worth noting that the bio-oil moisture content also tends to decrease with temperature. Thus, the apparent increase in bio-oil water insoluble content may only be due to a relative decrease in moisture content and water soluble content within the bio-oil, not simply a char yield decrease. Looking at the 400 micron particle size in Figure 32, it is evident that the moisture content decreases about 6 wt % as the temperature increases from 450 to 650 °C. Over the same range, the water insoluble content increases about 8 wt % in Figure 33. These observations suggest that as moisture content decreases with temperature, the water insoluble content increases by nearly the same amount. Apart from the decrease in moisture content, the apparent increase in bio-oil water insoluble content may also be attributed to a decrease in bio-oil water *soluble* content.

To truly see if the water insoluble content is increasing with temperature at the expense of char yield it is helpful to plot the bio-oil water insoluble content on a moisture free basis as a fraction of the biomass input along with the char and non-condensable gas yield.

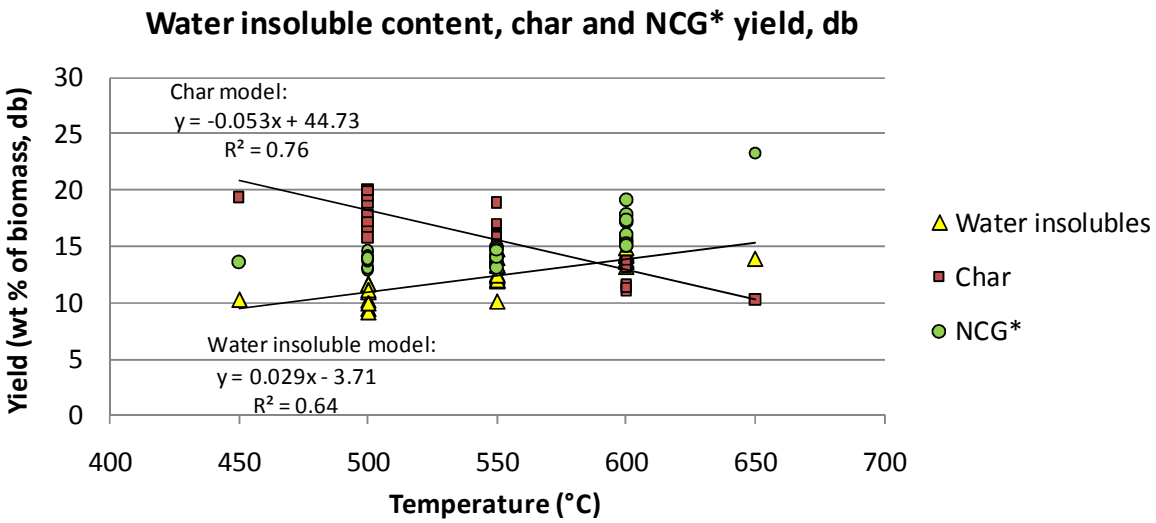

*NCG: non-condensable gas

Figure 34. Water insoluble content, char and non-condensable gas yield as a function of temperature

Figure 34 clearly indicates that bio-oil water insoluble content expressed as a fraction of the biomass input increases with temperature along with non-condensable gas yield while char yield decreases. The magnitude of the slope for the char yield model is slightly greater than the slope of the water insoluble content model indicating that the decrease in char yield is greater than the increase in water insoluble content over a given temperature range. The increasing yield of non-condensable gas with temperature likely makes up for this difference.

Presented a different way, one can see that bio-oil water insoluble content not only increases with temperature but that it increases with bio-oil organic liquid yield as indicated in Figure 35. In Figure 18, it was noted that the maximum organic liquid yield of 55.7 wt % occurred at a temperature of 600 °C. Therefore, it is evident that temperatures favorable for producing high bio-oil organic liquid yields correspond to conditions producing bio-oils with high water insoluble contents.

Though the bio-oil organic liquid yields from the highest (650°C) and lowest (450°C) temperature experiments are on the low end of the plot, the trend indicates that at high temperatures more lignin is converted to bio-oil water insolubles rather than dehydrating into char.

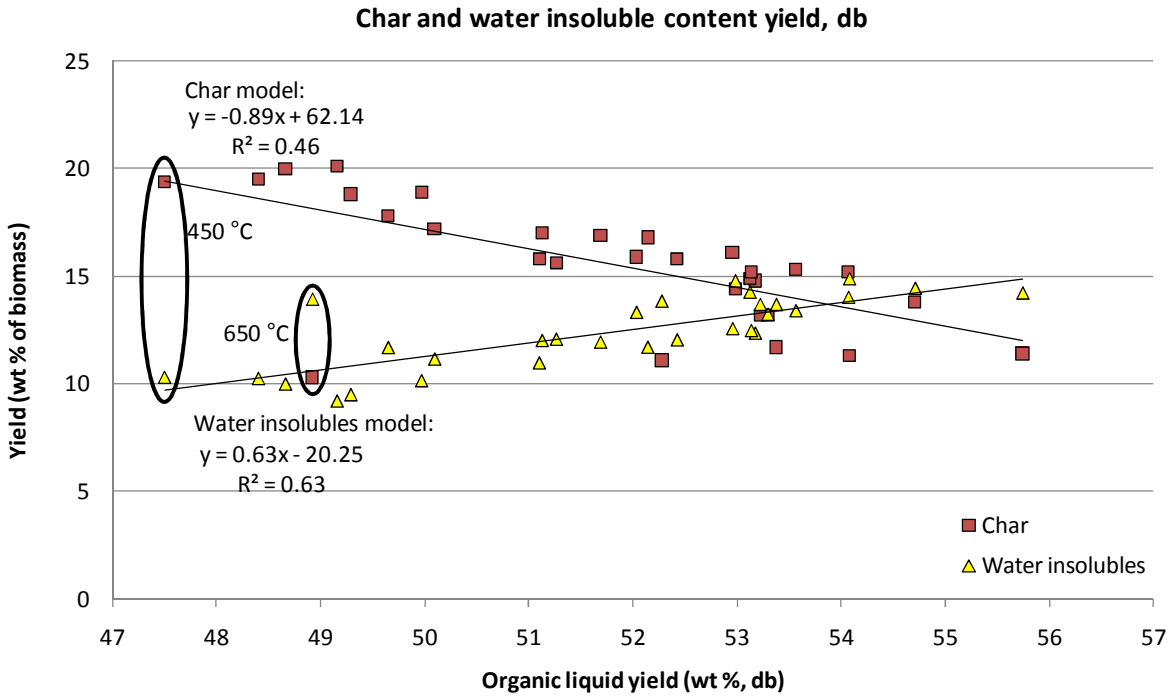

Figure 35. Bio-oil water insolubles and char yield with respect to organic liquid

5.5.1.3 Bio-oil Solids Content

The solids content was determined using the procedure in Appendix B. The solids content for stage fractions 1, 2 and 3was analyzed for all experiments. The solids content for the forth fraction however, was assumed to be the average of the fourth fraction in the 6 center point experiments or 0.77 wt %. Since the mass of the fourth stage fraction was small this amount often contributes less than 0.03 wt % to the whole bio-oil solids content.

The bio-oil solids content model was not significant and is not shown. Since the solids content is likely dependant on the biomass particle sized used, the average solids content is shown in Figure 36 for experiments using the same particle size. The figure indicates the results are not significant different from one another. The important thing to note is that the solids content is generally less than 1 wt %. This value is typically reported for bio-oils as noted in Table 14.

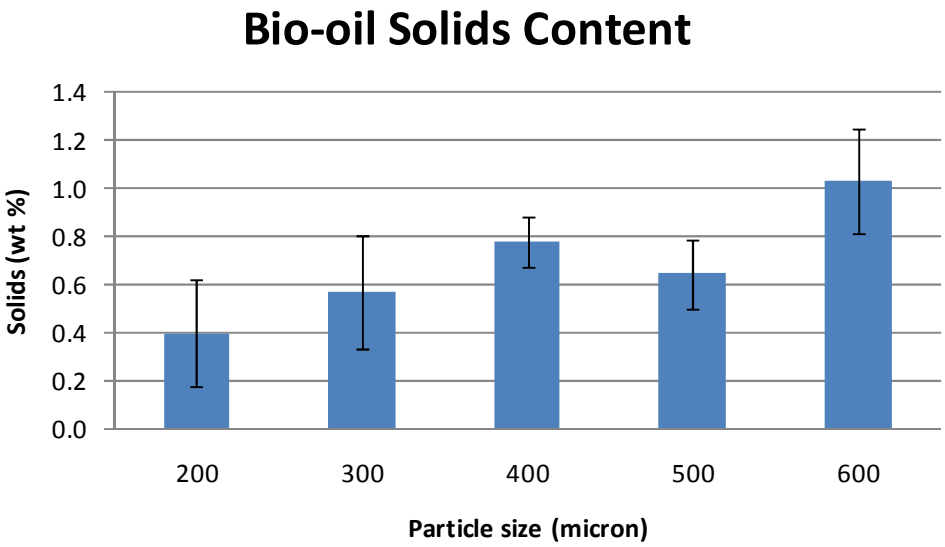

Figure 36. Bio-oil solids content with respect to particle size

5.5.1.4 Bio-oil Viscosity

Bio-oil fractions 1, 2 and 3 of the center point experiments were analyzed. The small quantity of stage fraction 4 did not permit any analysis yet it appeared water like in all cases. The resulting viscosity along with the bio-oil moisture content is reported in Table 15. Stage fraction 1and 3 clearly show a wide range of viscosities though the reactor operating conditions were consistent. None of the bio-oil viscosities fall within reported whole bio-oil viscosities ranging from 13-153 cSt when measured at 40 °C [75].

Table 15. Center point bio-oil viscosity, moisture and insoluble content

Stage Fraction	**SF1**		**SF2**		**SF3**			**SF4**	
Center point experiment	V[a] (cSt)	M[b] (wt %)	V (cSt)	M (wt %)	V (cSt)	M (wt %)	I[c] (wt %)	V -	M (wt %)
7-20090115A	223	12	4	43	703	13	37	water like	62
7-20090311A	937	6	5	41	470	13	29	water like	62
7-20090401A	177	13	4	42	632	12	31	water like	72
7-20090420A	910	8	5	42	735	12	34	water like	61
7-20090522A	285	11	4	43	469	13	30	water like	63
7-20090529A	538	8	4	42	417	13	31	water like	65

[a] Viscosity measured at 40 °C
[b] Moisture content
[c] Insoluble content

The wide range in viscosity can in part be explained by the corresponding moisture content of the bio-oil. As the moisture content increases, the viscosity decreases as shown in Figure 37 for stage fraction 1 center points. Stage fraction 3 is not as obviously linked to moisture content as this remained quite similar for all experiments. Instead, the range of viscosities may be depend on the quantity of water insolubles as this fraction is collected using an electrostatic precipitator.

The amount of water within the bio-oil is strongly linked to the temperature of the reactor as indicated in section 5.5.1.1 as well as the condenser temperature. Since the four bio-oil fractions are all collected at different temperatures each fraction condenses differing amounts of moisture and thus has a different viscosity. In order to collect uniform bio-oil fractions, the temperature of the condenser should be monitored and maintained at fixed conditions regardless of the reactor operating conditions.

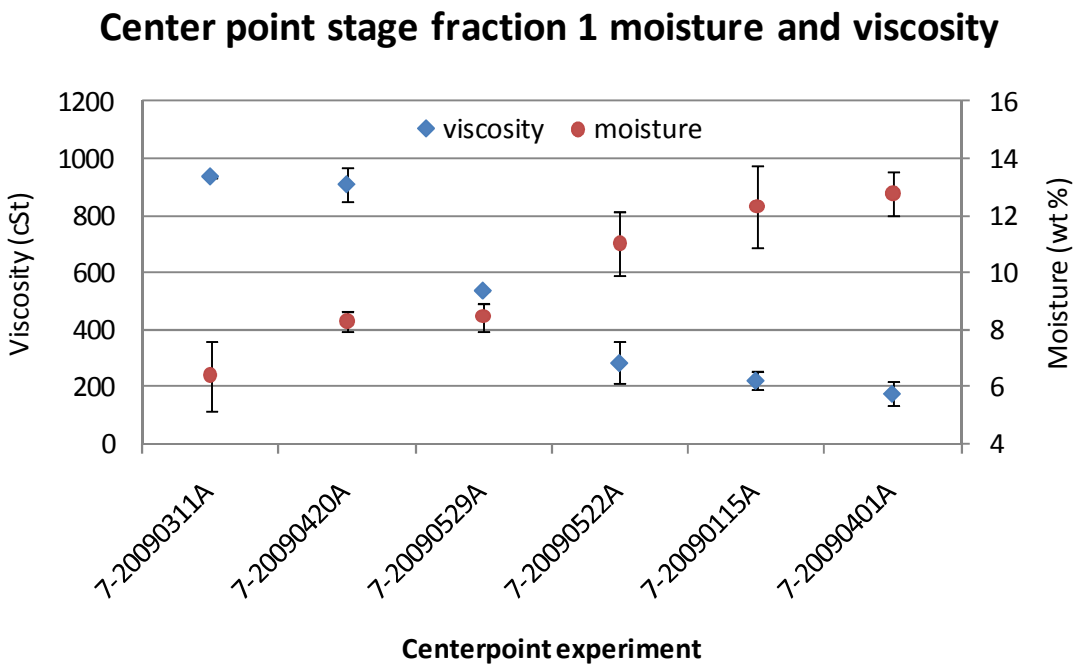

Figure 37. Center point stage fraction 1 viscosity and moisture content

5.5.1.5 Bio-oil Chemical Compounds

Chemical compounds within each bio-oil fraction were analyzed using GC/MS. The quantity of in each fraction was mathematically combined to find the total GC/MS

quantifiable portion of bio-oil. The 32 compounds identified and quantified are organized into seven groups as shown in Table 16.

Models generated from the chemical groups in Table 16 were insignificant and thus are not shown. Figure 38 shows the chemical groups quantified in bio-oil produced at temperatures 450 ˚C, 550 ˚C and 650 ˚C. The 95% confidence intervals in indicate that temperature though significant in many other bio-oil characteristics does not significantly affect the quantity of each chemical grouping within bio-oil.

The average quantity of each chemical group over all bio-oils is shown in Table 17. It is worth mentioning that between 35 – 40 wt % of typical bio-oils can be characterized and quantified using a GC/MS as noted by Oasmaa and Scholze [76, 77]. In this case, about 15 wt % of the bio-oils produced were quantified using GC/MS; though more chemicals were identified.

Table 16. GC/MS quantified compounds and groups within all bio-oil fractions

Acids	Guiacols
Acetic acid	Phenol, 2-methoxy-
Sugars	Phenol, 2-methoxy-4-methyl-
Levoglucosan	Phenol, 4-ethyl-2-methoxy-
Furans	Eugenol
2-Furancarboxaldehyde, 5-methyl-	Phenol, 2-methoxy-4-(1-propenyl)-, (E)-
Furfural	Vanillin
2-Furanmethanol	Syringols
2(5H)-Furanone, 3-methyl-	Phenol, 2,6-dimethoxy-
Phenols	4 methyl 2,6 dimethoxy phenol
Phenol	Ethanone, 1-(4-hydroxy-3,5-dimethoxyphen
Phenol, 2-methyl-	Other GC/MS quantified compounds
Phenol, 3-methyl-	2-Propanone, 1-hydroxy-
Phenol, 4-methyl-	2-Butanone, 3-hydroxy-
Phenol, 2-ethyl-	2-Cyclopenten-1-one, 2-methyl-
Phenol, 2,5-dimethyl-	2H-Pyran-2-one
2,4-Dimethylphenol	1,2-Cyclopentanedione, 3-methyl-
Phenol, 3-ethyl-	2-Furancarboxaldehyde, 5-(hydroxymethyl)
Phenol, 3,4-dimethyl-	Glycerin
Hydroquinone	

Table 17. Results from GC/MS analysis of whole bio-oils for all experiments

Group (wt %)	Average	St Dev	95% CI	Typical[a]
Acetic acid	3.27	1.18	0.42	0.1 - 1.8
Levoglucosan	2.13	1.11	0.40	0.4 - 1.4
Furans	0.76	0.10	0.04	0.3 - 0.58[b]
Phenols	0.65	0.07	0.03	2 – 5[c]
Guiacols	1.67	0.24	0.09	-
Syringols	2.80	0.46	0.17	-
Other	4.09	0.71	0.26	-
Total	15.37	-	-	~ 35

[a] Values reported by Girard and Diez unless otherwise stated [78]
[b] Recalculated from dry basis assuming 25 wt % moisture
[c] Values reported by Bridgwater et al [16]

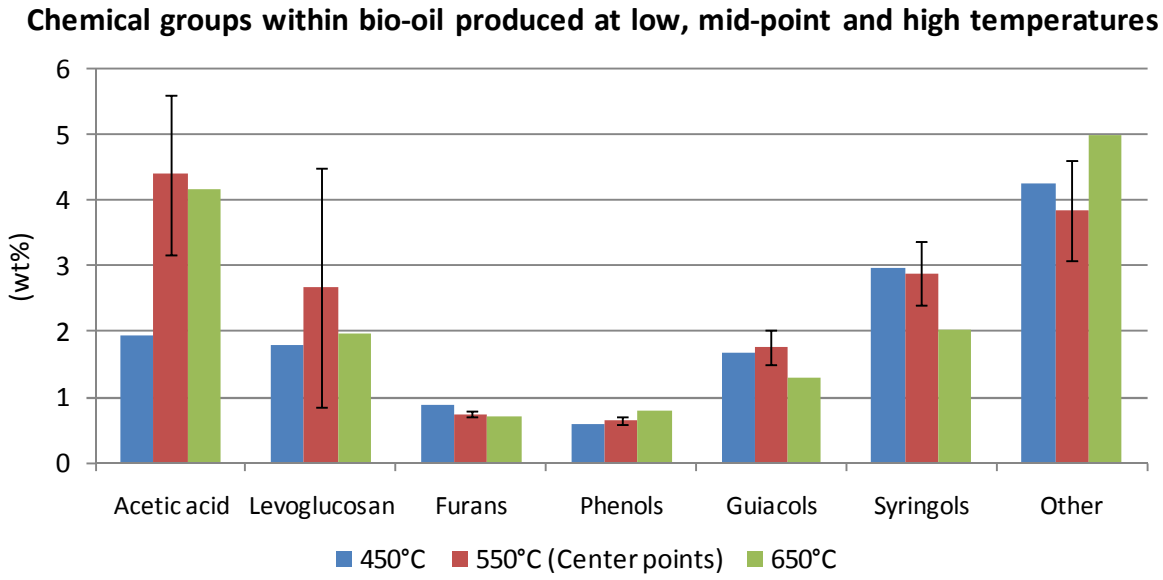

Figure 38. Chemical groupings within bio-oil produced at low, mid-point and high temperatures

Table 18 indicates the average amount of each chemical group present within the stage fraction for all 30 experiments. The weight distribution of chemical compounds among the stage fractions appears to be shifted towards the first condenser and trails off at the later. Since no apparent trends exist with respect to the reactor temperature, the distribution of chemical groups may be dependent upon the condenser temperature.

Table 18. Average GC/MS results for each stage fraction over all experiments

Group (wt %)	SF1	SF2	SF3	SF4
Acetic acid	1.31	1.33	0.57	0.06
Levoglucosan	1.18	0.46	0.50	-
Furans	0.41	0.20	0.13	0.01
Phenols	0.33	0.20	0.12	-
Guiacols	0.92	0.43	0.31	-
Syringols	1.61	0.64	0.54	0.01
Other	1.99	1.41	0.67	0.03
Total	7.76	4.66	2.85	0.10

5.5.1.6 Bio-oil Carbon Content

The carbon content of the bio-oil was determined using ASTM D5373 standard test method. The bio-oil carbon content reduced model is significant with a P-value less than 0.0001 and has an R^2 value of 0.67. Temperature and particle size are the only significant single terms with P-values less than 0.05. The only other significant term is interaction effect of temperature x particle size with a P-value of 0.034 as indicated in bio-oil carbon content model in Appendix D. The carbon content in the bio-oil increases with temperature shown in Figure 39.

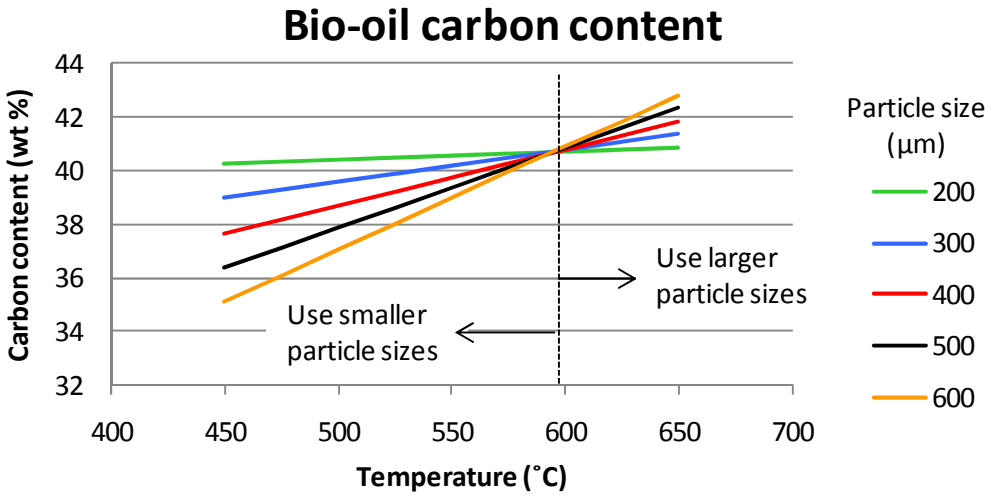

Fixed conditions: flow rate at 3 sL/min and feed rate at 1.5 kg/hr.

Figure 39. Bio-oil carbon content with respect to the operating conditions

At approximately 600 ˚C the bio-oil carbon content will be nearly the same no matter what particle size is chose. Below 600 ˚C, the bio-oil carbon content decreases as the biomass particle size increases from 200 – 600 micron. Above 600 ˚C the opposite occurs. As temperatures become greater than 570 ˚C bio-oil yields begin to decline. An overall carbon balance is discussed in section 5.5.3.1.

When the bio-oil carbon content is plotted on a dry bio-oil basis as in Figure 40, the effect of temperature is not nearly as profound. Again, since the relative carbon content is increasing with respect to temperature in Figure 39 another compound must be decreasing. As indicated in Figure 32, the moisture content of the bio-oil decreases with temperature and thus the oxygen content within the bio-oil is presumably decreasing. Therefore, when the bio-oil carbon content is plotted on a moisture free basis (ie. the carbon content is not relative to moisture) the increase in carbon content with temperature it is not nearly as pronounced.

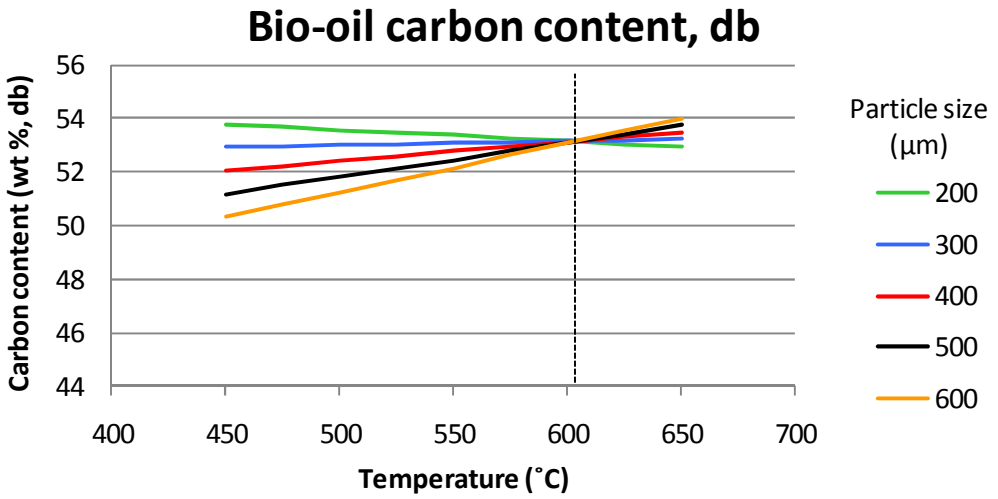

Fixed conditions: flow rate at 3 sL/min and feed rate at 1.5 kg/hr.

Figure 40. Bio-oil carbon content on a dry bio-oil basis

5.5.2 Char Characterization

Char samples were characterized by ultimate and proximate analysis and higher heating value. The results of the center point char samples are listed in Table 19 and compared with other oak wood char from an auger reactor operating at 450 °C.

Table 19. Center point char characteristics

	Char	Oak wood char[a]
HHV (MJ/kg)	30.68	31.06
Ultimate analysis (wt %)		
Carbon	78.17	82.83
Hydrogen	3.56	2.7
Nitrogen	0.13	0.31
Oxygen[b]	16.72	11.22
Sulfur	0.01	0.02
Proximate analysis (wt %)		
Ash	1.40	2.92
Moisture	3.51	3.17
Volatiles	26.91	15.58
Fixed Carbon	68.55	78.33

[a] Values from an auger reactor operating at 450 °C, Mohan [79]
[b] by difference

Proximate analysis of the char was determined using a Thermogravimetric Analyzer (TGA). The volatiles are determined by the difference in weight as the sample is heated from 100 ˚C to around 880 ˚C. Depending on the length of time at the various temperatures in the TGA, the fixed carbon and volatiles may change slightly. This may account for the difference in volatiles and fixed carbon.

5.5.2.1 Char Carbon Content

Temperature, particle size, flow rate and feed rate are all significant in the char carbon content model. Interactions between temperature and particle size as well as particle size and flow rate are also significant in the model. The reduced char carbon content model is listed in Equation 18 where x_1, x_2, x_3 and x_4 represent the coded temperature, particle size, flow rate and biomass feed rate, respectively.

$$Y_{biochar\ CC} = 77.04 + 0.65x_1 + 0.37x_2 + 0.28x_3 + 0.42x_4 + 0.46x_1x_2 + 0.55x_2x_3 \qquad \textbf{Equation 18.}$$

The interaction between temperature and particle size can be visualized in Figure 41. The char carbon content model is similar to the bio-oil model in that as the temperature is increased, the carbon content of the char also increases; with the exception of the 200 micron

particles. The same trend in the bio-oil carbon content model for increasing particle size is also evident in the char carbon content model; though the critical temperature is shifted down from around 600 ˚C to around 510 ˚C.

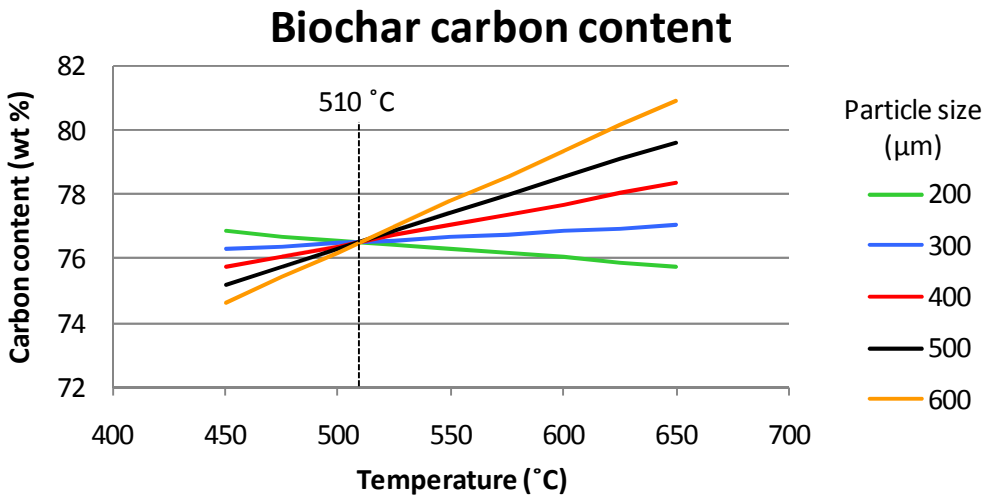

Figure 41. Char carbon content with respect to temperature and particle size

5.5.3 Non-condensable Gas Characterization

The non-condensable gas is primarily composed of carbon dioxide, carbon monoxide and methane as shown in Figure 42. Other gases include ethylene, ethane, hydrogen and oxygen. Trace amounts of acetylene and propane were occasionally detected though not shown. The system was purged with nitrogen before each experiment to remove oxygen and create an inert atmosphere. A vacuum pump regulated the pressure within the reactor and was maintained at 12 cm (5 inches) of water. The slightly positive pressure prevented oxygen from entering and in most experiments no oxygen was detected. Occasionally the vacuum pump would shift below atmospheric conditions and some oxygen would leak in as was the case in one of the center point experiments. The non-condensable gas yield model is given in section 5.4 in Equation 15.

The carbon monoxide content closely resembles the entire non-condensable gas yield as shown in Figure 20a and Figure 25. As temperatures comparable to low temperature gasification conditions are approached the carbon monoxide content becomes much greater.

The error on the carbon monoxide, carbon dioxide, methane and hydrogen yield is ± 0.35, 0.23, 0.05 and 0.01 wt %, respectively.

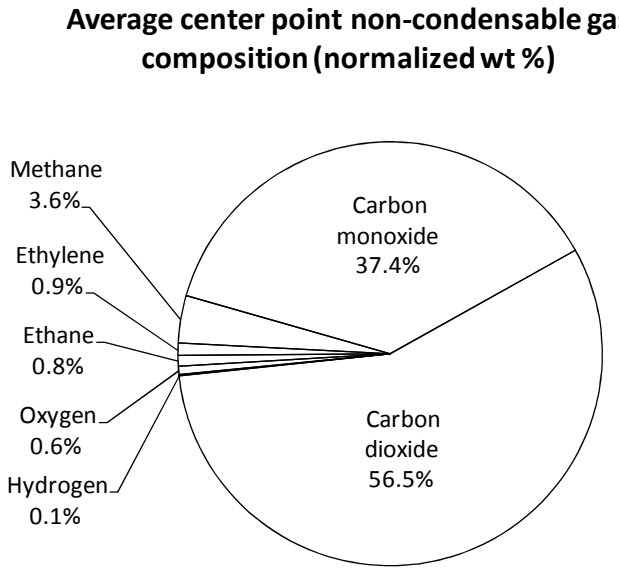

Figure 42. Average non-condensable gas composition from center points on a nitrogen free basis

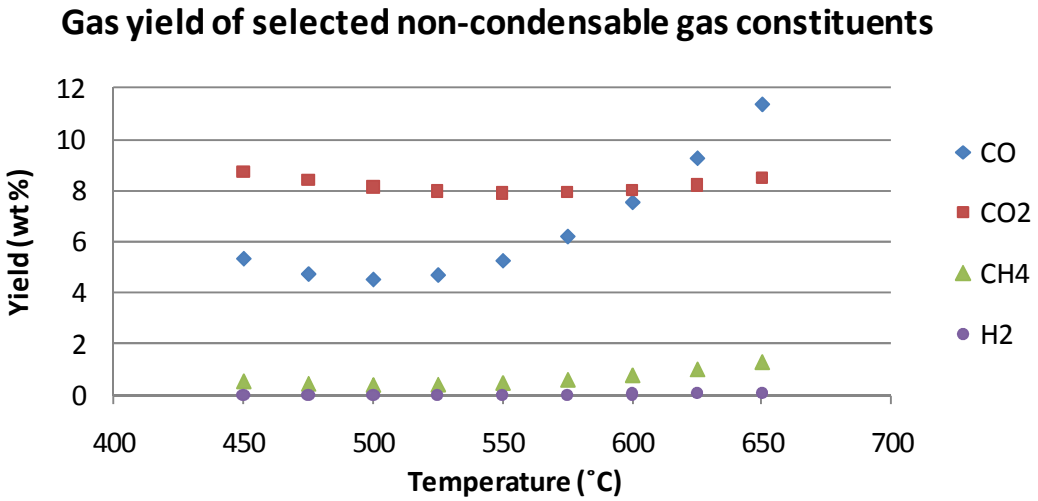

Fixed conditions: particle size at 400 micron, flow rate at 3 sL/min and feed rate at 1.5 kg/hr.

Figure 43. Gas yield of selected non-condensable gas constituents

5.5.3.1 Non-condensable Gas Carbon Content

The carbon content of the non-condensable gas is depicted in the model snapshot in Figure 44. The non-condensable gas yield follows a nearly identical trend. Temperature is

the most dominating factor, but particle size and feed rate are also significant. The interaction between temperature and particle size as well as that of particle size and flow rate is also significant. One might note that for bio-oil, char and non-condensable gas the carbon content increases with temperatures above 500 °C in all cases.

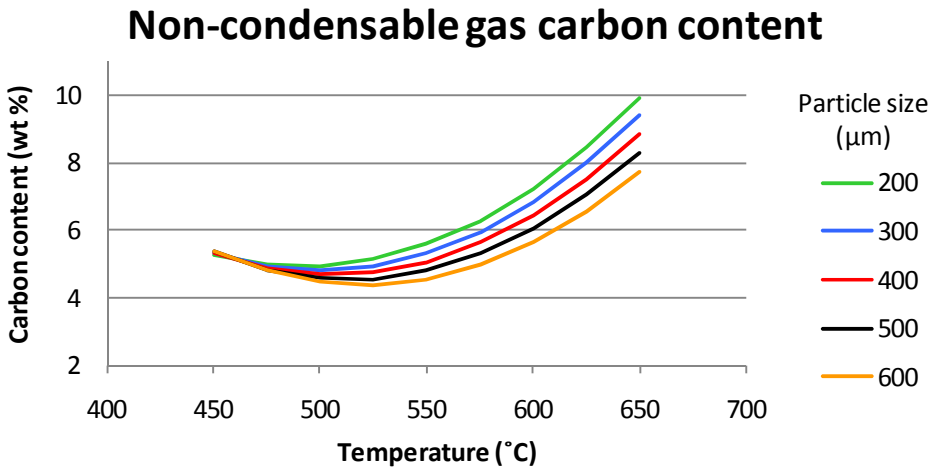

Fixed conditions: flow rate at 3 sL/min and feed rate at 1.5 kg/hr.

Figure 44. Non-condensable gas carbon content

Though the carbon content may increase the product the yield may decrease with increasing temperature. Thus a constant carbon balance can be maintained. Table 20 shows how the carbon content of each product can increase while maintaining a constant, total carbon yield. The table was produced using the product yield and carbon content models to calculate the carbon balance. The carbon out is the sum of the weighted average of the carbon within the respective products. The carbon content of the Red oak biomass is listed in Table 8 as 48.7± 3.56 wt %. This suggests that the overall carbon balance was roughly 92 wt % but may have been up to 100 wt %. The mass balance closure for the bio-oil, char and non-condensable gas models over the temperature range is always greater than 97 wt %. This is evidence that the product yield models account for temperature quite well.

It is noteworthy to mention that the maximum weighted bio-oil carbon content corresponds to the temperature (600 °C) where the maximum bio-oil yield was produced. Thus, conditions that favor maximum bio-oil yields correspond to conditions where bio-oil carbon content and bio-oil water insoluble content are at or near a maximum.

Table 20. Model mass balance and carbon closure[a]

Temp[b]	Yield (wt%)				Carbon content (wt%/wt%)			Weighted content (wt%)			Carbon Out
(°C)	Bio-oil	Char	NCG[c]	Total	Bio-oil	Char	NCG	Bio-oil	Char	NCG	(wt%)
450	64.42	20.03	14.89	99.34	37.14	75.90	37.08	23.92	15.20	5.52	44.65
500	67.93	18.35	13.36	99.64	38.43	76.67	37.17	26.11	14.07	4.97	45.14
550	69.48	16.02	14.03	99.53	39.56	77.37	37.58	27.49	12.39	5.27	45.15
600	69.07	13.05	16.92	99.04	40.51	77.97	38.31	27.98	10.17	6.48	44.64
650	66.70	9.43	22.00	98.14	41.30	78.49	39.35	27.55	7.40	8.66	43.61

[a] Fixed conditions: particle size at 400 μm, flow rate at 3 sL/min and feed rate at 1.5 kg/hr

[b] Temperature

[c] Non-condensable gas

CHAPTER 6: Conclusion

The free-fall fast pyrolysis reactor is a novel reactor type that employs radiant heat supplied by electrical heaters to convert raw, lignocellulosic biomass into bio-oil, char and non-condensable gases. The reactor is simple in design and operation yet the process of optimization is not trivial.

6.1. Experimental Conclusions

This work has successfully produced bio-oil from a novel free-fall reactor. Maximum bio-oil yields of 72 wt % were produced using small amounts of carrier gas and no heat carrier. The yield is comparable to traditional fast pyrolysis yields from a fluid bed reactor. Temperature and particle size were found to be the key factors in determining product yield and product characteristics. Though increasing flow rate would conceivably increase bio-oil yields by shortening the vapor residence time, its affect was determined not to be statistically significant.

Maximum bio-oil yields between 70 – 75 wt % will likely occur at temperatures around 575 °C, particle sizes just below 300 microns, nitrogen flow rates at 5 sL/min and feed rates at 2 kg/hr of sieved Red oak biomass.

A central composite design of experiments enabled the discovery of interaction affects between factors, specifically that of temperature and particle size. In general, higher operating temperatures lead to higher heating rates. The high heating rates are essential to fast pyrolysis in that secondary reactions are minimized because the particle is quickly vaporized. These parameters lend themselves to low moisture content and high carbon and water insoluble content bio-oils. Very high temperatures hinder bio-oil yields as the pyrolysis vapors are cracked into non-condensable gases. Char yield decreases at high temperatures but non-condensable gas yield increases. Smaller particle sizes are generally decomposed more quickly than larger particle sizes. Small particles allow for fast decomposition which minimizes opportunity for secondary reactions to occur within the particle creating secondary char. Using smaller biomass particle sizes results in higher bio-oil yield, lower char yield and higher non-condensable gas yield. Smaller particle sizes generally lower the bio-oil moisture content. Since both reactor temperature and biomass

particle size influence the same results, the interaction between the two should be considered when seeking to maximize or minimize product characteristics. The interaction between reactor temperature and particle size can be observed most clearly in the bio-oil moisture content, water insoluble content and carbon content models.

6.2. Validation of Free-fall Reactor

Evaluating the free-fall fast pyrolysis reactor by experimental operation, response surface methodology and product analysis provides a number of insights. Most notably, the free-fall reactor can in fact be utilized for the production of bio-oil and in so doing achieve competitive yields to that of the traditional fluidized bed. In addition, maximum bio-oil yields were found to be in agreement with bio-oil yields from other free-fall reactors operating at similar conditions as reported in literature. The reactor product characteristics were for the most part comparable to those cited elsewhere. Differences in the moisture content, higher heating value and viscosity may be due to the unique bio-oil collection system.

6.3. Future Opportunities

A few suggestions come to mind for the continued use of the free-fall reactor. First, alternatives to cyclone particulate removal may need to be used in conjunction with the free-fall reactor. One such possibility is the use of a swirl tube. Since the reactor was optimized using sieved Red oak biomass the use of un-sieved biomasses will negatively impact bio-oil yields and greatly increase the solids content within the bio-oil. It is necessary then to replace the current cyclone with a new heated particulate filtration device to achieve the same bio-oil characteristics as noted earlier. Second, a temperature controlled bio-oil collection system may improve and amplify some of the bio-oil characteristics that were found. Third, careful control of the biomass feed rate may improve the results of future experimental designs. And finally, a larger feeder or hopper along with a self unloading char catch will allow for increased operational time.

Performing fast pyrolysis with the reactor heating zones set to different temperatures or removing sections of the reactor to vary particle residence time may be interesting to

study. Completing fast pyrolysis experiments without any nitrogen carrier gas may prove that no carrier gas is needed. Additionally, running the system at the predicted optimum conditions would add validation to the design of experiments. Long term studies may include fast pyrolysis of pretreated and torrefied biomass as well as investigating the reactor as a fast torrefaction reactor.

References

1. Czernik, S. and A.V. Bridgwater, *Overview of Applications of Biomass Fast Pyrolysis Oil.* Energy & Fuels, 2004. **18**: p. 590-598.
2. Bridgwater, A.V. and G.V.C. Peacocke, *Fast pyrolysis processes for biomass.* Renewable and Sustainable Energy Reviews, 2000. **4**: p. 1-73.
3. Brown, R.C., *Biorenewable Resources: Engineering New Products from Agriculture*. 2003, Ames, Iowa: Iowa State Press.
4. Peterson, A.A., et al., *Thermochemical biofuel production in hydrothermal media: A review of sub- and supercritical water technologies.* Energy and Environmental Science, 2008. **1**: p. 32-65.
5. Bridgwater, A.V., *IEA Bioenergy 2006 Annual Report: Biomass Pyrolysis*. 2007. p. 4-19.
6. Mullaney, H., et al., *Technical, Environmental and Economic Feasibility of Bio-oil in New Hampshire's North County*. 2002, Universtiy of New Hampshire. p. 1-95.
7. Demirbas, A., *Biomass resource facilities and biomass conversion processing for fuels and chemicals.* Energy Conversion and Management, 2001. **42**: p. 1357-1378.
8. Meier, D. and O. Faix, *State of the art of applied fast pyrolysis of lignocellulosic materials -- a review.* Bioresource Technology, 1999. **68**: p. 71-77.
9. Bridgwater, A.V., *The production of biofuels and renewable chemicals by fast pyrolysis of biomass.* International Journal of Global Energy Issues, 2007. **27**: p. 160-203.
10. Bridgwater, A.V., *Principles and practice of biomass fast pyrolysis processes for liquids.* Journal of Analytical and Applied Pyrolysis, 1999. **51**: p. 3-22.
11. Mohan, D., C.U. Pittman, and P.H. Steele, *Pyrolysis of Wood/Biomass for Bio-oil: A Critical Review.* Energy and Fuels, 2006. **20**: p. 848-889.
12. Fahmi, R., et al., *The effect of lignin and inorganic species in biomass on pyrolysis oil yields, quality and stability.* Fuel, 2008. **87**: p. 1230-1240.
13. Oasmaa, A. and S. Czernik, *Fuel Oil Quality of Biomass Pyrolysis Oils State of the Art for the End Users.* Energy & Fuels, 1999. **13**: p. 914-921.
14. Raveendran, K., A. Ganesh, and K.C. Khilar, *Influence of mineral matter on biomass pyrolysis characteristics.* Fuel, 1995. **74**: p. 1812-1822.
15. Lee, K.-H., et al., *Influence of Reaction Temperature, Pretreatment, and a Char Removal System on the Production of Bio-oil from Rice Straw by Fast Pyrolysis, Using a Fluidized Bed.* Energy & Fuels, 2005. **19**: p. 2179-2184.
16. Bridgwater, A.V., S. Czernik, and J. Piskorz, *The Status of Biomass Fast Pyrolysis*, in *Fast Pyrolysis of Biomass: A Handbook*, A.V. Bridgwater, Editor. 2002, CPL Press Liberty House, The Enterprise Centre: Newbury, UK. p. 1-22.
17. Dynamotive. *BioOil Plus*. 2009 [cited; Available from: http://www.dynamotive.com/industrial-fuels/biooil-plus/].
18. Svoboda, K., et al., *Pretreatment and feeding of biomass for pressurized entrained flow gasification.* Fuel Processing Technology, 2009. **90**: p. 629-635.
19. Huber, G.W., S. Iborra, and C. Avelino, *Synthesis of Transportation Fuels from Biomass: Chemistry, Catalysts, and Engineering.* Chemical Reviews, 2006. **106**: p. 4044-4098.
20. Elliott, D.C., et al., *Developments in direct thermochemical liquefaction of biomass: 1983-1990.* Energy and Fuels, 1991. **5**: p. 399-410.

21. Bridgwater, A.V., *Renewable fuels and chemicals by thermal processing of biomass.* Chemical Engineering Journal, 2003. **91**: p. 87-102.
22. Radlein, D., *The Production of Chemicals From Fast Pyrolysis Bio-oils*, in *In Fast Pyrolysis of Biomass: A Handbook*, A.V. Bridgwater, Editor. 1999, CPL Press Liberty House, The Enterprise Centre. p. p. 164-188.
23. Scott, D.S., et al., *A second look at fast pyrolysis of biomass--the RTI process.* Journal of Analytical and Applied Pyrolysis, 1999. **51**: p. 23-37.
24. *NREL Turning Biomass into Adhesives and Plastics. NREL Technology Brief: Advances in Technology at the National Renewable Energy Laboratory (Fact sheet). (1994). 4 pp.; NREL Report No. MK-336-5819.* 1994.
25. Diebold, J.P. and J.W. Schahill, *Improvements in the Vortex Reactor Design*, in *Developments in Thermochemical Biomass Conversion*, A.V. Bridgwater and D.G.B. Boocock, Editors. 1997, Blackie Academic & Professional London. p. 242-252.
26. Czernik, S., J. Schahill, and J.P. Diebold, *The Production of Liquid Fuel by Fast Pyrolysis of Biomass.* Journal of Solar Energy Engineering, 1995. **117**: p. 2-6.
27. Lede, J., *The Cyclone: A Multifunctional Reactor for the Fast Pyrolysis of Biomass.* Industrial & Engineering Chemistry Research, 2000. **39**: p. 893-903.
28. BTG-BTL. *BTG-BTL.* 2008 [cited; Available from: http://www.btg-btl.com/index2.php.
29. Wagenaar, B.M., W. Prins, and W.P.M. van Swaaij, *Pyrolysis of biomass in the rotating cone reactor: modelling and experimental justification.* Chemical Engineering Science, 1994. **49**: p. 5109-5126.
30. Venderbosch, R.H., et al., *Pyrolysis of Palm Oil Residues in Malaysia*, in *PyNe Newsletter Issue 19*. 2006: Birmingham, UK.
31. Henrich, E., *Fast Pyrolysis of Biomass with a Twin Screw Reactor a First BTL Step*, in *PyNe Newsletter Issue 17*. 2004: Birmingham, UK.
32. Ingram, L., et al., *Pyrolysis of Wood and Bark in an Auger Reactor: Physical Properties and Chemical Analysis of the Produced Bio-oils.* Energy & Fuels, 2007. **22**: p. 614-625.
33. Badger, P.C. and P. Fransham, *Use of mobile fast pyrolysis plants to densify biomass and reduce biomass handling costs--A preliminary assessment.* Biomass and Bioenergy, 2006. **30**: p. 321-325.
34. Fransham, P., *Advances in Dry Distillation Technology*, in *PyNe Newsletter Issue 19*. 2006: Birmingham, UK.
35. Lee, J.G., et al., *Characteristics of entrained flow coal gasification in a drop tube reactor.* Fuel, 1996. **75**: p. 1035-1042.
36. Guo, R., J. Yang, and Z. Liu, *Behavior of trace elements during pyrolysis of coal in a simulated drop-tube reactor.* Fuel, 2004. **83**: p. 639-643.
37. Matsuoka, K., et al., *High-Pressure Coal Pyrolysis in a Drop Tube Furnace.* Energy and Fuels, 2003. **17**: p. 984-990.
38. Xu, W.C., et al., *High pressure hydropyrolysis of coals by using a continuous free-fall reactor.* Fuel, 2003. **82**: p. 677-685.
39. Karaduman, A., et al., *Flash pyrolysis of polystyrene wastes in a free-fall reactor under vacuum.* Journal of Analytical and Applied Pyrolysis, 2001. **60**: p. 179-186.
40. Mastral, J.F., C. Berrueco, and J. Ceamanos, *Pyrolysis of High-Density Polyethylene in Free-Fall Reactors in Series.* Energy and Fuels, 2006. **20**: p. 1365-1371.

41. Brown, A.L., et al., *Design and Characterization of an Entrained Flow Reactor for the Study of Biomass Pyrolysis Chemistry at High Heating Rates.* Energy and Fuels, 2001. **15**: p. 1276-1285.
42. Lehto, J., *Determination of kinetic parameters for Finnish milled peat using drop tube reactor and optical measurement techniques.* Fuel, 2007. **86**: p. 1656-1663.
43. Shuangning, X., Y. Weiming, and B. Li, *Flash pyrolysis of agricultural residues using a plasma heated laminar entrained flow reactor.* Biomass and Bioenergy, 2005. **29**: p. 135-141.
44. Yang, H., et al., *Pyrolysis of palm oil wastes for enhanced production of hydrogen rich gases.* Fuel Processing Technology, 2006. **87**: p. 935-942.
45. Zanzi, R., K. Sjöström, and E. Björnbom, *Rapid high-temperature pyrolysis of biomass in a free-fall reactor.* Fuel, 1996. **75**: p. 545-550.
46. Zhang, L., et al., *Co-pyrolysis of biomass and coal in a free fall reactor.* Fuel, 2007. **86**: p. 353-359.
47. Wei, L., et al., *Characteristics of fast pyrolysis of biomass in a free fall reactor.* Fuel Processing Technology, 2006. **87**: p. 863-871.
48. Onay, O. and O.M. Koçkar, *Pyrolysis of rapeseed in a free fall reactor for production of bio-oil.* Fuel, 2006. **85**: p. 1921-1928.
49. Li, S., et al., *Fast pyrolysis of biomass in free-fall reactor for hydrogen-rich gas.* Fuel Processing Technology, 2004. **85**: p. 1201-1211.
50. Zanzi, R., K. Sjöström, and E. Björnbom, *Rapid pyrolysis of agricultural residues at high temperature.* Biomass and Bioenergy, 2002. **23**: p. 357-366.
51. Kovac, R.J., et al., *Research on the Pyrolysis of Hardwood in an Entrained Bed Process Development Unit*. 1991, Georgia Institution of Technology: Atlanta, Georgia. p. 1-331.
52. Yu, Q., et al., *Temperature impact on the formation of tar from biomass pyrolysis in a free-fall reactor.* Journal of Analytical and Applied Pyrolysis, 1997. **40-41**: p. 481-489.
53. Yorgun, S., S. Sensöz, and Ö.M. Koçkar, *Flash pyrolysis of sunflower oil cake for production of liquid fuels.* Journal of Analytical and Applied Pyrolysis, 2001. **60**: p. 1-12.
54. Bohn, M.S. and C.B. Benham, *Biomass Pyrolysis with an Entrained Flow Reactor.* Industrial and Engineering Chemistry, Process Design and Development, 1984. **23**: p. 355-363.
55. Probstein, R.F. and R.E. Hicks, eds. *Synthetic Fuels*. 2006, Dover Publications, Inc.: New York. 280-291.
56. Piskorz, J., et al., *Fast pyrolysis of sweet sorghum and sweet sorghum bagasse.* Journal of Analytical and Applied Pyrolysis, 1998. **46**: p. 15-29.
57. Cengel, Y.A., *Heat Transfer: A Practical Approach*. 2nd ed. 2003, New York: McGraw-Hill.
58. Bailey, C. *Timber Thermal Properties*. [cited 2007; Available from: http://www.mace.manchester.ac.uk/project/research/structures/strucfire/materialInFire/Timber/thermalProperties.htm].
59. Kanury, A.M. and P.L. Blackshear Jr., *Some Considerations Pertaining to the Problem of Wood-Burning.* Combustion Science and Technology, 1970. **1**: p. 339-355.
60. Daugaard, D.E. and R.C. Brown, *Enthalpy for Pyrolysis for Several Types of Biomass.* Energy and Fuels, 2003. **17**: p. 934-939.

61. Scahill, J.W., J.P. Diebold, and C. Feik, *Removal of residual Char Fines from Pyrolysis Vapors by Hot Gas Filtration*, in *Developments in Themochemical Biomass Conversion Vol. 1*, A.V. Bridgwater and D.G.B. Boocock, Editors. 1997, Blackie Academic and Professional: London. p. 253-266.
62. Cooper, C.D. and F.C. Alley, *Cyclones*, in *Air Pollution Control: A Design Approach*. 1986, PWS Publisher: Boston, MA.
63. Hoffmann, A.C. and L.E. Stein, *Gas Cyclones and Swirl Tubes: Principles, Design and Operation*. 2nd ed. 2008, New York: Springer Berlin Heidelberg.
64. Horne, P.A. and P.T. Williams, *Influence of temperature on the products from the flash pyrolysis of biomass.* Fuel, 1996. **75**: p. 1051-1059.
65. Westerhout, R.J.M., et al., *Controlling the Water Content of Biomass Fast Pyrolysis Oil.* Industrial & Engineering Chemistry Research, 2007. **46**: p. 9238-9247.
66. Rekab, K. and M. Shaikh, *Statistical Design of Experiments with Engineering Applications*. 2005, Boca Raton, FL: CRC Press, Taylor & Francis Group.
67. Antal, J.M.J. and M. Gronli, *The Art, Science, and Technology of Charcoal Production.* Industrial & Engineering Chemistry Research, 2003. **42**.
68. Yang, H., et al., *Characteristics of hemicellulose, cellulose and lignin pyrolysis.* Fuel, 2007. **86**(12-13): p. 1781-1788.
69. Onay, O., *Fast and catalytic pyrolysis of pistacia khinjuk seed in a well-swept fixed bed reactor.* Fuel, 2007. **86**: p. 1452-1460.
70. Lede, J., et al., *The nature and properties of intermediate and unvaporized biomass pyrolysis materials: Intermediate liquid products of pyrolysis*, in *Developments in Thermochemical Biomass Conversion*, A.V. Bridgwater and D.G.B. Boocock, Editors. 1997, Blackie Academic & Professional London. p. 27-42.
71. Ba, T., et al., *Colloidal Properties of Bio-oils Obtained by Vacuum Pyrolysis of Softwood Bark. Characterization of Water-Soluble and Water-Insoluble Fractions.* Energy & Fuels, 2004. **18**(3): p. 704-712.
72. Piskorz, J., D.S. Scott, and D. Radlein. *Composition of Oils Obtained by Fast Pyrolysis of Different Woods*. in *Pyrolysis Oils from Biomass Producing, Analyzing and Upgrading*. 1988. Washington, DC: ACS Symposium Series.
73. Moens, L., et al., *Study of the Neutralization and Stabilization of a Mixed Hardwood Bio-Oil.* Energy & Fuels, 2009. **23**(5): p. 2695-2699.
74. Dupont, C., et al., *Biomass pyrolysis experiments in an analytical entrained flow reactor between 1073 K and 1273 K.* Fuel, 2008. **87**(7): p. 1155-1164.
75. Oasmaa, A., E. Kuoppala, and Y. Solantausta, *Fast Pyrolysis of Forestry Residue. 2. Physicochemical Composition of Product Liquid.* Energy & Fuels, 2003. **17**(2): p. 433-443.
76. Oasmaa, A. and D. Meier, *Analysis, Characterization and Test Methods of Fast Pyrolysis Liquids*, in *Fast Pyrolysis of Biomass: A Handbook*, A.V. Bridgwater, Editor. 2002, CPL Press Liberty House, The Enterprise Centre: Newbury, UK. p. 23-40.
77. Scholze, B. and D. Meier, *Characterization of the water-insoluble fraction from pyrolysis oil (pyrolytic lignin). Part I. PY-GC/MS, FTIR, and functional groups.* Journal of Analytical and Applied Pyrolysis, 2001. **60**(1): p. 41-54.
78. Girard, P. and C. Diez, *Environmental, Health and Safety Aspect Related to Fast Pyrolysis Oils - A Guideline to Notify a New Substance*, in *Fast Pyrolysis of Biomass: A*

Handbook, A.V. Bridgwater, Editor. 2002, CPL Press Liberty House, The Enterprise Centre: Newbury, UK. p. 69-84.
79. Mohan, D., et al., *Sorption of arsenic, cadmium, and lead by chars produced from fast pyrolysis of wood and bark during bio-oil production.* Journal of Colloid and Interface Science, 2007. **310**: p. 57-73.

Appendix A: Reactor design calculations

Heating rate for biomass particle as a function of wall temperature and particle density

Calculate the time required to heat a small particle from 25C to 450C:

Assume that biomass particles are solid spheres:

$D := 50\mu m, 60\mu m .. 1000\mu m$ diameter of particle

Biot number for biomass:

$L_c = \frac{V}{A_s}$ Characteristic length where V is the volume and A_s is the surface area.

$V(D) := \frac{1}{6}\pi \cdot D^3$ where D is the diameter of the particle

$A_s(D) := \pi D^2$

$L_c(D) := \frac{V(D)}{A_s(D)}$ $L_c(D) =$

	0
0	8.33
1	10
2	11.67
3	13.33
4	15

μm

$Bi = \frac{h \cdot L_c}{k}$ Biot number where h is the convection coefficient and k is the conduction coefficient.

Calculate h_rad:

$T_p := 25K + 273K$

$T_{wall} := (850 \;\; 950 \;\; 1050 \;\; 1150 \;\; 1250)K$ (assume a wall temperature minimum)

$\varepsilon := 1$ (assume emmisivity of one)

$\sigma := 5.67 \cdot 10^{-8} \frac{W}{m^2 \cdot K^4}$ (Stephan Boltzmann constant)

$\varepsilon_p := 1$ (assume blackbody radiation assumes veiw factor of 1)

$F_{p\_wall} := 0.7$ (view factor -see veiw factor calculations)

(radiation heat transfer between 2 surfaces: from 1 the *particle* to 2 the *surroundings*)

$$Q_{dot12} = \frac{\sigma \cdot \left(T_1^4 - T_2^4\right)}{\frac{1-\varepsilon_1}{A_1 \cdot \varepsilon_1} + \frac{1}{A_1 \cdot F_{12}} + \frac{1-\varepsilon_2}{A_2 \cdot \varepsilon_2}} = \frac{\sigma \cdot \left(T_2^2 + T_1^2\right)\left(T_2 + T_1\right)\left(T_1 - T_2\right)}{\frac{1-\varepsilon_1}{A_1 \cdot \varepsilon_1} + \frac{1}{A_1 \cdot F_{12}} + \frac{1-\varepsilon_2}{A_2 \cdot \varepsilon_2}} = W$$

$$q_{dot12} = \frac{\sigma\cdot\left(T_2^{\,2} + T_1^{\,2}\right)\left(T_2 + T_1\right)\left(T_1 - T_2\right)}{A_1\cdot\left(\frac{1-\varepsilon_1}{A_1\cdot\varepsilon_1} + \frac{1}{A_1\cdot F_{12}} + \frac{1-\varepsilon_2}{A_2\cdot\varepsilon_2}\right)} = \frac{\sigma\cdot\left(T_2^{\,2} + T_1^{\,2}\right)\left(T_2 + T_1\right)\left(T_1 - T_2\right)}{\frac{1-\varepsilon_1}{\varepsilon_1} + \frac{1}{F_{12}} + \frac{1-\varepsilon_2}{\varepsilon_2}\cdot\left(\frac{A_1}{A_2}\right)} = \frac{W}{m^2}$$

For a small object in a large cavity, we assume the following (p.628 Cengel):

$$\frac{A_1}{A_2} = 0 \qquad F_{12} := 1$$

Since F_{12} is not likely to equal 1 we leave it in the following equations.

$$q_{dot12} = \frac{\sigma\cdot\left(T_2^{\,2} + T_1^{\,2}\right)\left(T_2 + T_1\right)\left(T_1 - T_2\right)}{\frac{1}{\varepsilon_1} - 1 + \frac{1}{F_{12}} + \frac{1-\varepsilon_2}{\varepsilon_2}(0)} = \frac{\sigma\cdot\left(T_2^{\,2} + T_1^{\,2}\right)\left(T_2 + T_1\right)\left(T_1 - T_2\right)}{\frac{1}{\varepsilon_1} - 1 + \frac{1}{F_{12}}}$$

$$h_{rad} = \frac{Q_{dot12}}{A_s\cdot\left(T_s - T_{surr}\right)}$$

Therefore:

$$h_{rad} = \frac{\sigma\cdot\left(T_2^{\,2} + T_1^{\,2}\right)\left(T_2 + T_1\right)}{\frac{1}{\varepsilon_1} - 1 + \frac{1}{F_{12}}}$$

$$h_{rad}\left(T_{wall}\right) := \frac{\sigma\cdot\left(T_p^{\,2} + T_{wall}^{\,2}\right)\left(T_p + T_{wall}\right)}{\frac{1}{\varepsilon_p} - 1 + \frac{1}{F_{p\_wall}}}$$

(Cengel p. 628 -derived radiation due to convection without assuming view factor of 1.)

$$h_{rad}\left(T_{wall}\right) = \varepsilon\cdot\sigma\cdot\left(T_p^{\,2} + T_{wall}^{\,2}\right)\left(T_p + T_{wall}\right)$$

(Cengel, pg. 130)

$$h_{rad}\left(T_{wall_{0,0}}\right) = 36.97\,\frac{W}{m^2\cdot K}$$

which is greater than the assumed: $h_{conv} = 10\,\frac{W}{m^2\cdot K}$

Therefore use h_rad and neglect h_{conv} to be conservative.

Calculate the radiation heat transfer coefficient for each wall temperature.

Wall temp: 850K

$$h_{rad}\left(T_{wall_{0,0}}\right) = 36.97\frac{W}{m^2\cdot K}$$

Wall temp: 1050K

$$h_{rad}\left(T_{wall_{0,2}}\right) = 63.74\frac{W}{m^2\cdot K}$$

Wall temp: 1250K

$$h_{rad}\left(T_{wall_{0,4}}\right) = 101.46\frac{W}{m^2\cdot K}$$

Wall temp: 950K

$$h_{rad}\left(T_{wall_{0,1}}\right) = 49.1\frac{W}{m^2\cdot K}$$

Wall temp: 1150K

$$h_{rad}\left(T_{wall_{0,3}}\right) = 81.11\frac{W}{m^2\cdot K}$$

$k_{biomass} := 0.10\frac{W}{m\cdot K}$ (thermal condutivity of softwood)

$Bi(D, T_{wall}) := \frac{h_{rad}(T_{wall})\cdot L_c(D)}{k_{biomass}}$ (Biot number)

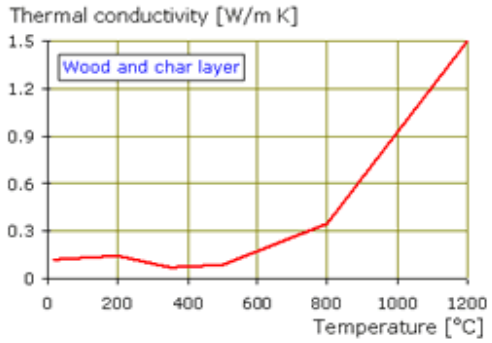

Conduction coefficient of softwood at about 500C.
http://www.mace.manchester.ac.uk/project/research/structures/strucfire/materialInFire/Timber/thermalProperties.htm

Calculate the Biot number for different wall temperatures:

$Bi\left(D, T_{wall_{0,0}}\right) =$

	0
0	3.081·10-3
1	3.697·10-3
2	4.313·10-3
3	4.929·10-3
4	5.545·10-3
5	6.161·10-3
6	6.777·10-3
7	7.393·10-3
8	8.009·10-3
9	8.625·10-3

Bi<0.1 for entire range

$Bi\left(D, T_{wall_{0,1}}\right) =$

	0
0	4.092·10-3
1	4.91·10-3
2	5.729·10-3
3	6.547·10-3
4	7.365·10-3
5	8.184·10-3
6	9.002·10-3
7	9.82·10-3
8	0.011
9	0.011

Bi<0.1 @ ≤850micron

$Bi\left(D, T_{wall_{0,2}}\right) =$

	0
0	5.311·10-3
1	6.374·10-3
2	7.436·10-3
3	8.498·10-3
4	9.561·10-3
5	0.011
6	0.012
7	0.013
8	0.014
9	0.015

Bi<0.1 @ ≤650micron

$Bi\left(D, T_{wall_{0,3}}\right)$ =

	0
0	6.759·10-3
1	8.111·10-3
2	9.463·10-3
3	0.011
4	0.012
5	0.014
6	0.015
7	0.016
8	0.018
9	0.019

$Bi\left(D, T_{wall_{0,4}}\right)$ =

	0
0	8.455·10-3
1	0.01
2	0.012
3	0.014
4	0.015
5	0.017
6	0.019
7	0.02
8	0.022
9	0.024

Bi<0.1 @ ≤510micron Bi<0.1 @ ≤410micron

To assume lumped capacitance analysis: $Bi \le 0.1$

Therefore lumped capacitance can be assumed at the conditions given for the respective particle sizes.

Calculate the time required to heat a particle to 500C using the lumped system analysis:

$T_o := 500K + 273.15K$ final temp of particle

$T_{wall} := T_{wall}$ temp of surroundings

$T_i := 25K + 273.15K$ initial temp of particle

$\rho := (450 \;\; 525 \;\; 600 \;\; 880 \;\; 1350)\frac{kg}{m^3}$ (density of various biomasses)

Some considerations Pertaining to the Problem of Wood Burning, Kanury and Blackshear, 1970 p. 346

$C_p := 2.273\frac{kJ}{kg \cdot K}$ (specific heat capacity of biomass)

Computational calorimetric investigation of the reactions during thermal conversion of wood biomass, Strezov et al. Biomass and Bioenergy 27 (2004) p. 5

$b\left(D, T_{wall}, \rho\right) := \frac{h_{rad}\left(T_{wall}\right) \cdot A_s(D)}{\rho \cdot V(D) \cdot C_p}$ (inverse time constant Cengel, p. 210)

$\frac{T_o - T_{wall}}{T_i - T_{wall}} = e^{-b(D) \cdot t}$ (derivation from energy balance of a solid over a finite time interval, Cengel, p. 211)

$$t\left(D, T_{wall}, \rho\right) := \frac{\ln\left(\frac{T_o - T_{wall}}{T_i - T_{wall}}\right)}{-b\left(D, T_{wall}, \rho\right)}$$

(rearanging and solving for t provides the equation on the left)

Solve for the time, t, required to heat a particle to 500C as a function of the wall temperature:

Particle Diameter

$D =$

	0
0	50
1	60
2	70
3	80
4	90
5	100

μm

Wall temp: 850K(576C)
Bi<0.1 for entire range

$t\left(D, T_{wall_{0,0}}, \rho_{0,4}\right) =$

	0
0	1.364
1	1.636
2	1.909
3	2.182
4	2.455
5	2.727

s

Wall temp: 950K(676C)
Bi<0.1 @ ≤850micron

$t\left(D, T_{wall_{0,1}}, \rho_{0,4}\right) =$

	0
0	0.679
1	0.815
2	0.951
3	1.087
4	1.223
5	1.359

s

Wall temp: 1050K(776C)
Bi<0.1 @ ≤650micron

$t\left(D, T_{wall_{0,2}}, \rho_{0,4}\right) =$

	0
0	0.401
1	0.481
2	0.561
3	0.641
4	0.721
5	0.802

s

Wall temp: 1150K(876C)
Bi<0.1 @ ≤510micron

$t\left(D, T_{wall_{0,3}}, \rho_{0,4}\right) =$

	0
0	0.257
1	0.309
2	0.36
3	0.411
4	0.463
5	0.514

s

Wall temp: 1250K(976C)
Bi<0.1 @ ≤410micron

$t\left(D, T_{wall_{0,4}}, \rho_{0,4}\right) =$

	0
0	0.174
1	0.209
2	0.244
3	0.279
4	0.314
5	0.348

s

Plot the results for various wall temperatures and biomass densities.

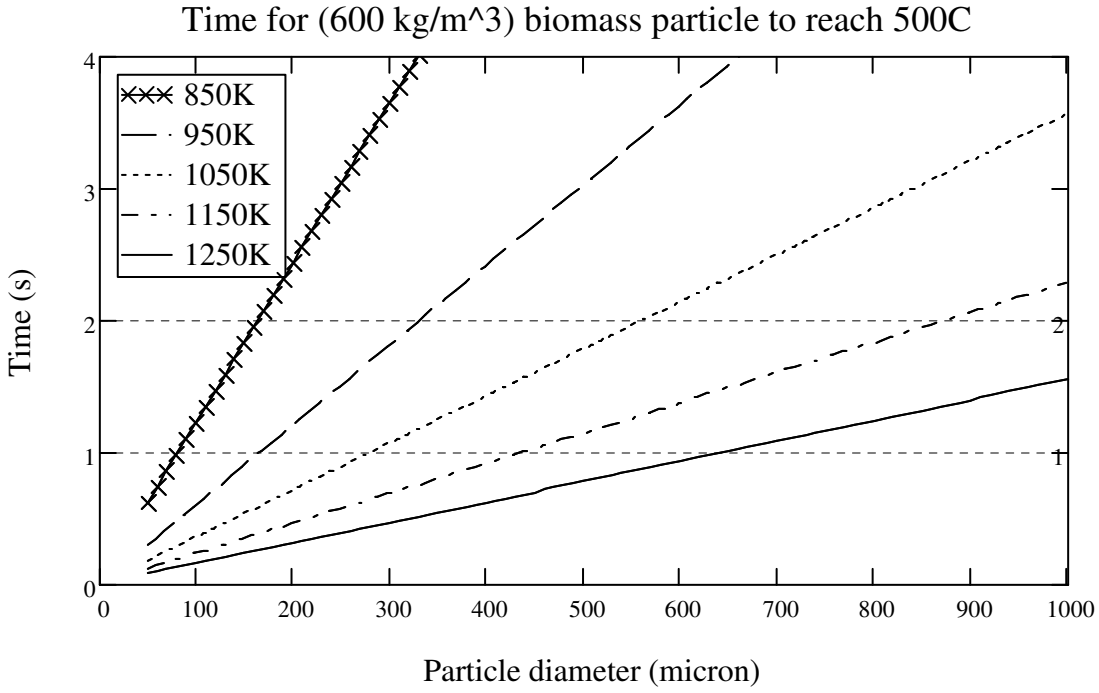

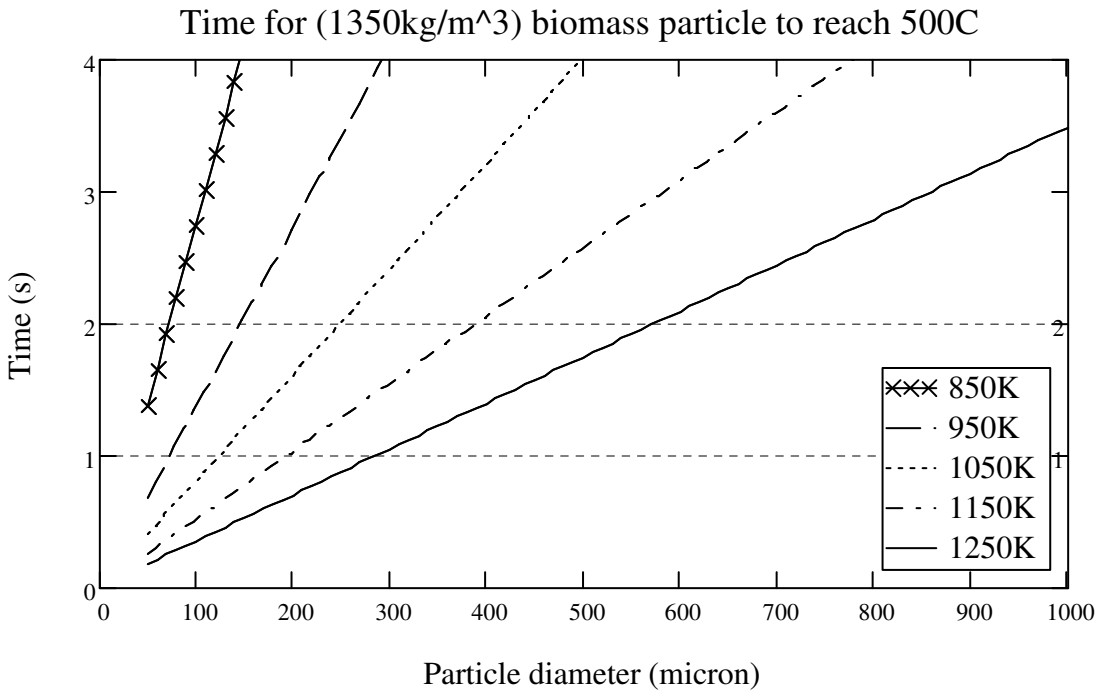

Determine the terminal velocity of a range of particle sizes

Calculate the terminal/settling velocity of a small particle using Stokes' Law:

$$u_t = \sqrt{\frac{4 \cdot g \cdot 2 \cdot r_o \cdot (\rho_p - \rho_f)}{3 \cdot \rho_f \cdot C_D}}$$ (0.1 < Re < 1000) See Perry's Chemical Engineers' Handbook, 7th ed. 1997. (terminal and settling velocity p. 6-50)

where:
u_t is the particle settling velocity
r is the Stokes radius
g is gravity
ρ_p is density of the particle
ρ_f is the density of the fluid
η is the fluid viscosity and
C_D is the drag coefficient

$$Re(r_o) = \frac{\rho_f \cdot (2 \cdot r_o) \cdot v_t(r_o)}{\mu}$$ (Reynolds number, function of particle diameter and terminal velocity)

$$C_D(r_o) = \left(\frac{24}{Re(r_o)}\right)\left(1 + 0.14 \cdot Re(r_o)^{0.70}\right)$$ (Coefficient of drag, function of Reynolds number)

$$u_t = \sqrt{\frac{4 \cdot g \cdot 2 \cdot r_o \cdot (\rho_p - \rho_f)}{3 \cdot \rho_f \cdot C_D}}$$ (terminal velocity; insert Reynolds number into coefficient of drag and insert coefficient of drag into terminal velocity equation - see below) (0.1 < Re < 1000)

$r_o := 100\text{micron}, 200\text{micron}.. 1000\text{micron}$ (outer radius of particle)

Range of densities used to determine terminal velocity:

$\rho_{char} := 450 \frac{kg}{m^3}$ (bulk density of char)

$\rho_{wood} := 525 \frac{kg}{m^3}$ (density of wood at 300K; assumed constant as heated: Cengel, Table A-8, pg. 867)

$\rho_p := 600 \frac{kg}{m^3}$ (density of wood, Kanury and Blackshear, 1970 pg. 346)

$\rho_{pelletizedconrnstover} := 880 \frac{kg}{m^3}$ (density of cornstover, Kaliyan and Morey, 2005 pg. 6)

$\rho_{coal} := 1350 \frac{kg}{m^3}$ (density of coal at 300K, Cengel, Table A-8, pg. 867)

Fluid properties:

$\rho_f := 0.4880 \frac{kg}{m^3}$ (density of fluid (air) at 450C -less dense than pyrolysis vapors therefore particle will have a higher ψ)

$\mu := 3.415\,10^{-5} \frac{kg}{m \cdot s}$ (dynamic viscosity of air at 450C)

Use a solve block to iterate the value of the terminal velocity:

Guess $u_t := 3 \cdot \frac{m}{s}$ (enter a guess value for the terminal velocity)

Given

$r_o := \frac{300}{2} micron$ (enter **radius** of particle)

$$u_t = \sqrt{\frac{4 \cdot g \cdot 2 \cdot r_o \cdot (\rho_{coal} - \rho_f)}{3 \cdot \rho_f \left[\left[\frac{24}{\frac{\rho_f \cdot (2 \cdot r_o) \cdot u_t}{\mu}}\right]\left[1 + 0.14\left[\frac{\rho_f \cdot (2 \cdot r_o) \cdot u_t}{\mu}\right]^{0.70}\right]\right]}}$$

$T_{vpart} := Find(u_t)$

$T_{vpart} = 1.3177 \frac{m}{s}$ $T_{vpart} = 4.3233 \frac{ft}{s}$ (calculate terminal velocity)

Coefficient of Drag:
(used to find velocity and free-fall distance as a function of time)

$v_t(r_o) := T_{vpart}$

$Re(r_o) := \frac{\rho_f \cdot (2 \cdot r_o) \cdot v_t(r_o)}{\mu}$

$C_D(r_o) := \left(\frac{24}{Re(r_o)}\right)\left(1 + 0.14 \cdot Re(r_o)^{0.70}\right)$

$C_D(r_o) = 6.247$

Terminal velocities of particles ranging from 100 to 1000 um in diameter for various densities:

Density of char:
450 kg/m^3

$$T_{v450} := \begin{pmatrix} 0.0698 \\ 0.1517 \\ 0.2577 \\ 0.3818 \\ 0.5185 \\ 0.6634 \\ 0.8135 \\ 0.9663 \\ 1.1202 \\ 1.2743 \\ 1.4277 \\ 1.5799 \\ 1.7307 \\ 1.8799 \\ 2.0274 \\ 2.1732 \\ 2.3171 \\ 2.4593 \\ 2.5998 \end{pmatrix} \frac{m}{s}$$

Density of wood:
525 kg/m^3

$$T_{v525} := \begin{pmatrix} 0.0812 \\ 0.1758 \\ 0.2975 \\ 0.4388 \\ 0.5934 \\ 0.7563 \\ 0.9241 \\ 1.0942 \\ 1.265 \\ 1.4354 \\ 1.6047 \\ 1.7724 \\ 1.9383 \\ 2.1022 \\ 2.2641 \\ 2.4239 \\ 2.5817 \\ 2.7375 \\ 2.8913 \end{pmatrix} \frac{m}{s}$$

Density of wood:
600 kg/m^3

$$T_{v600} := \begin{pmatrix} 0.0925 \\ 0.1998 \\ 0.3367 \\ 0.4946 \\ 0.6663 \\ 0.8463 \\ 1.0308 \\ 1.2173 \\ 1.4039 \\ 1.5897 \\ 1.7739 \\ 1.9561 \\ 2.1362 \\ 2.3139 \\ 2.4893 \\ 2.6623 \\ 2.8330 \\ 3.0015 \\ 3.1678 \end{pmatrix} \frac{m}{s}$$

Density of cornstover:
880 kg/m^3

$$T_{v880} := \begin{pmatrix} 0.1344 \\ 0.2871 \\ 0.478 \\ 0.6937 \\ 0.9239 \\ 1.1616 \\ 1.4023 \\ 1.6431 \\ 1.8824 \\ 2.1192 \\ 2.3529 \\ 2.5833 \\ 2.8102 \\ 3.0337 \\ 3.2538 \\ 3.4706 \\ 3.6843 \\ 3.895 \\ 4.1028 \end{pmatrix} \frac{m}{s}$$

Density of charcoal:
1350 kg/m^3

$$T_{v1350} := \begin{pmatrix} 0.2033 \\ 0.428 \\ 0.7014 \\ 1.0027 \\ 1.3177 \\ 1.6379 \\ 1.9581 \\ 2.2755 \\ 2.5887 \\ 2.8969 \\ 3.1999 \\ 3.4975 \\ 3.79 \\ 4.0775 \\ 4.3603 \\ 4.6385 \\ 4.9125 \\ 5.1824 \\ 5.4485 \end{pmatrix} \frac{m}{s}$$

Diameter of particle:

$$D_p := \begin{pmatrix} 100 \\ 150 \\ 200 \\ 250 \\ 300 \\ 350 \\ 400 \\ 450 \\ 500 \\ 550 \\ 600 \\ 650 \\ 700 \\ 750 \\ 800 \\ 850 \\ 900 \\ 950 \\ 1000 \\ 1050 \end{pmatrix} \text{micron}$$

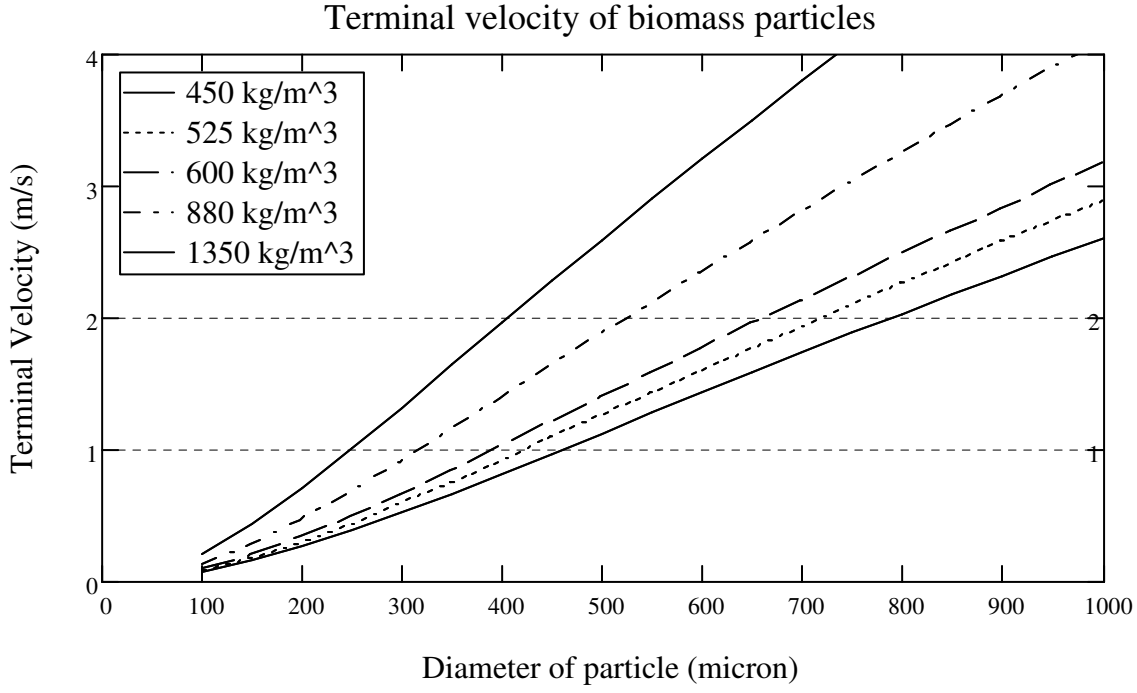

Calculation of velocity and free-fall length with respect to time using Euler's method

Define the differential equation:

$$F = m \cdot a = m \cdot \left(\frac{d}{dt} v \right) = F_B + F_D - F_g$$ (force balance on particle)

$$F_B = \rho_f \cdot g \cdot V_p$$ (bouyant force)

$$F_D = \frac{1}{2} C_D \cdot \rho_f \cdot A_c \cdot v^2$$ (drag force)

$$F_g = M \cdot g$$ (gravitational force)

$$M \cdot \left(\frac{d}{dt} v \right) = \rho_f \cdot g \cdot V_p + \frac{1}{2} C_D \cdot \rho_f \cdot A_c \cdot v^2 - M \cdot g$$

$$\frac{\Delta v}{\Delta t} = \frac{\rho_f \cdot g \cdot V_p}{M} - g + \frac{C_D \cdot \rho_f \cdot A_c}{2 \cdot M} \cdot v^2$$ (differential equation)

Define particle and fluid properties:

$\Delta t := .005$ (delta t is the step size "s")

$\rho_f := 0.4880$ (density of air at 450C "kg/m 3")

$\mu := 3.415 \cdot 10^{-5}$ (dynamic viscosity of air at 450C "kg/m*s)

$D_p := 300$ (particle diameter "micron")

$r_o := \frac{D_p \cdot 10^{-6}}{2}$ $\quad r_o = 1.5 \times 10^{-4}$ (radius of particle "m")

$\rho_p := 1350$ (density of particle "kg/m 3")

$A_c := \pi \cdot r_o^2$ $\quad A_c = 7.069 \times 10^{-8}$ (cross sectional area of particle "m 2")

$V_p := \frac{4}{3} \cdot \pi \cdot r_o^3$ $\quad V_p = 1.414 \times 10^{-11}$ (volume of particle "m 3")

$Mass := \rho_p \cdot V_p$ $\quad Mass = 1.909 \times 10^{-8}$ (mass of particle "kg")

$grav := 9.81$ (gravity "m/s 2")

$v_t := 1.3177$ (define terminal velocity from previous calculations based on particle size and density "m/s")

$Re(r_o) := \frac{\rho_f \cdot (2 \cdot r_o) \cdot v_t}{\mu}$ (Reynolds number)

$C_D(r_o) := \left(\frac{24}{Re(r_o)}\right)\left(1 + 0.14 \cdot Re(r_o)^{0.70}\right)$ (Coefficient of drag on particle)

$C_D(r_o) = 6.247$ (calculate the drag coefficient)

$h(\Delta t) := \Delta t$ (elapsed time in seconds)

$vel(v) := -1\left(\frac{\rho_f \cdot grav \cdot V_p}{Mass} - grav + \frac{C_D(r_o) \cdot \rho_f \cdot A_c}{2 \cdot Mass} \cdot v^2\right)$ (velocity at elepsed time)

$t_0 := 0s$ (initial conditions for time)

$v_0 := 0\frac{m}{s}$ (initial conditions for velocity)

$x_0 := 0m$ (initial conditions for distance)

$num := 500$ (number of iterations desired)

Calculate the velocity and free-fall distance using Euler's method:

$Mat(iter) :=$ | $k \leftarrow 1$
| $M_{0,0} \leftarrow t_0$
| $M_{0,1} \leftarrow v_0$
| $M_{0,2} \leftarrow x_0$
| for $i \in 1, 2 .. iter$
| $M_{k,0} \leftarrow M_{k-1,0} + h(\Delta t)$ time
| $M_{k,1} \leftarrow M_{k-1,1} + vel(M_{k-1,1})\,\Delta t$ velocity
| $M_{k,2} \leftarrow M_{k-1,2} + M_{k,1} \cdot \Delta t$ length
| $k \leftarrow k + 1$
| M

Table of values using Euler's method:

time (s) velocity (m/s) length (m)

Mat (num) =

	0	1	2
0	0	0	0
1	$5 \cdot 10^{-3}$	0.049032269	$2.451613467 \cdot 10^{-4}$
2	0.01	0.097996673	$7.351447103 \cdot 10^{-4}$
3	0.015	0.146757854	$1.46893398 \cdot 10^{-3}$
4	0.02	0.195182141	$2.444844687 \cdot 10^{-3}$
5	0.025	0.243139016	$3.660539765 \cdot 10^{-3}$
6	0.03	0.290502512	$5.113052325 \cdot 10^{-3}$
7	0.035	0.33715253	$6.798814973 \cdot 10^{-3}$
8	0.04	0.382976013	$8.713695037 \cdot 10^{-3}$
9	0.045	0.427867989	0.010853035
10	0.05	0.471732437	0.013211697
11	0.055	0.514482975	0.015784112
12	0.06	0.556043364	0.018564329
13	0.065	0.596347824	0.021546068
14	0.07	0.635341169	0.024722774
15	0.075	0.672978765	0.028087668

Plot the velocity and the free-fall distance over time:

$j := 0, 1 .. num$

$t_j := 0 + j \cdot \Delta t$ $vel_j := Mat(num)_{j,1}$ $dist_j := Mat(num)_{j,2}$

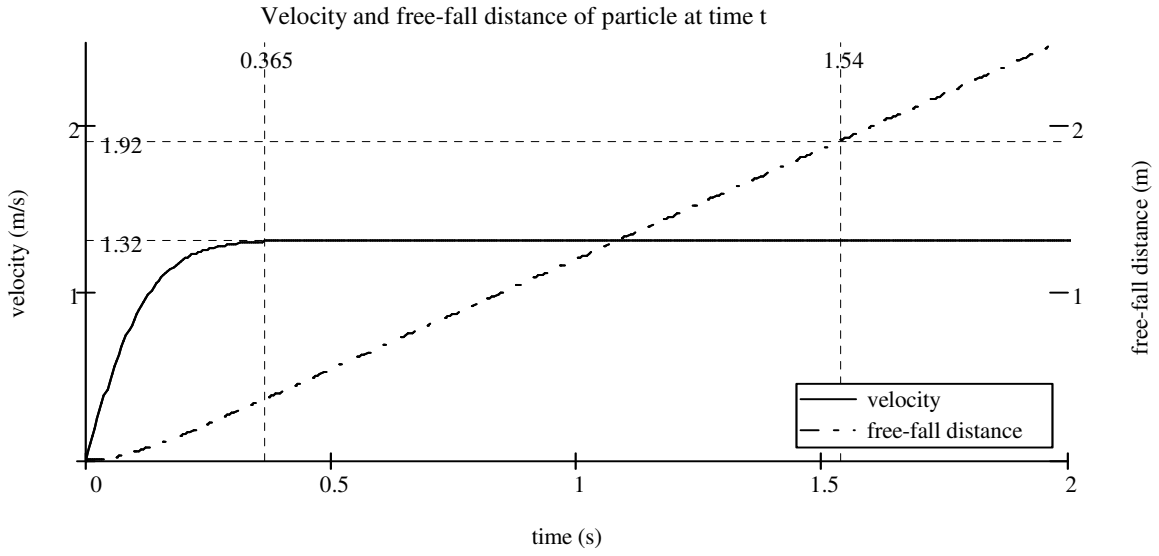

Heat required to vaporize biomass and heat carrier gas to 500C:

Reactor dimensions:

$D_{id} := 0.824in$

$L_{pipe} := 6ft$

$A_{sid} := \pi \cdot D_{id} \cdot L_{pipe}$

$kmol := 1000mol$

$kJ := 1000J$

$MJ := 10^6 J$

Operating temperature: 500C

$T_{in} := 25K + 273.15K$

$T_{out} := 500K + 273.15K$

$T_{ave} := \frac{T_{in} + T_{out}}{2}$ $T_{ave} = 262.5°C$ (Find properties at this temp.)

Properties of biomass:

$MW_{biomass} := 23.02\frac{gm}{mol}$

$MW_{biooil} := 88\frac{kg}{kmol}$

$C_{pbiomass} := 2.273\frac{kJ}{kg \cdot K}$

$h_{pcornstover} := 1.53\frac{MJ}{kg}$ (Daugaard and Brown 2003: heat of pyrolysis)

Properties of N2:

$\rho_{N2} := 0.5956\frac{kg}{m^3}$ (specific heat at 300C)

$C_{pN2} := 1070\frac{J}{kg \cdot K}$ (specific heat at 300C)

Set biomass flowrate:

$m_{dotbio} := 1\frac{kg}{hr}$

$m_{dotbio} = m_{dotchar} + m_{dotvap} + m_{dotncg}$

$m_{dotchar} := 0.15 \cdot m_{dotbio}$ (estimated char mass flowrate) $m_{dotchar} = 0.15\frac{kg}{hr}$

Set carrier gas flowrate:

$V_{dotcg} := 30\frac{cm^3}{min}$ Ligang, Characteristics of fast pyrolysis of biomass in a free fall reactor, Fuel Proc. Tech. 87, (2006)

$m_{dotcg} := V_{dotcg} \cdot \rho_{N2}$ (carrier gas massflow rate) $m_{dotcg} = 1.072 \times 10^{-3}\frac{kg}{hr}$

Mass flowrate into reactor:

$m_{dotin} := m_{dotbio} + m_{dotcg}$ (input flowrate: biomass + c.g.) $m_{dotin} = 1.001\frac{kg}{hr}$

Mass flowrate out of reactor:

$m_{dotgas} := 0.85 m_{dotbio} + m_{dotcg}$ (vapor exiting reactor) $m_{dotgas} = 0.851 \frac{kg}{hr}$

$m_{dotout} := m_{dotchar} + m_{dotgas}$ (char + vapor combined) $m_{dotout} = 1.001 \frac{kg}{hr}$

Heat required to vaporize biomass and bring N2 to temperature(500C):

$Q_{biomass} := m_{dotbio} \cdot h_{pcornstover}$ (heat needed to pyrolize biomass) $Q_{biomass} = 425\,W$

$Q_{N2} := m_{dotcg} \cdot C_{pN2} \cdot (T_{out} - T_{in})$ (heat needed to heat c.g.) $Q_{N2} = 0.151 W$

$Q_{dottot} := Q_{biomass} + Q_{N2}$ (total heat required) $Q_{dottot} = 425.151 W$

Heat Transfer calculations from surface of the ceramic heater to the center of the drop tube

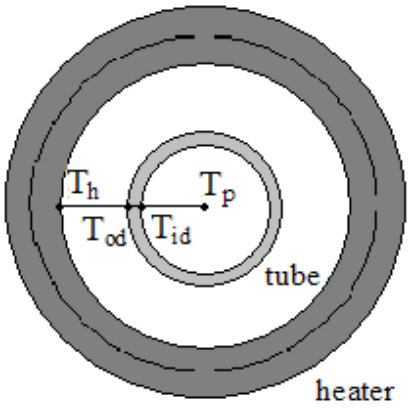

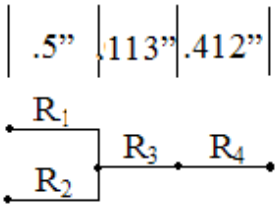

see pages 130, 466, 475, 874 in Heat Transfer, Cengal.

$R_1 = R_{conv} = \frac{1}{h_1 \cdot A_s}$ (neglect)

$R_2 = R_{rad} = \frac{1}{h_{rad} \cdot A_s}$

$R_3 = R_{condcyl} = \frac{\ln\left(\frac{r_{odw}}{r_{idw}}\right)}{2 \cdot \pi \cdot L \cdot k}$

$R_4 = R_{rad} = \frac{1}{h_{rad2} \cdot A_s}$

$D_h := 2in$ (diameter of heater)

$r_h := \frac{D_h}{2}$ (radius of heater wall)

$D_{od} := 1.05in$ (outside diameter of pipe)

$r_{odw} := \frac{D_{od}}{2}$ (outside radius of pipe)

$D_{id} := 0.824in$ (inside diameter of pipe -Sched. 40)

$r_{idw} := \frac{D_{id}}{2}$ (inside radius of pipe)

$L_{pipe} := 6ft$ (length of heated pipe)

$A_{sod} := \pi \cdot (D_{od}) \cdot L_{pipe}$ (surface area of pipe ouside)

$A_{sid} := \pi \cdot (D_{id}) \cdot L_{pipe}$ (surface area of pipe inside)

Find R.1 (convection) between surfaces T.s and T.a:

$T_h := (650.26 + 273.15)K$ (Set heater temp)

$T_{od} := (592.31 + 273.15)K$ (assume outside wall temp)

$T_{ave} := \frac{T_h + T_{od}}{2}$ (temp at which properties are evaluated) $T_{ave} = 621.285°C$

$\beta := \frac{1}{T_{ave}}$ (volume expansion coefficient of an ideal gas p. 462)

$T_{inf} := T_{ave}$ (temp of fluid)

$L_c := 6ft$ (characteristic length)

$\nu := 9.515\,10^{-5}\,\frac{m^2}{s}$ (kinematic viscosity of air at 1 atm and 600C. Cengal, p. 874)

$$Gr_L := \frac{g \cdot \beta \cdot (T_h - T_{inf}) \cdot L_c^{\,3}}{\nu^2}$$

(Grashof number, dimensionless number representing natural convection effects). Cengal, p. 465

$$\frac{35.6\,ft}{Gr_L^{.25}} = 21\,in$$

(which is greater than D_{od} (1in) therefore vertical cylinder **cannot** be modeled as a vertical plate where curvature effects are negligable. Cengel, p. 467)

Properties of air at 900C:

$Pr = 0.7206$

$k = 0.07465 \frac{W}{m \cdot K}$

Properties of air at 600C:

$Pr := 0.7037$

$k := 0.06093 \frac{W}{m \cdot K}$

$L_c := \frac{D_h - D_{od}}{2}$ $\quad L_c = 0.012\,m$

$$Ra_L := \frac{g \cdot \beta \cdot (T_h - T_{od}) \cdot L_c^{\,3}}{\nu^2} \cdot Pr$$

(Rayleigh number: product of the Grashof and Prandtl number

For two long and concentric cylinders maintained at uniform but different temperature, the rate of heat transfer between them through the annular space between the natural convection unit is (Cengal, p. 481):

$$Q_{dot} = \frac{2 \cdot \pi \cdot k_{eff}}{\ln\left(\frac{D_h}{D_{od}}\right)} \cdot (T_h - T_{od})$$

$$F_{cyl} := \frac{\ln\left(\frac{D_h}{D_{od}}\right)^4}{L_c^{\,3} \cdot \left(D_{od}^{\frac{-3}{5}} + D_h^{\frac{-3}{5}}\right)^5}$$

(geometric factor for concentric cylinders p. 481)

$$k_{eff} := k \cdot 0.386 \left(\frac{Pr}{0.861 + Pr}\right)^{0.25} \cdot (F_{cyl} \cdot Ra_L)^{0.25}$$

(effective thermal conductivity p. 481)
valid for $0.70<Pr<6000$ and
$100<F_{cyl}Ra_L<10^7$

$F_{cyl} \cdot Ra_L = 12.091$

(For $F_{cyl}Ra_L<100$, natural convection currents are negligable and thus k_eff = k. Cengal, p. 481)

$$Q_{dot} := \frac{2\cdot\pi\cdot k_{eff}}{\ln\left(\frac{D_h}{D_{od}}\right)}\cdot\left(T_h - T_{od}\right) \qquad Q_{dot} = 20.295\frac{W}{m}$$ (For interests sake)

Neglect R.1 due to convection and find R.2 due to radiation:
(from the heaters to the reactor)

$\varepsilon_h := 0.9$ (emmisivity of heater)

$\varepsilon_{odw} := 0.3$ (emmisivity of reactor wall) Assume value of 0.3 that of unpolished metal pg. 581 Cengel

$\sigma := 5.67\cdot 10^{-8}\frac{W}{m^2\cdot K^4}$ (Stefan Boltzmann constant)

$$h_{rad} := \frac{\sigma\cdot\left(T_h^{\,2} + T_{od}^{\,2}\right)\left(T_h + T_{od}\right)}{\frac{1}{\varepsilon_{odw}} + \frac{1-\varepsilon_h}{\varepsilon_h}\cdot\left(\frac{r_{odw}}{r_h}\right)}$$ (Emsick thesis appendix section 17) radiative heat transfer between heater and tube $h_{rad} = 47.9\frac{W}{m^2\cdot K}$

$R_{rad} := \frac{1}{h_{rad}\cdot A_{sod}}$ (Thermal resistance due to radiation) $\boxed{R_{rad} = 0.136\frac{K}{W}}$

Calculate R.3 due to conduction:

$t := \frac{D_{od} - D_{id}}{2}$ $t = 0.113in$ (thickness of the reactor wall)

$k_{cond} := 13.4\frac{W}{m\cdot K}$ (conductivity of 316 stainless steel p. 859 Cengel)

$$R_{condcyl} := \frac{\ln\left(\frac{r_{odw}}{r_{idw}}\right)}{2\cdot\pi\cdot L_{pipe}\cdot k_{cond}}$$ (thermal resistance due to conduction in a cylinder p. 147 Cengel) $\boxed{R_{condcyl} = 1.574\times 10^{-3}\frac{K}{W}}$

Calculate R.4 due to Radiation:

$T_{pin} := 25K + 273K$ (temperature of biomass and carrier gas coming in)

$T_{id} := 591.64K + 273K$ (assume a 900C wall temperature)

$\varepsilon_p := 1$ (assume blackbody radiation)

$F_{p\_wall} := 0.7$ (view factor -see veiw factor calculations)

$$h_{rad2} := \frac{\sigma \cdot \left(T_{pin}^{\ 2} + T_{id}^{\ 2} \right) \left(T_{pin} + T_{id} \right)}{\frac{1}{\varepsilon_p} - 1 + \frac{1}{F_{p\_wall}}}$$

(Cengel p. 628 -derived radiation due to convection without assuming view factor of 1.)

$h_{rad2} = 38.596 \frac{W}{m^2 \cdot K}$

view factor of 0.7:

$$R_{rad2} := \frac{1}{h_{rad2} \cdot A_{sid}}$$

$R_{rad2} = 0.163$

$R_{rad2} = 0.215 \frac{K}{W}$

$$R_{tot} := R_{rad} + R_{condcyl} + R_{rad2}$$

$R_{tot} = 0.313$

$R_{tot} = 0.353 \frac{K}{W}$

Knowing the energy required to vaporize biomass is equal to Q.tot we can calculate the temperature of the unknowns by setting T.p=500C.

$T_p := 500K + 273.15K$ (temperature of vapor and gas leaving reactor)

Sched 40

Pipe ID=0.824"

$Q_{dottot} := 425.151W$ (From "Heat required to vaporize biomass and heat carrier gas" calculations)

$T_p = 500°C$

$T_{id} := T_p + Q_{dottot} \cdot R_{rad2}$

$T_{id} = 591.61°C$

$T_{od} := T_{id} + Q_{dottot} \cdot R_{condcyl}$

$T_{od} = 592.27°C$

$T_h := T_{od} + Q_{dottot} \cdot R_{rad}$

$T_h = 650.2°C$

The minimum temperature that is needed to maintain the inner temperature of the tube at 500C is about 650C not accounting for heat losses which may be significant considering the size of the reactor.

View factor considerations

Mass flow rate:

$m_{dotbiomass} := 1 \frac{kg}{hr}$ (mass flow for biomass)

Particle size:

$D_p := 400micron$ (diameter of particle)

$$Vol_p := \frac{4}{3} \cdot \pi \left(\frac{D_p}{2} \right)^3$$

(volume of particle)

$Vol_p = 3.351 \times 10^{-5} cm^3$

Volume of reactor:

$r_{tube} := \frac{0.824in}{2}$ (droptube radius)

$L_{tube} := 1cm$ (length of tube)

$Vol_{tube} := \pi \cdot r_{tube}^{\ 2} \cdot L_{tube}$ (volume of tube)

$Vol_{tube} = 1.215 \times 10^{-4} ft^3$

If we feed biomass at 1kg/hr how much biomass is in the tube at any given second?

$u_{tbiomass} := 1.95\frac{m}{s}$ (terminal velocity for 1350Kg/m^3 biomass particle: 400micron)

$part_{density}\left(u_{tbiomass}\right) := \frac{m_{dotbiomass}}{u_{tbiomass}}$ (bulk density of particles in reactor)

$part_{density}\left(u_{tbiomass}\right) = 1.425\times 10^{-3}\,\frac{gm}{cm}$

$w := 1350\frac{kg}{m^3}\cdot Vol_p$ (weight of particles)

$w = 4.524\times 10^{-5}\,gm$

$\#P := \frac{part_{density}\left(u_{tbiomass}\right)}{w}$ (number of particles per unit length)

$\#P = 3.149\frac{1}{mm}$

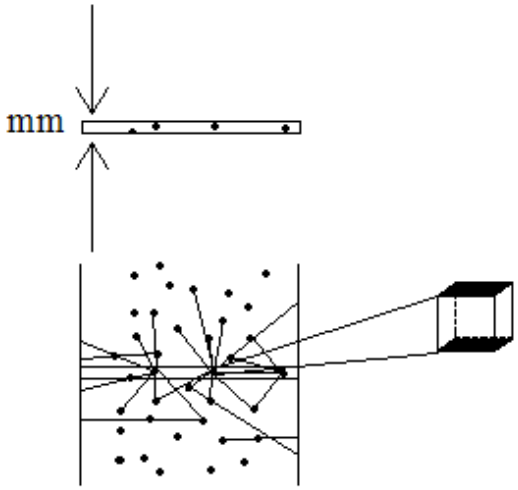

Consider the 1 mm length to the left. If there are 3.1 particles in this cross section, one can see that the view factor between the particle and the reactor wall **is not 1**. Other particles will interfere with the radiation from the wall.

If we look at the particle as a cube it is reasonable to assume that much of the radiation is blocked form above and below it due to the other particles in the tube. On the other hand, the particle can "see" most of the tube wall in the horizontal direction. It is fair to say that the view factor lies between 4/6ths or 2/3rds and 1. Assume a value of **0.7**.

Vapors produced and exiting at the bottom of the reactor

$kmol := 1000mol$

Set biomass flowrate:

$m_{dotbio} := 1\frac{kg}{hr}$

$m_{dotbio} = m_{dotchar} + m_{dotvap} + m_{dotncg}$

$m_{dotchar} := 0.15 \cdot m_{dotbio}$ $\quad m_{dotchar} = 0.15\frac{kg}{hr}$

$m_{dotncg} := 0.15 \cdot m_{dotbio}$

Combine the mass flow rates of the vapors and non condensible gases.

$m_{dotcomb} = m_{dotvap} + m_{dotncg}$

$m_{dotcomb} := 0.85 \cdot m_{dotbio}$ $\quad m_{dotcomb} = 2.4 \times 10^{-4}\ \frac{kg}{s}$

Calculate the length of the reactor by setting the vapor residence time equal to a maximum of 2s.

$$t_{vap} = \frac{L}{v_{vap}} = \frac{L \cdot \rho_{vap} \cdot A_{cross}}{m_{dotcomb}}$$

where: $t_{vap} := 2s$ (vapor residence time)

$r := \frac{0.824in}{2}$ (radius of the reactor tube Schedule 40 3/4" pipe)

$A_{cross} := \pi \cdot r^2$ (cross sectional area of the tube) $\quad A_{cross} = 3.44 \times 10^{-4}\ m^2$

Use the Ideal Gas Law to calculate the volumetric flowrate of the vapor:

$$P \cdot V_{dot} = n_{dot} \cdot R \cdot T = \frac{m_{dotvap}}{MW_{vap}} \cdot R \cdot T \qquad V_{dot} = \frac{m_{dotvap} \cdot R \cdot T}{P \cdot MW_{vap}}$$

Set the following:

$P := 1.1atm$

$$M = \frac{m}{n} \qquad n_{dot} = \frac{m_{dotvap}}{MW_{vap}}$$

$MW_{comb} := 88\frac{kg}{kmol}$ (Molecular weight of everything leaving the reactor -weighted average of MW of bio-oil and NCG)

$MW_{biooil} := 100\frac{kg}{kmol}$ (Molecular weight of bio-oil.)

$MW_{biooil} := 100\frac{kg}{kmol}$ (Molecular weight of bio-oil.)

$MW_{ncgas} := 33\frac{kg}{kmol}$ (Molecular weight of non-condensable gas)

$R_{bar} := 8.314\frac{J}{mol \cdot K}$ (Ideal gas constant) $R = \frac{R_{bar}}{MW}$

$T := 500°C$ (Temperature of vapors exiting the reactor)

$V_{dot} := \frac{m_{dotcomb} \cdot R_{bar} \cdot T}{P \cdot MW_{comb}}$ (volume of vapor produced in one minute) $V_{dot} = 9.284\frac{L}{min}$

$T_{amb} := 293K$ (Temperature of vapors exiting the condensers)

$V_{dotncgas} := \frac{m_{dotncg} \cdot R_{bar} \cdot T_{amb}}{P \cdot MW_{ncgas}}$ (volumetric flowrate of non condensible gases PRODUCED leaving condensers -does not include carrier gas) $V_{dotncgas} = 3.508\frac{ft^3}{hr}$

$v_{vap} := \frac{V_{dot}}{A_{cross}}$ (velocity of vapor at exit of reactor) $v_{vap} = 0.45\frac{m}{s}$

$\rho_{vap} := \frac{P \cdot MW_{comb}}{R_{bar} \cdot T}$ (density of vapors) $\rho_{vap} = 1.526\frac{kg}{m^3}$

$L := t_{vap} \cdot v_{vap}$ (distance vapors travel in 2 sec.) $L = 0.9m$

$D_{exit} := \frac{3}{16}in, \frac{1}{4}in .. \frac{3}{4}in$

$r_{exit}(D_{exit}) := \frac{D_{exit}}{2}$

$A_{exit}(D_{exit}) := \pi \cdot r_{exit}(D_{exit})^2$

Calculate the velocity of the vapors as a function of tube diameter:

$$v_{vap}(D_{exit}) := \frac{V_{dot}}{A_{exit}(D_{exit})}$$

$$D(D_{exit}) := v_{vap}(D_{exit}) \cdot 1s$$

$v_{vap}(D_{exit})$ =		D_{exit} =			$D(D_{exit})$ =	
8.686	m/s	0.187	in	Velocity of vapors exiting the reactor for a given pipe size.	8.686	m
4.886		0.25			4.886	
3.127		0.313		Select 1/2in (OD) tubing with 7/16in (ID).	3.127	
2.172		0.375			2.172	
1.595		0.438			1.595	
1.222		0.5			1.222	
0.965		0.563			0.965	
0.782		0.625			0.782	
0.646		0.688			0.646	
0.543		0.75			0.543	

Distance the vapours travel in 1 second based on the diameter of the tube.

Compare the velocity of the carrier gas to that of the particle:

$$V_{cargas} := 5\frac{l}{min} \cdot \left(\frac{500K + 273K}{25K + 273K} \right)$$

$$V_{cargas} = 2.162 \times 10^{-4} \frac{m^3}{s}$$

$$v_{cg} := \frac{V_{cargas}}{A_{cross}} \qquad v_{cg} = 0.628\frac{m}{s}$$ (velocity of the carrier gas through the reactor)

How long will it take the vapors to travel through the reactor?

$$L_{reactor} := 2.13m$$

$$t := \frac{L_{reactor}}{0.45\frac{m}{s}} \qquad t = 4.733\,s$$

If we add 5 SLPM of carrier gas, how long will it take?

$$t := \frac{L_{reactor}}{0.45\frac{m}{s} + v_{cg}} \qquad t = 1.975\,s$$

How fast will the vapors be travelling?

$$v := \frac{L_{reactor}}{t} \qquad v = 1.078\frac{m}{s}$$

The terminal velocity of a 1350 kg/m^3, 300 um particle is 1.3 m/s. Therefore, the carrier gas flow rates will need to be greater than 5 SLPM before they affect the velocity of the particle.

Char collector size:

Assume roughly 20% of biomass feed rate will become char (conservative):

$\rho_{char} := 400\frac{kg}{m^3}$ Bulk density of char (400kg/m3), pg 48, Joe Ritzert thesis

$char_{produced} := \frac{0.20 m_{dotbiomass}}{\rho_{char}} \cdot t$ (char produced)

$char_{produced} = 1\,L$

$char_{produced} = 0.035 ft^3$

$t = 2\,hr$ (test time)

$m_{dotbiomass} = 1\frac{kg}{hr}$ (mass flow/feed rate)

After 2 hours, the volume of char that will be produced when operating at 1 kg/hr is 1L.

Dimensions of container:
Assume that 1/3rd of the container is filled after 2 hours to prevent the container from filling up so full that the particles are re-entrained.

$r := 3in$ (radius of char container)

$A_{cross} := \pi \cdot r^2$ (cross sectional area of container) $A_{cross} = 28\,in^2$

$h := \frac{3 \cdot char_{produced}}{A_{cross}}$ (height of char catch) $h = 6\,in$

$V := A_{cross} \cdot h$ (volume of char catch) $V = 3\,L$

Determine the velocity in the char container as a function of diameter:

$kPa := 1000Pa$

$m_{dot} = \rho \cdot A \cdot v$ (continuity principle)

$m_{dottube} = m_{dotchar}$

$D_{char} := (4 \;\; 5 \;\; 6)in$ (char container diameter)

$r_{exit}(D_{char}) := \frac{D_{char}}{2}$ (radius char container)

$r_{tube} := 0.412in$ (radius of the reactor)

$A_{tube} := \pi \cdot r_{tube}^2$ (cross sectional area of tube)

$A_{char}(D_{char}) := \pi \cdot r_{exit}(D_{char})^2$ (cross sectional area char container)

$m_{dottube} := 1\frac{kg}{hr}$ (mass flow through reactor tube)

$m_{dotchar} := 1\frac{kg}{hr}$ (mass flow into char container)

$\rho_1 := 1.526\frac{kg}{m^3}$ (density of vapors exiting) $\rho_2 := \rho_1$

$p_1 := 1atm$ (atmospheric pressure after cyclone)

$v_{tube} := \frac{m_{dottube}}{\rho_1 \cdot A_{tube}}$ (Velocity of vapors through reactor tube) $v_{tube} = 0.529\frac{m}{s}$

$m_{dottube} := \rho_1 \cdot A_{tube} \cdot v_{tube}$ $m_{dotchar} = \rho_2 \cdot A_{char} \cdot v_{char}$

$\rho_1 \cdot A_{tube} \cdot v_{tube} = \rho_2 \cdot A_{char} \cdot v_{char}$

$v_{char}(D_{char}) := \frac{\rho_1 \cdot A_{tube} \cdot v_{tube}}{\rho_2 \cdot A_{char}(D_{char})}$ (Velocity of vapors through char container)

$v_{char}\left(D_{char_{0,0}}\right) = 0.022\frac{m}{s}$ (4in diameter char container)

$v_{char}\left(D_{char_{0,1}}\right) = 0.014\frac{m}{s}$ (5in diameter char container)

$v_{char}\left(D_{char_{0,2}}\right) = 0.01\frac{m}{s}$ (6in diameter char container)

Determine the char particles terminal velocity to find char catch size:

Fluid properties:

$\rho_f := 0.4880\frac{kg}{m^3}$ (density of fluid (air) at 450C -less dense than pyrolysis vapors therefore particle will have a higher u_t)

$\mu := 3.415\,10^{-5}\frac{kg}{m \cdot s}$ (dynamic viscosity of air at 450C)

Char properties:

$\rho_{char} := 450\frac{kg}{m^3}$ (Bulk density of char)

$\rho_p := \rho_{char}$ (density of particle is equal to the density of char)

$r_o := 5micron, 10micron .. 50micron$ (outer radius of particle)

$D_p(r_o) := 2 \cdot r_o$ (particle diameter)

$Re_p(r_o, D_{char}) := \frac{\rho_f \cdot (2 \cdot r_o) \cdot v_{char}(D_{char})}{\mu}$ (Reynolds number, function of particle diameter and the velocity in the char container)

Choose drag coefficient based on Reynolds number, since all values are below 0.4 use $24/Re_p$.

$C_d = \frac{24}{Re_p}$ for Re_p <0.4

$C_d = \frac{10}{\sqrt{Re_p}}$ for 0.4< Re_p < 500

$C_d = 0.43$ for 500 < Re_p < 200,000

$Re_p(r_o, D_{char_{0,0}})$	$Re_p(r_o, D_{char_{0,1}})$	$Re_p(r_o, D_{char_{0,2}})$
208·10-3	053·10-3	426·10-3
417·10-3	107·10-3	852·10-3
625·10-3	.16·10-3	278·10-3
0.013	214·10-3	704·10-3
0.016	0.01	.13·10-3
0.019	0.012	556·10-3
0.022	0.014	982·10-3
0.026	0.016	0.011
0.029	0.018	0.013
0.032	0.021	0.014

$u_t = \sqrt{\frac{4 \cdot g \cdot 2 \cdot r_o \cdot (\rho_p - \rho_f)}{3 \cdot \rho_f \cdot C_d}}$

$u_t(r_o, D_{char}) := \sqrt{\frac{4 \cdot g \cdot 2 \cdot r_o \cdot (\rho_p - \rho_f)}{3 \cdot \rho_f \cdot \frac{24}{Re_p(r_o, D_{char})}}}$ (Particle terminal velocity)

Particle terminal velocities:

Char container diameter = 4in

$u_t\left(r_o, D_{char_{0,0}}\right) =$

	0
0	4.013·10-3
1	8.025·10-3
2	0.012
3	0.016
4	0.02
5	0.024
6	0.028
7	0.032
8	0.036
9	0.04

$\frac{m}{s}$

Char container diameter = 5in

$u_t\left(r_o, D_{char_{0,1}}\right) =$

	0
0	3.21·10-3
1	6.42·10-3
2	9.63·10-3
3	0.013
4	0.016
5	0.019
6	0.022
7	0.026
8	0.029
9	0.032

$\frac{m}{s}$

Char container diameter = 6in

$u_t\left(r_o, D_{char_{0,2}}\right) =$

	0
0	2.675·10-3
1	5.35·10-3
2	8.025·10-3
3	0.011
4	0.013
5	0.016
6	0.019
7	0.021
8	0.024
9	0.027

$\frac{m}{s}$

Char diameter:

$D_p\left(r_o\right) =$

	0
0	10
1	20
2	30
3	40
4	50
5	60
6	70
7	80
8	90
9	100

micron

Fluid velocity in char container for respective cross-sectional areas:

$v_{char}\left(D_{char_{0,0}}\right) = 0.022\frac{m}{s}$ (4in diameter char container)

$v_{char}\left(D_{char_{0,1}}\right) = 0.014\frac{m}{s}$ (5in diameter char container)

$v_{char}\left(D_{char_{0,2}}\right) = 0.01\frac{m}{s}$ (6in diameter char container)

If the velocity in the char container is lower than the terminal velocity, the particle will disengage from the flow (ie. the terminal velocity of the particle is higher than that of the fluid flow):

Four inch diameter: catches particles 60micons and larger.
Five inch diameter: catches particles 50 microns and larger.
Six inch diameter: catches particles 40 microns and larger.

Appendix B: Bio-oil sample preparation procedure and analysis for water insolubles and solids content methods

Bio-oil Sample Preparation Procedure

This is procedure is intended to create a homogenized mixture of bio-oil in preparation for bio-oil sampling for further analyses.

This procedure must be performed to prepare the bio-oil *before* the following analyses:

- Karl-Fischer moisture content
- Total Acid Number (TAN)
- Water Insolubles content
- Solids content
- Thermogravimetric analysis (TGA)
- CHNSO (Ultimate analysis)
- GC/MS
- Higher Heating Value (HHV)
- Viscosity

For bio-oil samples that are SOLID at room temperature:

1. Obtain large (250, 500 or 1000 ml) bio-oil storage containers from fridge.
2. Place bio-oil storage container in beaker of water. Heat beaker of water and bio-oil sample to 80°C on a hot plate. Monitor with a thermometer.
3. Maintain bio-oil temperature at 80°C for about 1 minute.
4. Stir bio-oil storage container for 1 minute using the electric stirrer. Stir both top and bottom to create a *homogenous* mixture. Clean impeller when completed.
5. Place container back into 80°C water.
6. If using a 1000 ml bio-oil container and the bio-oil is difficult to reach with a syringe, create a new storage container by pouring the bio-oil into a smaller, *labeled* container.
7. Proceed with prescribed bio-oil analysis procedure while bio-oil is maintained at 80°C.
8. Once all samples are prepared or analysis is complete, return storage container and lid to refrigerator.

For bio-oil samples that are LIQUID (flow) at room temperature:

1. Obtain large (250, 500 or 1000 ml) bio-oil storage containers from fridge.
2. Let containers sit out and approach room temperature. Shake containers intermittently to speed process.
3. Stir bio-oil storage containers for 1 minute using the electric stirrer. Stir both top and bottom to create a *homogenous* mixture. Clean impeller when completed.
4. Proceed with prescribed bio-oil analysis procedure.
5. Once all samples are prepared or analysis is complete, return storage container and lid to refrigerator.

Water Insolubles

SOP for Water Extraction of Insolubles in bio-oil.

1. Shake large bio-oil containers well. Place about 20 mL of the bio-oil sample into a centrifuge tube.
2. Sonicate centrifuge tube for 30 minutes. Then place tube on shaker table for 30 minutes.
3. Complete the following in triplicate. For example, use the bio-oil from the above centrifuge tube to prepare three of the following water/bio-oil samples.
4. Obtain a new centrifuge tube. Weigh and record mass of centrifuge tube.
5. Using a syringe, place about 10g of room temperature DI water into tube. Tare balance.
6. Add 2g of bio-oil. Record mass of bio-oil added by weighing syringe before and after. Mix on vortex mixer for 1 minute.
7. Add an additional 10g of DI water. Mix for 1 minute.
8. Repeat 2 more times. Total water added 40g. Total bio-oil added 2g. Ratio 20:1
9. Place centrifuge tube in sonicator for 30 minutes. Place tube on shaker table for 1 hour at maximum speed.
10. Place centrifuge tube in centrifuge for 20 minutes at 2500 rpm. Ensure that it is balanced; equal # of samples on each side.
11. Place size 42 filter paper in the oven at 105°C for 15 minutes to remove any moisture.
12. Remove filter paper from the oven and place in the desiccant to cool for 15 minutes.
13. Remove filter paper from the desiccant record the 1st mass that appears stable (little "g" shows up) of the filter paper.
14. Obtain flask and funnel. Place filter paper in funnel and pour centrifuge tube into funnel.
15. Turn on vacuum pump.
16. Pour centrifuge tube with water/bio-oil mixture onto filter paper. Ensure that the mixture does not touch the sides of the funnel.
17. Take filter paper, centrifuge tube and lid and place in oven at 50C for 20 hours. Keep lid off of tube.
18. Remove filter paper, centrifuge tube and lid from oven and place in desiccant to cool for 15 minutes.
19. Remove filter paper from the desiccant record the 1st mass that appears stable (little "g" shows up) of the filter paper.
20. Record mass of tube and lid.
21. Calculate the percentage of insolubles:

$$\text{wt-\% insolubles} = \frac{\text{final mass: filter paper, tube \& lid} - \text{initial mass: filter paper, tube \& lid}}{\text{mass of bio-oil sample}} \ (\text{x } 100)$$

22. Record weight percentage of insolubles beside sample name and weight of bio-oil added within Insoluble record manual.

Note: Insolubles includes ash content. To calculate only insoluble wt %, subtract ash content.

Solids

(everything not soluble in methanol)

1. Place size 42 filter paper (2.5 micron retention) in the oven at 105°C for 15 minutes.
2. Cool the filter to room temperature in the desiccant containers for 15 minutes.
3. Using a 5 ml syringe (without the needle), obtain 3 ml of **well-mixed** bio-oil. Cap bio-oil container.
4. Place about 1 gram of bio-oil into centrifuge tube. Record mass of bio-oil added by weighing syringe before and after.
5. Pour about 12 grams of methanol (ACS grade) in centrifuge tube.
6. Mix bio-oil and methanol in centrifuge tube on vortex mixer for about a minute.
7. Weigh filter paper that has been sitting in the desiccant containers. (Do so quickly so that a significant amount of moisture does not adhere to filter). Record initial mass of filter paper.
8. Place filter paper on a funnel and wet with methanol.
9. Turn on vacuum pump.
10. Pour centrifuge tube with solution into the center of the filter paper. Do not allow solution to touch funnel sides.
11. Rinse lid and centrifuge tube with methanol into filter paper.
12. Remove filter paper and let air dry under the fume hood for 15 minutes.
13. Place the filter paper in the oven for ½ hour at 105°C.
14. Cool the filter to room temperature in the desiccant containers for 15 minutes.
15. Remove filter paper and record mass. (Do so quickly so that a significant amount of moisture does not adhere to filter).
16. Dispose of filter in bio-oil waste container.
17. Pour filtrate into bio-oil and methanol waste container.
18. Clean glassware if not being used again.
19. Calculate the percentage of solids using the calculation below:

$$\text{wt-\% solids} = \frac{\text{final filter paper mass} - \text{initial filter paper mass}}{\text{mass of bio-oil sample}} \ (\text{x } 100\%)$$

20. Record calculation and result in appropriate Solids laboratory notebook.

Appendix C: Experimental operating conditions, mass distribution and product analysis

Chrono order	Sorted order	Run ID	Operating conditions				Yield w.b. (wt-%)				
			Temperature (℃)	Particle size (μm)	N2 flow rate (SLPM)	Feed rate (kg/hr)	Bio-oil	Bio-char	NCG	Total	Unaccounted
1	30	7-20090112A	500	300	2	1.25	67.3	15.8	14.6	97.7	2.3
2	10	7-20090113A	550	400	1	1.5	70.4	14.8	14.9	100.1	-0.1
3	**1**	7-20090115A	550	400	3	1.5	70.2	15.3	13.6	99.1	0.9
4	17	7-20090219A	600	500	2	1.75	69.1	13.2	15.6	97.9	2.1
5	23	7-20090225A	500	500	4	1.75	68.0	18.8	13.0	99.8	0.2
6	7	7-20090228A	550	400	3	2	71.1	15.2	13.4	99.7	0.3
7	19	7-20090604B	600	300	4	1.75	72.0	11.4	16.1	99.5	0.5
8	20	7-20090309A	600	300	4	1.25	69.1	11.7	17.8	98.6	1.4
9	**2**	7-20090311A	550	400	3	1.5	68.9	16.9	13.5	99.3	0.7
10	16	7-20090313A	600	500	4	1.25	69.0	14.9	15.3	99.2	0.8
11	12	7-20090316A	550	200	3	1.5	69.7	14.4	15.0	99.1	0.9
12	25	7-20090317A	500	500	2	1.75	67.1	19.5	13.1	99.7	0.3
13	28	7-20090319A	500	300	4	1.25	67.4	17.8	14.0	99.2	0.8
14	**3**	7-20090401A	550	400	3	1.5	68.2	17.0	14.3	99.5	0.5
15	18	7-20090403A	600	500	2	1.25	68.4	13.2	17.2	98.8	1.2
16	9	7-20090414A	550	400	5	1.5	69.2	16.1	13.9	99.2	0.8
17	**5**	7-20090420A	550	400	3	1.5	69.7	15.9	14.1	99.7	0.3
18	13	7-20090423A	650	400	3	1.5	64.4	10.3	23.3	98.0	2.0
19	11	7-20090407A	550	600	3	1.5	67.2	18.9	13.1	99.2	0.8
20	22	7-20090425A	600	300	2	1.25	68.3	11.1	19.1	98.5	1.5
21	8	7-20090512A	550	400	3	1	69	15.6	14.8	99.4	0.6
22	**4**	7-20090522A	550	400	3	1.5	69.8	15.8	14	99.6	0.4
23	15	7-20090430A	600	500	4	1.75	70.7	13.8	15.1	99.6	0.4
24	27	7-20090505A	500	300	4	1.75	69.3	16.8	13.7	99.8	0.2
25	24	7-20090508A	500	500	4	1.25	65.7	20.1	14.1	99.9	0.1
26	29	7-20090513A	500	300	2	1.75	67.8	17.2	13.9	98.9	1.1
27	**6**	7-20090529A	550	400	3	1.5	70.1	15.2	14.7	100	0
28	21	7-20090514A	600	300	2	1.75	70.4	11.3	17.4	99.1	0.9
29	26	7-20090525A	500	500	2	1.25	66.1	20.0	13.9	100	0
30	14	7-20090526A	450	400	3	1.5	66.7	19.4	13.6	99.7	0.3

*Shaded lines indicate center point experiments

Chrono order	Mass yield w.b. (g)				Yield (wt-%)				Bio-oil yield d.b. (wt %)	Organic liquid (wt %)	Reaction water (wt %)	Carried water (wt %)	Biomass moisture (wt %)	Actual feedrate (kg/hr)	Difference in feed rate (kg/hr)
	Biomass fed	Bio-oil	Bio-char	NCG	SF1	SF2	SF3	SF4							
1	1312.1	883.1	207.3	191.3	56.2	28.2	14.7	0.9	65.4	51.10	14.30	1.9	5.44	1.28	0.03
2	1595.1	1122.9	236.0	238.0	48.1	38.6	12.6	0.7	68.9	53.17	15.73	1.5	4.92	1.59	0.09
3	1597.6	1121.0	244.1	217.7	45.7	34.9	17.8	1.6	68.4	53.56	14.84	1.8	5.50	1.59	0.09
4	1891.8	1306.4	249.2	294.6	38.4	41.7	18.0	1.9	67.3	53.29	14.01	1.8	5.45	1.88	0.13
5	1806.6	1228.1	339.2	235.2	44.5	35.7	17.4	2.3	66.2	49.29	16.91	1.8	5.18	1.79	0.04
6	2250.6	1599.3	342.5	302.7	35.6	44.1	17.7	2.6	69.5	54.07	15.43	1.6	5.05	2.20	0.20
7	1871.1	1347.4	213.9	301.9	38.1	37.8	21.0	3.1	70.3	55.74	14.56	1.7	5.63	1.86	0.11
8	1344.0	929.0	156.9	239.8	34.6	39.0	23.7	2.7	67.4	53.37	14.03	1.7	5.29	1.32	0.07
9	1668.1	1149.1	281.2	224.4	32.9	46.3	19.0	1.8	67.2	51.69	15.51	1.7	5.20	1.66	0.16
10	1287.1	888.7	191.6	197.1	37.1	38.7	22.2	2.1	67.3	53.12	14.18	1.7	5.38	1.28	0.03
11	1649.9	1150.1	238.1	248.0	32.1	45.4	20.4	2.1	68.1	52.98	15.12	1.6	5.04	1.63	0.13
12	1860.1	1248.2	362.6	243.5	41.2	43.1	14.2	1.4	65.3	48.40	16.90	1.8	5.19	1.82	0.07
13	1409.6	950.0	250.3	197.0	41.7	35.5	20.4	2.4	65.6	49.65	15.95	1.8	5.12	1.36	0.11
14	1532.0	1045.5	259.8	218.4	41.6	39.1	18.0	1.4	66.6	51.13	15.47	1.6	4.89	1.51	0.01
15	1300.0	888.9	172.2	224.0	39.5	42.4	17.2	1.0	66.8	53.22	13.58	1.6	4.88	1.27	0.02
16	1452.9	1005.2	233.8	202.0	32.9	41.2	23.0	2.8	67.5	52.95	14.55	1.7	5.04	1.44	-0.06
17	1678.8	1170.0	267.6	236.0	33.8	46.7	17.8	1.7	68.1	52.03	16.07	1.6	5.1	1.67	0.17
18	1519.0	979.0	156.8	354.3	35.9	36.2	24.4	3.6	62.6	48.92	13.68	1.8	5.02	1.51	0.01
19	1523.8	1024.5	287.3	199.2	35.6	45.8	17.3	1.3	65.6	49.97	15.63	1.6	4.82	1.51	0.01
20	1342.22	917.1	148.6	255.92	43.9	34.9	19.0	2.2	66.6	52.27	14.33	1.7	5.29	1.34	0.09
21	1158.2	798.9	180.34	171.09	41.2	39.3	18.5	1.0	67.3	51.26	16.04	1.7	5.05	1.16	0.16
22	1563.59	1091.1	247.7	219.42	40.0	39.7	18.8	1.6	67.9	52.42	15.48	1.9	5.79	1.55	0.05
23	1735.7	1227.6	239.35	262.66	40.6	35.8	20.9	2.8	69.1	54.71	14.39	1.6	5.21	1.71	-0.04
24	1789.32	1240.3	300.4	245.88	33.2	42.0	21.4	3.4	67.7	52.14	15.56	1.6	5.08	1.78	0.03
25	1263.19	829.8	254.39	177.9	40.6	38.0	19.6	1.8	63.9	49.16	14.74	1.8	5.01	1.21	-0.04
26	1710.36	1160.1	294.11	238.21	40.9	42.1	15.7	1.4	66.1	50.09	16.01	1.7	5.16	1.70	-0.05
27	1501.64	1053.1	227.8	220.36	36.6	41.8	19.8	1.8	68.4	53.13	15.27	1.7	5.62	1.5	0.00
28	1669.73	1175.7	188.8	290	43.0	36.4	18.6	2.1	68.9	54.08	14.82	1.5	4.99	1.66	-0.09
29	1310.76	866	261.7	182.11	46.6	37.7	14.7	1.1	64.2	48.66	15.54	1.9	5.09	1.28	0.03
30	1569.71	1047.1	304.3	213.43	41.6	39.6	17.0	1.8	64.7	47.50	17.20	2.0	5.62	1.56	0.06

Chrono order	Average steady state temperature (℃)									Max reactor temp
	R1	R2	R3	R4	R5	R6	R7	Char catch inlet	Condenser inlet	
1	68.76	251.00	395.22	411.69	440.33	451.00	452.05	444.04	457.39	452.05
2	81.04	295.19	449.59	456.48	480.32	490.45	491.71	451.93	459.52	491.71
3	70.34	280.22	430.95	444.16	469.72	483.98	488.05	450.93	457.08	488.05
4	85.53	332.69	485.88	495.87	510.31	521.06	531.47	462.93	458.50	531.47
5	62.98	262.24	390.17	399.64	414.83	429.25	435.95	433.79	456.19	435.95
6	71.98	280.57	415.17	431.32	455.25	468.73	477.60	448.60	458.43	477.60
7	78.47	345.54	384.24	450.79	489.87	512.57	511.18	465.25	462.89	512.57
8	68.19	308.28	454.30	483.34	514.10	524.88	539.98	464.07	457.83	539.98
9	68.79	282.35	400.48	429.52	452.30	466.88	2398.72	440.73	456.90	466.88
10	85.28	379.79	416.11	488.28	505.86	519.67	518.93	461.99	456.79	519.67
11	68.97	292.37	351.66	414.30	461.34	472.05	472.93	447.72	458.93	472.93
12	80.56	316.41	335.04	394.58	415.46	424.83	421.94	425.20	454.96	425.20
13	67.40	287.11	312.55	375.14	416.89	428.22	427.78	428.80	457.92	428.80
14	85.60	321.99	360.52	430.26	458.83	469.48	471.39	446.31	457.94	471.39
15	102.50	401.60	433.32	502.73	519.30	526.88	531.23	461.52	456.81	531.23
16	76.14	317.79	358.51	425.75	425.75	457.41	452.09	453.92	458.69	457.41
17	83.73	322.03	360.52	428.77	457.02	453.34	475.87	453.74	459.45	475.87
18	95.31	400.78	467.05	521.78	546.33	563.76	573.58	482.37	459.56	573.58
19	87.17	364.37	375.92	445.39	453.79	465.08	479.18	443.88	459.06	479.18
20	90.13	373.90	428.77	484.16	521.73	535.33	535.29	467.27	457.62	535.33
21	82.12	343.35	386.74	442.68	468.79	488.68	485.29	457.77	459.00	488.68
22	81.17	321.43	364.67	422.08	451.86	480.21	480.42	455.45	459.77	480.42
23	84.22	371.03	407.99	470.18	494.85	520.40	520.36	468.28	457.51	520.40
24	66.94	267.24	314.25	367.13	405.98	425.66	430.63	436.42	458.64	436.42
25	72.63	317.08	340.51	392.11	413.19	435.00	434.27	437.42	458.12	437.42
26	72.94	282.51	325.79	374.64	411.16	430.01	433.15	436.79	458.93	436.79
27	81.09	321.80	370.28	426.23	455.38	482.93	473.47	459.39	460.49	482.93
28	88.20	353.80	414.78	469.33	506.37	519.88	523.78	467.09	462.33	523.78
29	83.76	319.96	343.94	396.31	414.35	444.22	440.22	440.00	459.93	444.22
30	71.90	247.51	291.45	338.60	365.35	388.83	390.86	427.92	459.37	427.92

*R1 indicates reactor temperature beginning at the top of the reactor. Temperatures measured every 30 cm from one another.

Chrono order	MW (NCG)	mol (NCG)	Non-condensable gas composition vol-% (nitrogen free)								
			Hydrogen	Carbon monoxide	Methane	Oxygen	Propane	Ethane	Ethylene	Carbon dioxide	Acetylene
1	34.1	5.6	2.038	42.334	7.109	0.093	0.014	0.922	1.102	46.388	0.000
2	33.2	7.2	2.730	44.492	7.808	0.122	0.000	1.034	1.433	42.380	0.000
3	33.8	6.4	1.703	42.683	7.946	0.181	0.020	1.107	1.430	44.929	0.000
4	32.0	9.2	3.461	47.346	9.166	0.038	0.038	0.905	1.867	37.179	0.000
5	34.6	6.8	1.036	41.838	7.417	0.000	0.000	0.820	0.644	48.245	0.000
6	33.6	9.0	1.691	44.530	8.104	0.009	0.000	0.924	0.904	43.838	0.000
7	31.5	9.6	3.441	51.922	8.259	0.000	0.000	0.909	1.770	33.654	0.045
8	30.6	7.8	5.138	50.709	9.419	0.307	0.000	0.904	2.029	31.493	0.000
9	33.8	6.6	1.902	43.851	7.418	0.000	0.000	0.845	0.968	45.015	0.000
10	32.1	6.1	3.552	48.525	8.330	0.000	0.000	0.840	1.607	37.145	0.000
11	32.8	7.6	2.488	47.086	8.087	0.000	0.000	0.953	1.288	40.098	0.000
12	34.7	7.0	0.960	40.981	7.679	0.000	0.000	0.835	0.657	48.889	0.000
13	34.2	5.8	1.014	43.489	7.618	0.000	0.000	0.928	0.801	46.150	0.000
14	33.6	6.5	1.805	44.962	7.602	0.000	0.000	0.872	1.043	43.715	0.000
15	30.9	7.2	4.619	50.475	9.376	0.000	0.000	0.906	1.956	32.634	0.033
16	33.9	6.0	1.203	45.063	7.546	0.000	0.000	0.859	0.983	44.322	0.024
17	33.7	7.0	1.322	43.175	7.391	3.863	0.000	0.838	0.945	42.450	0.016
18	28.5	12.4	8.500	51.936	10.941	0.003	0.000	1.017	2.406	25.129	0.069
19	34.6	5.8	1.050	42.555	6.939	0.000	0.000	0.722	0.809	47.907	0.018
20	30.3	8.4	5.242	51.747	9.821	0.006	0.000	0.923	2.203	30.017	0.041
21	33.3	5.1	1.586	47.395	7.530	0.000	0.000	0.822	1.246	41.395	0.025
22	33.5	6.5	1.358	46.779	7.659	0.000	0.000	0.883	1.106	42.194	0.021
23	32.3	8.1	2.354	49.049	8.724	0.000	0.000	0.892	1.608	37.341	0.031
24	34.2	7.2	0.929	43.888	7.617	0.000	0.000	0.923	0.809	45.834	0.000
25	34.9	5.1	0.666	42.420	6.662	0.000	0.000	0.748	0.757	48.749	0.000
26	34.0	7.0	1.081	44.538	7.616	0.000	0.000	0.918	0.858	44.988	0.000
27	33.3	6.6	1.451	47.944	7.669	0.000	0.000	0.909	1.178	40.828	0.021
28	31.0	9.4	4.094	51.416	9.468	0.000	0.000	0.960	1.980	32.049	0.033
29	34.5	5.3	0.892	43.496	6.749	0.000	0.000	0.776	0.817	47.270	0.000
30	34.7	6.2	0.688	42.634	7.153	0.000	0.000	0.846	0.710	47.969	0.000

Chrono order	Non-condensable gas yield (wt %) (nitrogen free)								
	Hydrogen	Carbon monoxide	Methane	Oxygen	Propane	Ethane	Ethylene	Carbon dioxide	Acetylene
1	0.02	5.07	0.49	0.01	0.00	0.12	0.13	8.73	0.00
2	0.02	5.60	0.56	0.02	0.00	0.14	0.18	8.39	0.00
3	0.01	4.82	0.51	0.02	0.00	0.13	0.16	7.96	0.00
4	0.03	6.46	0.72	0.01	0.01	0.13	0.25	7.97	0.00
5	0.01	4.41	0.45	0.00	0.00	0.09	0.07	7.99	0.00
6	0.01	4.99	0.52	0.00	0.00	0.11	0.10	7.71	0.00
7	0.04	7.44	0.68	0.00	0.00	0.14	0.25	7.58	0.01
8	0.06	8.28	0.88	0.06	0.00	0.16	0.33	8.08	0.00
9	0.02	4.88	0.47	0.00	0.00	0.10	0.11	7.87	0.00
10	0.03	6.49	0.64	0.00	0.00	0.12	0.22	7.81	0.00
11	0.02	6.04	0.59	0.00	0.00	0.13	0.17	8.08	0.00
12	0.01	4.33	0.46	0.00	0.00	0.09	0.07	8.12	0.00
13	0.01	4.97	0.50	0.00	0.00	0.11	0.09	8.29	0.00
14	0.02	5.34	0.52	0.00	0.00	0.11	0.12	8.15	0.00
15	0.05	7.88	0.84	0.00	0.00	0.15	0.31	8.00	0.00
16	0.01	5.18	0.50	0.00	0.00	0.11	0.11	8.00	0.00
17	0.01	5.04	0.49	0.52	0.00	0.10	0.11	7.78	0.00
18	0.14	11.89	1.43	0.00	0.00	0.25	0.55	9.04	0.01
19	0.01	4.50	0.42	0.00	0.00	0.08	0.09	7.97	0.00
20	0.07	9.12	0.99	0.00	0.00	0.17	0.39	8.31	0.01
21	0.01	5.88	0.54	0.00	0.00	0.11	0.15	8.07	0.00
22	0.01	5.49	0.51	0.00	0.00	0.11	0.13	7.78	0.00
23	0.02	6.43	0.65	0.00	0.00	0.13	0.21	7.69	0.00
24	0.01	4.94	0.49	0.00	0.00	0.11	0.09	8.10	0.00
25	0.01	4.80	0.43	0.00	0.00	0.09	0.09	8.67	0.00
26	0.01	5.10	0.50	0.00	0.00	0.11	0.10	8.10	0.00
27	0.01	5.92	0.54	0.00	0.00	0.12	0.15	7.93	0.00
28	0.05	8.08	0.85	0.00	0.00	0.16	0.31	7.91	0.00
29	0.01	4.90	0.44	0.00	0.00	0.09	0.09	8.37	0.00
30	0.01	4.68	0.45	0.00	0.00	0.10	0.08	8.28	0.00

Chrono order	Moisture Content (wt %)					Water insoluble (wt %)	Solids content (wt %)	Carbon (wt %)	Hydrogen (wt %)	Nitrogen (wt %)	Oxygen (wt %)	Sulpher (wt %)	Ash (wt %)	TAN (mg KOH/g)	HHV (MJ/kg)
	SF1	SF2	SF3	SF4	Whole	Whole	Whole	Whole	Whole	Whole	Whole	Whole	Whole	Whole	Whole
1	16.1	45.3	10.9	71.7	24.1	16.28	0.42	41.604	7.56	0.039	50.58	0.011	0.202		
2	11.4	44.7	10.1	64.2	24.5	17.52	0.76	40.764	7.42	0.039	51.68	0.009	0.081		
3	12.3	42.5	12.7	61.9	23.7	19.05	1.24	40.749	7.59	0.050	51.58	0.001	0.030	102.1	17.0
4	7.8	39.4	11.8	70.2	22.9	19.13	0.71	41.311	7.55	0.054	51.01	0.011	0.070		
5	15.2	46.2	15.2	69.5	27.5	13.93	0.38	38.971	7.70	0.048	53.17	0.007	0.105		
6	7.3	39.7	12.2	64.8	24.0	19.70	0.81	40.344	7.44	0.011	52.19	0.010	0.007		
7	8.0	40.7	11.2	59.0	22.6	19.73	0.42	40.831	7.42	0.028	51.15	0.016	0.557		
8	6.1	42.2	10.6	62.6	22.8	19.79	0.94	41.559	7.38	0.010	49.53	0.011	1.515		
9	6.4	41.4	13.5	62.2	25.0	17.30	0.98	39.269	7.34	0.031	53.29	0.005	0.064	102.2	16.8
10	10.3	40.2	9.9	70.3	23.0	20.64	0.58	40.033	7.49	0.008	52.34	0.009	0.111		
11	6.2	40.2	11.4	66.5	24.0	21.20	0.40	40.165	7.46	0.008	52.13	0.012	0.225		
12	11.5	46.8	14.3	62.6	27.9	15.24	0.91	36.960	7.45	0.008	55.39	0.012	0.185		
13	12.8	47.6	11.8	69.0	26.3	17.31	0.08	38.935	7.55	0.008	52.59	0.013	0.905		
14	12.8	42.4	12.0	72.4	25.0	17.59	0.67	39.405	7.41	0.027	53.04	0.014	0.107	102.9	16.8
15	7.5	40.0	9.4	69.6	22.2	19.99	0.56	42.266	7.71	0.008	49.60	0.013	0.407		
16	6.7	40.7	11.4	65.7	23.5	18.14	1.03	39.884	7.49	0.008	51.98	0.014	0.618		
17	8.3	41.6	11.7	61.0	25.3	19.09	1.40	39.169	7.22	0.015	53.53	0.001	0.072	99.6	16.8
18	8.0	43.5	13.3	60.7	24.0	21.62	0.88	40.853	7.53	0.008	51.25	0.014	0.336	88.3	
19	7.9	43.0	13.1	67.9	25.6	15.07	1.03	38.527	7.60	0.008	53.28	0.015	0.565		
20	10.7	44.0	11.3	57.2	23.5	20.24	0.99	40.541	7.51	0.008	51.23	0.014	0.690		
21	9.8	49.1	9.5	61.4	25.7	17.48	0.64	39.763	7.51	0.008	52.35	0.015	0.350		
22	11.0	42.8	13.3	63.0	24.9	17.22	1.36	39.228	7.49	0.005	53.17	0.001	0.106	101.0	16.7
23	9.6	40.3	12.7	58.8	22.6	20.41	0.41	40.597	7.44	0.008	50.92	0.013	1.028		
24	10.6	38.9	13.7	59.1	24.8	16.85	0.45	39.041	7.50	0.008	52.89	0.017	0.537		
25	14.2	41.5	12.3	69.5	25.2	13.97	0.92	37.942	7.70	0.008	54.12	0.009	0.221		
26	11.5	44.0	12.7	66.4	26.1	16.43	0.31	38.718	7.57	0.008	52.95	0.011	0.750		
27	8.5	41.7	12.9	64.7	24.2	17.77	1.14	39.528	7.49	0.010	52.94	0.001	0.026	99.1	16.6
28	10.3	41.8	13.0	54.2	23.2	21.13	0.92	40.841	7.46	0.008	51.29	0.012	0.385		
29	14.4	45.2	12.8	70.6	26.4	15.08	0.67	37.838	7.58	0.029	53.93	0.017	0.606		
30	12.9	50.0	14.2	67.9	28.8	15.42	0.66	37.355	7.66	0.021	54.33	0.017	0.608	107.6	

*Oxygen content found by difference

Chrono order	Bio-oil chemical group (wt %)							
	Acetic acid	Levo-glucosan	Furans	Phenols	Guiacols	Syringols	Other	Total
1	3.247	1.852	0.731	0.623	1.595	2.684	3.012	13.744
2	3.304	4.379	0.693	0.630	1.598	2.598	3.710	16.913
3	7.018	7.306	0.822	0.825	2.412	4.086	5.648	28.118
4	3.944	1.931	0.576	0.619	1.517	2.463	3.307	14.357
5	3.378	1.912	0.718	0.618	1.649	2.917	3.466	14.659
6	1.572	2.404	0.737	0.759	2.133	3.633	4.642	15.880
7	1.543	1.885	0.688	0.643	1.582	2.576	3.653	12.570
8	3.698	2.110	0.529	0.676	1.539	2.345	4.684	15.581
9	3.811	1.732	0.651	0.633	1.662	2.793	3.559	14.841
10	3.610	2.949	1.033	0.863	2.407	4.092	5.626	20.580
11	2.699	1.710	0.720	0.664	1.661	2.641	4.017	14.112
12	2.316	1.696	0.770	0.613	1.659	3.015	3.586	13.656
13	2.456	1.558	0.780	0.616	1.688	2.863	3.967	13.928
14	3.345	1.755	0.776	0.618	1.679	2.837	3.985	14.994
15	2.995	1.949	0.728	0.677	1.535	2.516	3.387	13.788
16	2.390	1.699	0.758	0.601	1.608	2.697	3.805	13.559
17	4.252	1.769	0.720	0.597	1.568	2.623	3.219	14.748
18	4.157	1.955	0.708	0.789	1.299	2.012	4.974	15.894
19	2.001	1.831	0.803	0.583	1.649	2.952	4.260	14.079
20	3.500	1.971	0.635	0.716	1.448	2.263	5.030	15.563
21	2.958	1.854	0.782	0.610	1.656	2.717	4.011	14.587
22	2.742	1.751	0.749	0.586	1.621	2.340	2.915	12.704
23	3.382	1.708	0.714	0.610	1.541	2.566	4.146	14.667
24	1.389	1.683	0.873	0.614	1.666	2.833	4.532	13.591
25	2.566	1.714	0.942	0.602	1.626	2.897	4.713	15.060
26	4.613	1.701	0.855	0.626	1.662	2.782	4.657	16.895
27	5.174	1.703	0.724	0.622	1.619	2.655	3.779	16.276
28	4.635	1.954	0.730	0.631	1.479	2.392	4.779	16.600
29	3.475	1.792	0.864	0.603	1.778	3.147	3.521	15.179
30	1.938	1.785	0.877	0.599	1.671	2.961	4.258	14.089

Char analysis:

Chrono order	Char Ultimate Analysis (wt %)						HHV
	Carbon	Hydrogen	Nitrogen	Oxygen	Sulfur	Ash	(MJ/kg)
1	76.34	3.82	0.2404	19.58	0.0157		
2	76.97	3.62	0.1912	17.42	0.0170	1.7756	
3	77.71	3.43	0.0614	17.69	0.0079	1.0980	31.74
4	77.22	3.59	0.2182	17.14	0.0164	1.8146	
5	77.18	3.70	0.2293	18.14	0.0130	0.7364	
6	77.06	3.66	0.3466	17.47	0.0161	1.4389	
7	76.74	4.03	0.3164	18.90	0.0168		
8	76.80	3.68	0.2919	16.90	0.0170	2.3097	
9	76.74	3.65	0.2631	18.22	0.0127	1.1158	29.65
10	79.36	3.50	0.2844	14.87	0.0151	1.9710	
11	75.39	4.05	0.2320	18.50	0.0161	1.8134	
12	77.21	3.74	0.3241	17.46	0.0131	1.2539	
13	75.51	3.95	0.3079	20.22	0.0167		
14	77.39	3.65	0.0040	17.58	0.0101	1.3671	29.81
15	77.13	3.69	0.2859	16.92	0.0174	1.9544	
16	76.88	3.91	0.2895	17.90	0.0162	1.0024	
17	77.95	3.53	0.2600	16.70	0.0075	1.5546	32.36
18	78.42	3.56	0.3332	15.20	0.0198	2.4735	
19	77.40	3.79	0.3762	16.49	0.0160	1.9262	
20	75.86	3.84	0.2715	17.99	0.0190	2.0187	
21	76.68	3.94	0.2527	19.11	0.0149		
22	77.26	3.82	0.2328	17.14	0.0088	1.5479	30.75
23	80.02	3.59	0.3032	14.29	0.0200	1.7791	
24	77.43	3.92	0.3052	16.98	0.0149	1.3475	
25	76.76	3.97	0.3097	17.87	0.0100	1.0825	
26	76.99	3.89	0.1570	17.40	0.0166	1.5457	
27	77.14	3.87	0.1322	17.13	0.0130	1.7136	29.78
28	78.22	3.69	0.2873	15.46	0.0162	2.3239	
29	73.86	4.39	0.2784	19.78	0.0138	1.6798	
30	75.66	4.25	0.2900	18.30	0.0144	1.4908	

*Oxygen content found by difference

Appendix D: Models and ANOVA tables

Bio-oil yield Model (full model)

Summary of Fit		Hypothesis		
RSquare	0.72	Model:	H_o: $\beta_i=\beta_j=\beta_{ii}=\beta_{jj}=\beta_{ij}=0$	Reject H_o if $F_o > F_{0.05,14,15}$
RSquare Adj	0.47	LOF:	H_o: LOF is significant	Reject H_o if $F_o < F_{0.05,10,5}$
Root Mean Square Error	1.24	Term:	H_o: β_i is insignificant	Reject H_o if $F_o > F_{0.05,1,15}$
Mean of Response	68.68	Intercep	H_o: β is insignificant	Reject H_o if $\lvert t_o \rvert > t_{0.05,15}$
Observations (or Sum Wgts)	30	Alternatively, if $p < 0.05$ the parameter is significant		

Analysis of Variance						Model	
Source	DF	SS	MS			F test	Significance
Model	14	60.5	4.321	2.817	F ratio (F_o)	2.424	YES
Error	15	23.0	1.534	0.028	Prob > F		
C. Total	29	83.5	.	.			

Lack Of Fit						Lack of Fit	
Source	DF	SS	MS			F test	Significance
Lack Of Fit	10	20.0	1.998	3.298	F ratio (F_o)	4.735	NO
Pure Error	5	3.0	0.606	0.100	Prob > F		
Total Error	15	23.0	.	0.964	Max RSq		

Term						Term	
Source	Estimate	DF	SS	F ratio (F_o)	Prob > F	F test	Significance
Temperature (x_1)	0.57083	1	7.820	5.099	0.039	4.543	YES
Particle size (x_2)	-0.52083	1	6.510	4.245	0.057	4.543	NO
Flow rate (x_3)	0.17917	1	0.770	0.502	0.489	4.543	NO
Feed rate (x_4)	0.72083	1	12.470	8.131	0.012	4.543	YES
Temperature*Particle size (x_1x_2)	0.14375	1	0.331	0.216	0.649	4.543	NO
Temperature*Flow rate (x_1x_3)	0.15625	1	0.391	0.255	0.621	4.543	NO
Particle size*Flow rate (x_2x_3)	-0.08125	1	0.106	0.069	0.797	4.543	NO
Temperature*Feed rate (x_1x_4)	0.10625	1	0.181	0.118	0.736	4.543	NO
Particle size*Feed rate (x_2x_4)	-0.10625	1	0.181	0.118	0.736	4.543	NO
Flow rate*Feed rate (x_3x_4)	0.28125	1	1.266	0.825	0.378	4.543	NO
Temperature*Temperature (x_1x_1)	-0.98021	1	26.354	17.184	0.001	4.543	YES
Particle size*Particle size (x_2x_2)	-0.25521	1	1.786	1.165	0.298	4.543	NO
Flow rate*Flow rate (x_3x_3)	0.08229	1	0.186	0.121	0.733	4.543	NO
Feed rate*Feed rate (x_4x_4)	0.14479	1	0.575	0.375	0.549	4.543	NO

Intercept				Intercept	
Source	Estimate	t Ratio	Prob > |t|	t test	Significance
Intercept (β)	69.4833	137.435	1.13E-24	2.131	YES

Bio-oil yield Model (reduced)

Summary of Fit		Hypothesis		
RSquare	0.65	Model:	H_o: $\beta_i=\beta_j=\beta_{ii}=\beta_{jj}=\beta_{ij}=0$	Reject H_o if $F_o > F_{0.05,14,15}$
RSquare Adj	0.59	LOF:	H_o: LOF is significant	Reject H_o if $F_o < F_{0.05,10,5}$
Root Mean Square Error	1.08	Term:	H_o: β_i is insignificant	Reject H_o if $F_o > F_{0.05,1,15}$
Mean of Response	68.68	Intercept:	H_o: β is insignificant	Reject H_o if $\|t_o\| > t_{0.05,15}$
Observations (or Sum Wgts)	30	Alternatively, if $p < 0.05$ the parameter is significant		

Analysis of Variance						Model	
Source	DF	SS	MS			F test	Significance
Model	4	54.3	13.574	11.623	F ratio (F_o)	2.759	YES
Error	25	29.2	1.168	1.8E-05	Prob > F		
C. Total	29	83.5	.	.			

Lack Of Fit						Lack of Fit	
Source	DF	SS	MS			F test	Significance
Lack Of Fit	10	20.6	2.062	3.608	F ratio (F_o)	2.544	YES
Pure Error	15	8.6	0.572	0.013	Prob > F		
Total Error	25	29.2	.	0.897	Max RSq		

Term						Term	
Source	Estimate	DF	SS	F ratio (F_o)	Prob > F	F test	Significance
Temperature (x_1)	0.57083	1	7.820	6.696	0.016	4.183	YES
Particle size (x_2)	-0.52083	1	6.510	5.575	0.026	4.183	YES
Flow rate (x_3)							
Feed rate (x_4)	0.72083	1	12.470	10.678	0.003	4.183	YES
Temperature*Particle size (x_1x_2)							
Temperature*Flow rate (x_1x_3)							
Particle size*Flow rate (x_2x_3)							
Temperature*Feed rate (x_1x_4)							
Particle size*Feed rate (x_2x_4)							
Flow rate*Feed rate (x_3x_4)							
Temperature*Temperature (x_1x_1)	-0.97708	1	27.495	23.543	0.000	4.183	YES
Particle size*Particle size (x_2x_2)							
Flow rate*Flow rate (x_3x_3)							
Feed rate*Feed rate (x_4x_4)							

Intercept				Intercept	
Source	Estimate	t Ratio	Prob > |t|	t test	Significance
Intercept (β)	69.4833	272.684	6.02E-45	2.060	YES

Bio-char yield reduced model

Summary of Fit			Hypothesis	
RSquare	0.95	Model:	H_o: $\beta_i=\beta_j=\beta_{ii}=\beta_{jj}=\beta_{ij}=0$	Reject H_o if $F_o > F_{0.05,14,15}$
RSquare Adj	0.94	LOF:	H_o: LOF is significant	Reject H_o if $F_o < F_{0.05,10,5}$
Root Mean Square Error	0.69	Term:	H_o: β_i is insignificant	Reject H_o if $F_o > F_{0.05,1,15}$
Mean of Response	15.58	Intercept	H_o: β is insignificant	Reject H_o if $\lvert t_o \rvert > t_{0.05,15}$
Observations (or Sum Wgts)	30	Alternatively, if $p < 0.05$ the parameter is significant		

Analysis of Variance						Model	
Source	DF	SS	MS			F test	Significance
Model	4	208.9	52.22	110.477	F ratio (F_o)	2.759	YES
Error	25	11.8	0.47	1.6E-15	Prob > F		
C. Total	29	220.7	.	.			

Lack Of Fit						Lack of Fit	
Source	DF	SS	MS			F test	Significance
Lack Of Fit	10	5.1	0.506	1.123	F ratio (F_o)	2.544	NO
Pure Error	15	6.8	0.451	0.407	Prob > F		
Total Error	25	11.8	.	0.969	Max RSq		

Term						Term	
Source	Estimate	DF	SS	F ratio (F_o)	Prob > F	F test	Significance
Temperature (x_1)	-2.65	1	168.540	356.547	2.61E-16	4.242	YES
Particle size (x_2)	1.225	1	36.015	76.190	4.63E-09	4.242	YES
Flow rate (x_3)	0.275	1	1.815	3.840	0.061	4.242	NO
Feed rate (x_4)							
Temperature*Particle size (x_1x_2)							
Temperature*Flow rate (x_1x_3)							
Particle size*Flow rate (x_2x_3)							
Temperature*Feed rate (x_1x_4)							
Particle size*Feed rate (x_2x_4)							
Flow rate*Feed rate (x_3x_4)							
Temperature*Temperature (x_1x_1)	-0.29583	1	2.521	5.332	0.029	4.242	YES
Particle size*Particle size (x_2x_2)							
Flow rate*Flow rate (x_3x_3)							
Feed rate*Feed rate (x_4x_4)							

Intercept				Intercept	
Source	Estimate	t Ratio	Prob > |t|	t test	Significance
Intercept (β)	15.8167	97.602	8.37E-34	2.060	YES

Non-condensable gas yield reduced model

Summary of Fit			Hypothesis	
RSquare	0.94	Model:	H_o: $\beta_i=\beta_j=\beta_{ii}=\beta_{jj}=\beta_{ij}=0$	Reject H_o if $F_o > F_{0.05,14,15}$
RSquare Adj	0.92	LOF:	H_o: LOF is significant	Reject H_o if $F_o < F_{0.05,10,5}$
Root Mean Square Error	0.60	Term:	H_o: β_i is insignificant	Reject H_o if $F_o > F_{0.05,1,15}$
Mean of Response	15.00	Intercept:	H_o: β is insignificant	Reject H_o if $\lvert t_o \rvert > t_{0.05,15}$
Observations (or Sum Wgts)	30	Alternatively, if $p < 0.05$ the parameter is significant		

Analysis of Variance						Model	
Source	DF	SS	MS			F test	Significance
Model	7	127.6	18.229	50.838	F ratio (F_o)	2.464	YES
Error	22	7.9	0.359	4.0E-12	Prob > F		
C. Total	29	135.5	.	.			

Lack Of Fit						Lack of Fit	
Source	DF	SS	MS			F test	Significance
Lack Of Fit	17	6.9	0.406	2.042	F ratio (F_o)	4.590	NO
Pure Error	5	1.0	0.199	0.221	Prob > F		
Total Error	22	7.9	.	0.993	Max RSq		

Term						Term	
Source	Estimate	DF	SS	F ratio (F_o)	Prob > F	F test	Significance
Temperature (x_1)	1.77917	1	75.970	193.201	1.12E-12	4.301	YES
Particle size (x_2)	-0.54583	1	7.150	18.184	2.91E-04	4.301	YES
Flow rate (x_3)	-0.32083	1	2.470	6.283	0.020	4.301	YES
Feed rate (x_4)	-0.45417	1	4.950	12.589	0.002	4.301	YES
Temperature*Particle size (x_1x_2)	-0.31875	1	1.626	4.134	0.054	4.301	NO
Temperature*Flow rate (x_1x_3)							
Particle size*Flow rate (x_2x_3)							
Temperature*Feed rate (x_1x_4)							
Particle size*Feed rate (x_2x_4)							
Flow rate*Feed rate (x_3x_4)							
Temperature*Temperature (x_1x_1)	1.09097	1	34.278	87.174	2.75E-09	4.301	YES
Particle size*Particle size (x_2x_2)							
Flow rate*Flow rate (x_3x_3)							
Feed rate*Feed rate (x_4x_4)							

Intercept				Intercept	
Source	Estimate	t Ratio	Prob > |t|	t test	Significance
Intercept (β)	14.1306	95.605	2.06E-31	2.074	YES

Bio-oil moisture content reduced model

Summary of Fit		Hypothesis	
RSquare	0.78	Model:	H_o: $\beta_i=\beta_j=\beta_{ii}=\beta_{jj}=\beta_{ij}=0$ Reject H_o if $F_o > F_{0.05,14,15}$
RSquare Adj	0.74	LOF:	H_o: LOF is significant Reject H_o if $F_o < F_{0.05,10,5}$
Root Mean Square Error	0.84	Term:	H_o: β_i is insignificant Reject H_o if $F_o > F_{0.05,1,15}$
Mean of Response	24.64	Intercept	H_o: β is insignificant Reject H_o if $\lvert t_o \rvert > t_{0.05,15}$
Observations (or Sum Wgts)	30	Alternatively, if $p < 0.05$ the parameter is significant	

Analysis of Variance						Model	
Source	DF	SS	MS			F test	Significance
Model	4	60.7	15.185	21.532	F ratio (F_o)	2.759	YES
Error	25	17.6	0.705	8.5E-08	Prob > F		
C. Total	29	78.4	.	.			

Lack Of Fit						Lack of Fit	
Source	DF	SS	MS			F test	Significance
Lack Of Fit	4	3.9	0.983	1.507	F ratio (F_o)	2.840	NO
Pure Error	21	13.7	0.652	0.236	Prob > F		
Total Error	25	17.6	.	0.825	Max RSq		

Term						Term	
Source	Estimate	DF	SS	F ratio (F_o)	Prob > F	F test	Significance
Temperature (x_1)	-1.46	1	51.158	72.543	7.4E-09	4.242	YES
Particle size (x_2)	0.31992	1	2.456	3.483	0.074	4.242	NO
Flow rate (x_3)							
Feed rate (x_4)							
Temperature*Particle size (x_1x_2)	-0.43388	1	3.012	4.271	0.049	4.242	YES
Temperature*Flow rate (x_1x_3)							
Particle size*Flow rate (x_2x_3)							
Temperature*Feed rate (x_1x_4)							
Particle size*Feed rate (x_2x_4)							
Flow rate*Feed rate (x_3x_4)							
Temperature*Temperature (x_1x_1)	0.3779	1	4.113	5.832	0.023	4.242	YES
Particle size*Particle size (x_2x_2)							
Flow rate*Flow rate (x_3x_3)							
Feed rate*Feed rate (x_4x_4)							

Intercept				Intercept	
Source	Estimate	t Ratio	Prob > |t|	t test	Significance
Intercept (β)	24.3368	122.953	2.64E-36	2.060	YES

Bio-oil water insolubles reduced model

Summary of Fit			Hypothesis	
RSquare	0.86	Model:	H_o: $\beta_i=\beta_j=\beta_{ii}=\beta_{jj}=\beta_{ij}=0$	Reject H_o if $F_o > F_{0.05,14,15}$
RSquare Adj	0.84	LOF:	H_o: LOF is significant	Reject H_o if $F_o < F_{0.05,10,5}$
Root Mean Square Error	0.88	Term:	H_o: β_i is insignificant	Reject H_o if $F_o > F_{0.05,1,15}$
Mean of Response	18.01	Intercept	H_o: β is insignificant	Reject H_o if $\lvert t_o \rvert > t_{0.05,15}$
Observations (or Sum Wgts)	30	Alternatively, if $p < 0.05$ the parameter is significant		

Analysis of Variance						Model	
Source	DF	SS	MS			F test	Significance
Model	3	120.9	40.29	52.585	F ratio (F_o)	2.975	YES
Error	26	19.9	0.77	3.6E-11	Prob > F		
C. Total	29	140.8	.	.			

Lack Of Fit						Lack of Fit	
Source	DF	SS	MS			F test	Significance
Lack Of Fit	10	5.0	8.234	1.647	2.96	4.735	NO
Pure Error	5	21.0	11.687	0.557	0.04		
Total Error	15	26.0	19.921	.	0.92		

Term						Term	
Source	Estimate	DF	SS	F ratio (F_o)	Prob > F	F test	Significance
Temperature (x_1)	2.01495	1	97.441	127.177	1.6E-11	4.225	YES
Particle size (x_2)	-0.90135	1	19.498	25.449	3.0E-05	4.225	YES
Flow rate (x_3)							
Feed rate (x_4)							
Temperature*Particle size (x_1x_2)	0.49569	1	3.931	5.131	0.032	4.225	YES
Temperature*Flow rate (x_1x_3)							
Particle size*Flow rate (x_2x_3)							
Temperature*Feed rate (x_1x_4)							
Particle size*Feed rate (x_2x_4)							
Flow rate*Feed rate (x_3x_4)							
Temperature*Temperature (x_1x_1)							
Particle size*Particle size (x_2x_2)							
Flow rate*Flow rate (x_3x_3)							
Feed rate*Feed rate (x_4x_4)							

Intercept				Intercept	
Source	Estimate	t Ratio	Prob > |t|	t test	Significance
Intercept (β)	18.0098	112.694	1.68E-36	2.056	YES

Bio-oil carbon content reduced model

Summary of Fit			Hypothesis	
RSquare	0.67	Model:	H_o: $\beta_i=\beta_j=\beta_{ii}=\beta_{jj}=\beta_{ij}=0$	Reject H_o if $F_o > F_{0.05,14,15}$
RSquare Adj	0.63	LOF:	H_o: LOF is significant	Reject H_o if $F_o < F_{0.05,10,5}$
Root Mean Square Error	0.79	Term:	H_o: β_i is insignificant	Reject H_o if $F_o > F_{0.05,1,15}$
Mean of Response	39.77	Intercept	H_o: β is insignificant	Reject H_o if $\lvert t_o \rvert > t_{0.05,15}$
Observations (or Sum Wgts)	30	Alternatively, if $p < 0.05$ the parameter is significant		

Analysis of Variance						Model	
Source	DF	SS	MS			F test	Significance
Model	3	32.7	10.912	17.673	F ratio (F_o)	2.975	YES
Error	26	16.1	0.617	1.8E-06	Prob > F		
C. Total	29	48.8	.	.			

Lack Of Fit						Lack of Fit	
Source	DF	SS	MS			F test	Significance
Lack Of Fit	5	1.8	0.353	0.519	F ratio (F_o)	2.685	NO
Pure Error	21	14.3	0.680	0.759	Prob > F		
Total Error	26	16.1	.	0.707	Max RSq		

Term						Term	
Source	Estimate	DF	SS	F ratio (F_o)	Prob > F	F test	Significance
Temperature (x_1)	1.04	1	25.958	42.043	7.1E-07	4.225	YES
Particle size (x_2)	-0.3925	1	3.697	5.988	0.021	4.225	YES
Flow rate (x_3)							
Feed rate (x_4)							
Temperature*Particle size (x_1x_2)	0.43875	1	3.080	4.989	0.034	4.225	YES
Temperature*Flow rate (x_1x_3)							
Particle size*Flow rate (x_2x_3)							
Temperature*Feed rate (x_1x_4)							
Particle size*Feed rate (x_2x_4)							
Flow rate*Feed rate (x_3x_4)							
Temperature*Temperature (x_1x_1)							
Particle size*Particle size (x_2x_2)							
Flow rate*Flow rate (x_3x_3)							
Feed rate*Feed rate (x_4x_4)							

Intercept				Intercept	
Source	Estimate	t Ratio	Prob > |t|	t test	Significance
Intercept (β)	39.766	277.193	1.18E-46	2.056	YES

Bio-char carbon content reduced model

Summary of Fit			Hypothesis	
RSquare	0.72	Model:	H_o: $\beta_i=\beta_j=\beta_{ii}=\beta_{jj}=\beta_{ij}=0$	Reject H_o if $F_o > F_{0.05,14,15}$
RSquare Adj	0.64	LOF:	H_o: LOF is significant	Reject H_o if $F_o < F_{0.05,10,5}$
Root Mean Square Error	0.69	Term:	H_o: β_i is insignificant	Reject H_o if $F_o > F_{0.05,1,15}$
Mean of Response	77.04	Intercept	H_o: β is insignificant	Reject H_o if $\lvert t_o \rvert > t_{0.05,15}$
Observations (or Sum Wgts)	30	Alternatively, if $p < 0.05$ the parameter is significant		

Analysis of Variance						Model	
Source	DF	SS	MS			F test	Significance
Model	6	27.9	4.648	9.769	F ratio (F_o)	2.528	YES
Error	23	10.9	0.476	2.2E-05	Prob > F		
C. Total	29	38.8	.	.			

Lack Of Fit						Lack of Fit	
Source	DF	SS	MS			F test	Significance
Lack Of Fit	18	10.0	0.557	3.047	F ratio (F_o)	4.579	NO
Pure Error	5	0.9	0.183	0.111	Prob > F		
Total Error	23	10.9	.	0.976	Max RSq		

Term						Term	
Source	Estimate	DF	SS	F ratio (F_o)	Prob > F	F test	Significance
Temperature (x_1)	0.64958	1	10.127	21.285	0.000	4.279	YES
Particle size (x_2)	0.36958	1	3.278	6.890	0.015	4.279	YES
Flow rate (x_3)	0.28292	1	1.921	4.038	0.056	4.279	NO
Feed rate (x_4)	0.42292	1	4.293	9.022	0.006	4.279	YES
Temperature*Particle size (x_1x_2)	0.46063	1	3.395	7.135	0.014	4.279	YES
Temperature*Flow rate (x_1x_3)							
Particle size*Flow rate (x_2x_3)	0.55188	1	4.873	10.242	0.004	4.279	YES
Temperature*Feed rate (x_1x_4)							
Particle size*Feed rate (x_2x_4)							
Flow rate*Feed rate (x_3x_4)							
Temperature*Temperature (x_1x_1)							
Particle size*Particle size (x_2x_2)							
Flow rate*Flow rate (x_3x_3)							
Feed rate*Feed rate (x_4x_4)							

Intercept				Intercept	
Source	Estimate	t Ratio	Prob > |t|	t test	Significance
Intercept (β)	77.0427	611.772	6.09E-50	2.069	YES

Non-condesnable gas carbon content reduced model

Summary of Fit		Hypothesis	
RSquare	0.94	Model:	H_o: $\beta_i=\beta_j=\beta_{ii}=\beta_{jj}=\beta_{ij}=0$ Reject H_o if $F_o > F_{0.05,14,15}$
RSquare Adj	0.93	LOF:	H_o: LOF is significant Reject H_o if $F_o < F_{0.05,10,5}$
Root Mean Square Error	0.28	Term:	H_o: β_i is insignificant Reject H_o if $F_o > F_{0.05,1,15}$
Mean of Response	5.47	Intercept	H_o: β is insignificant Reject H_o if $\|t_o\| > t_{0.05,15}$
Observations (or Sum Wgts)	30	Alternatively, if $p < 0.05$ the parameter is significant	

Analysis of Variance						Model	
Source	DF	SS	MS			F test	Significance
Model	6	29.0	4.832	63.455	F ratio (F_o)	2.528	YES
Error	23	1.8	0.076	3.71E-13	Prob > F		
C. Total	29	30.7	.	.			

Lack Of Fit						Lack of Fit	
Source	DF	SS	MS			F test	Significance
Lack Of Fit	18	1.5	0.085	1.945	F ratio (F_o)	4.579	NO
Pure Error	5	0.2	0.044	0.238	Prob > F		
Total Error	23	1.8	.	0.993	Max RSq		

Term						Term	
Source	Estimate	DF	SS	F ratio (F_o)	Prob > F	F test	Significance
Temperature (x_1)	0.87833	1	18.515	243.164	1.0E-13	4.279	YES
Particle size (x_2)	-0.25833	1	1.602	21.035	0.000	4.279	YES
Flow rate (x_3)	-0.13833	1	0.459	6.032	0.022	4.279	YES
Feed rate (x_4)	-0.1775	1	0.756	9.931	0.004	4.279	YES
Temperature*Particle size (x_1x_2)	-0.1425	1	0.325	4.267	0.050	4.279	NO
Temperature*Flow rate (x_1x_3)							
Particle size*Flow rate (x_2x_3)							
Temperature*Feed rate (x_1x_4)							
Particle size*Feed rate (x_2x_4)							
Flow rate*Feed rate (x_3x_4)							
Temperature*Temperature (x_1x_1)	0.50458	1	7.333	96.300	1.1E-09	4.279	YES
Particle size*Particle size (x_2x_2)							
Flow rate*Flow rate (x_3x_3)							
Feed rate*Feed rate (x_4x_4)							

Intercept				Intercept	
Source	Estimate	t Ratio	Prob > |t|	t test	Significance
Intercept (β)	5.06167	77.824	2.30E-29	2.069	YES

Hydrogen gas yield reduced model

Summary of Fit		Hypothesis	
RSquare	0.87	Model:	H_o: $\beta_i=\beta_j=\beta_{ii}=\beta_{jj}=\beta_{ij}=0$ Reject H_o if $F_o > F_{0.05,14,15}$
RSquare Adj	0.85	LOF:	H_o: LOF is significant Reject H_o if $F_o < F_{0.05,10,5}$
Root Mean Square Error	0.01	Term:	H_o: β_i is insignificant Reject H_o if $F_o > F_{0.05,1,15}$
Mean of Response	0.03	Intercept	H_o: β is insignificant Reject H_o if $\lvert t_o \rvert > t_{0.05,15}$
Observations (or Sum Wgts)	30	Alternatively, if $p < 0.05$ the parameter is significant	

Analysis of Variance						Model	
Source	DF	SS	MS			F test	Significance
Model	4	0.019	0.005	42.983	F ratio (F_o)	2.759	YES
Error	25	0.003	1.1E-04	7.44E-11	Prob > F		
C. Total	29	0.022	.	.			

Lack Of Fit						Lack of Fit	
Source	DF	SS	MS			F test	Significance
Lack Of Fit	4	0.002	4E-04	6.255	F ratio (F_o)	2.840	YES
Pure Error	21	1E-03	6E-05	0.002	Prob > F		
Total Error	25	0.003	.	0.942	Max RSq		

Term						Term	
Source	Estimate	DF	SS	F ratio (F_o)	Prob > F	F test	Significance
Temperature (x_1)	0.02167	1	0.011	102.012	2.6E-10	4.242	YES
Particle size (x_2)	-0.005	1	0.001	5.433	0.028	4.242	YES
Flow rate (x_3)							
Feed rate (x_4)							
Temperature*Particle size (x_1x_2)	-0.005	1	4.0E-04	3.622	0.069	4.242	NO
Temperature*Flow rate (x_1x_3)							
Particle size*Flow rate (x_2x_3)							
Temperature*Feed rate (x_1x_4)							
Particle size*Feed rate (x_2x_4)							
Flow rate*Feed rate (x_3x_4)							
Temperature*Temperature (x_1x_1)	0.01528	1	0.007	60.865	3.7E-08	4.242	YES
Particle size*Particle size (x_2x_2)							
Flow rate*Flow rate (x_3x_3)							
Feed rate*Feed rate (x_4x_4)							

Intercept				Intercept	
Source	Estimate	t Ratio	Prob > |t|	t test	Significance
Intercept (β)	0.01278	5.158	2.47E-05	2.060	YES

Carbon monoxide gas yield reduced model

Summary of Fit		Hypothesis		
RSquare	0.96	Model:	H_o: $\beta_i=\beta_j=\beta_{ii}=\beta_{jj}=\beta_{ij}=0$	Reject H_o if $F_o > F_{0.05,14,15}$
RSquare Adj	0.94	LOF:	H_o: LOF is significant	Reject H_o if $F_o < F_{0.05,10,5}$
Root Mean Square Error	0.40	Term:	H_o: β_i is insignificant	Reject H_o if $F_o > F_{0.05,1,15}$
Mean of Response	5.97	Intercept	H_o: β is insignificant	Reject H_o if $\lvert t_o \rvert > t_{0.05,15}$
Observations (or Sum Wgts)	30	Alternatively, if $p < 0.05$ the parameter is significant		

Analysis of Variance						Model	
Source	DF	SS	MS			F test	Significance
Model	6	78.5	13.083	83.078	F ratio (F_o)	2.528	YES
Error	23	3.6	0.157	2.0E-14	Prob > F		
C. Total	29	82.1	.	.			

Lack Of Fit						Lack of Fit	
Source	DF	SS	MS			F test	Significance
Lack Of Fit	18	2.7	0.152	0.865	F ratio (F_o)	4.579	NO
Pure Error	5	0.9	0.176	0.632	Prob > F		
Total Error	23	3.6	.	0.989	Max RSq		

Term						Term	
Source	Estimate	DF	SS	F ratio (F_o)	Prob > F	F test	Significance
Temperature (x_1)	1.50333	1	54.240	344.443	2.5E-15	4.279	YES
Particle size (x_2)	-0.4325	1	4.489	28.509	2.0E-05	4.279	YES
Flow rate (x_3)	-0.1675	1	0.673	4.276	0.050	4.279	NO
Feed rate (x_4)	-0.25417	1	1.550	9.846	0.005	4.279	YES
Temperature*Particle size (x_1x_2)	-0.25125	1	1.010	6.414	0.019	4.279	YES
Temperature*Flow rate (x_1x_3)							
Particle size*Flow rate (x_2x_3)							
Temperature*Feed rate (x_1x_4)							
Particle size*Feed rate (x_2x_4)							
Flow rate*Feed rate (x_3x_4)							
Temperature*Temperature (x_1x_1)	0.75764	1	16.532	104.982	4.8E-10	4.279	YES
Particle size*Particle size (x_2x_2)							
Flow rate*Flow rate (x_3x_3)							
Feed rate*Feed rate (x_4x_4)							

Intercept				Intercept	
Source	Estimate	t Ratio	Prob > |t|	t test	Significance
Intercept (β)	5.35889	57.294	2.55E-26	2.069	YES

Methane gas yield reduced model

Summary of Fit		Hypothesis	
RSquare	0.93	Model:	H_o: $\beta_i=\beta_j=\beta_{ii}=\beta_{jj}=\beta_{ij}=0$ Reject H_o if $F_o > F_{0.05,14,15}$
RSquare Adj	0.91	LOF:	H_o: LOF is significant Reject H_o if $F_o < F_{0.05,10,5}$
Root Mean Square Error	0.06	Term:	H_o: β_i is insignificant Reject H_o if $F_o > F_{0.05,1,15}$
Mean of Response	0.60	Intercept	H_o: β is insignificant Reject H_o if $\lvert t_o \rvert > t_{0.05,15}$
Observations (or Sum Wgts)	30	Alternatively, if $p < 0.05$ the parameter is significant	

Analysis of Variance						Model	
Source	DF	SS	MS			F test	Significance
Model	5	1.24	0.248	62.704	F ratio (F_o)	2.621	YES
Error	24	0.10	0.004	5.5E-13	Prob > F		
C. Total	29	1.34	.	.			

Lack Of Fit						Lack of Fit	
Source	DF	SS	MS			F test	Significance
Lack Of Fit	9	0.05	0.006	2.151	F ratio (F_o)	2.588	NO
Pure Error	15	0.04	0.003	0.091	Prob > F		
Total Error	24	0.10	.	0.969	Max RSq		

Term						Term	
Source	Estimate	DF	SS	F ratio (F_o)	Prob > F	F test	Significance
Temperature (x_1)	0.18542	1	0.825	208.313	2.5E-13	4.260	YES
Particle size (x_2)	-0.04542	1	0.050	12.498	0.002	4.260	YES
Flow rate (x_3)	-0.02875	1	0.020	5.008	0.035	4.260	YES
Feed rate (x_4)							
Temperature*Particle size (x_1x_2)							
Temperature*Flow rate (x_1x_3)	-0.03313	1	0.018	4.432	0.046	4.260	YES
Particle size*Flow rate (x_2x_3)							
Temperature*Feed rate (x_1x_4)							
Particle size*Feed rate (x_2x_4)							
Flow rate*Feed rate (x_3x_4)							
Temperature*Temperature (x_1x_1)	0.10701	1	0.330	83.269	2.8E-09	4.260	YES
Particle size*Particle size (x_2x_2)							
Flow rate*Flow rate (x_3x_3)							
Feed rate*Feed rate (x_4x_4)							

Intercept				Intercept	
Source	Estimate	t Ratio	Prob > |t|	t test	Significance
Intercept (β)	0.51639	34.811	4.68E-22	2.064	YES

Carbon dioxide gas yield reduced model

Summary of Fit			Hypothesis	
RSquare	0.45	Model:	H_o: $\beta_i=\beta_j=\beta_{ii}=\beta_{jj}=\beta_{ij}=0$	Reject H_o if $F_o > F_{0.05,14,15}$
RSquare Adj	0.41	LOF:	H_o: LOF is significant	Reject H_o if $F_o < F_{0.05,10,5}$
Root Mean Square Error	0.25	Term:	H_o: β_i is insignificant	Reject H_o if $F_o > F_{0.05,1,15}$
Mean of Response	8.09	Intercept	H_o: β is insignificant	Reject H_o if $\lvert t_o \rvert > t_{0.05,15}$
Observations (or Sum Wgts)	30	Alternatively, if $p < 0.05$ the parameter is significant		

Analysis of Variance						Model	
Source	DF	SS	MS			F test	Significance
Model	2	1.3	0.661	10.889	F ratio (F_o)	3.354	YES
Error	27	1.6	0.061	3.4E-04	Prob > F		
C. Total	29	3.0	.	.			

Lack Of Fit						Lack of Fit	
Source	DF	SS	MS			F test	Significance
Lack Of Fit	6	1.0	0.159	4.894	F ratio (F_o)	2.573	YES
Pure Error	21	0.7	0.033	0.003	Prob > F		
Total Error	27	1.6	.	0.769	Max RSq		

Term						Term	
Source	Estimate	DF	SS	F ratio (F_o)	Prob > F	F test	Significance
Temperature (x_1)							
Particle size (x_2)							
Flow rate (x_3)							
Feed rate (x_4)	-0.14667	1	0.516	8.507	7.0E-03	4.210	YES
Temperature*Particle size (x_1x_2)							
Temperature*Flow rate (x_1x_3)							
Particle size*Flow rate (x_2x_3)							
Temperature*Feed rate (x_1x_4)							
Particle size*Feed rate (x_2x_4)							
Flow rate*Feed rate (x_3x_4)							
Temperature*Temperature (x_1x_1)	0.16722	1	0.805	13.271	0.001	4.210	YES
Particle size*Particle size (x_2x_2)							
Flow rate*Flow rate (x_3x_3)							
Feed rate*Feed rate (x_4x_4)							

Intercept	`			Intercept	
Source	Estimate	t Ratio	Prob > |t|	t test	Significance
Intercept (β)	7.95722	137.044	6.34E-40	2.052	YES

Maximum vapor temperature within the reactor full model

Summary of Fit			Hypothesis	
RSquare	0.97	Model:	H_o: $\beta_i=\beta_j=\beta_{ii}=\beta_{jj}=\beta_{ij}=0$	Reject H_o if $F_o > F_{0.05,14,15}$
RSquare Adj	0.94	LOF:	H_o: LOF is significant	Reject H_o if $F_o < F_{0.05,10,5}$
Root Mean Square Error	9.78	Term:	H_o: β_i is insignificant	Reject H_o if $F_o > F_{0.05,1,15}$
Mean of Response	481.53	Intercept:	H_o: β is insignificant	Reject H_o if $\lvert t_o \rvert > t_{0.05,15}$
Observations (or Sum Wgts)	30	Alternatively, if $p < 0.05$ the parameter is significant		

Analysis of Variance						Model	
Source	DF	SS	MS			F test	Significance
Model	14	44401	3172	33.130	F ratio (F_o)	2.424	YES
Error	15	1436	95.731	1.0E-08	Prob > F		
C. Total	29	45837	.	.			

Lack Of Fit						Lack of Fit	
Source	DF	SS	MS			F test	Significance
Lack Of Fit	10	1134	113.392	1.877	F ratio (F_o)	4.735	NO
Pure Error	5	302	60.408	0.252	Prob > F		
Total Error	15	1436	.	0.993	Max RSq		

Term						Term	
Source	Estimate	DF	SS	F ratio (F_o)	Prob > F	F test	Significance
Temperature (x_1)	42.0375	1	42411.6	443.030	1.5E-12	4.543	YES
Particle size (x_2)	-0.31917	1	2.445	0.026	0.875	4.543	NO
Flow rate (x_3)	-4.89417	1	574.869	6.005	0.027	4.543	YES
Feed rate (x_4)	-3.67833	1	324.723	3.392	0.085	4.543	NO
Temperature*Particle size (x_1x_2)	0.14875	1	0.354	0.004	0.952	4.543	NO
Temperature*Flow rate (x_1x_3)	-0.595	1	5.664	0.059	0.811	4.543	NO
Particle size*Flow rate (x_2x_3)	0.71875	1	8.266	0.086	0.773	4.543	NO
Temperature*Feed rate (x_1x_4)	-0.61625	1	6.076	0.063	0.805	4.543	NO
Particle size*Feed rate (x_2x_4)	1.6925	1	45.833	0.479	0.500	4.543	NO
Flow rate*Feed rate (x_3x_4)	1.56625	1	39.250	0.410	0.532	4.543	NO
Temperature*Temperature (x_1x_1)	5.51146	1	833.175	8.703	0.010	4.543	YES
Particle size*Particle size (x_2x_2)	-0.66229	1	12.031	0.126	0.728	4.543	NO
Flow rate*Flow rate (x_3x_3)	-1.03604	1	29.441	0.308	0.587	4.543	NO
Feed rate*Feed rate (x_4x_4)	1.10896	1	33.731	0.352	0.562	4.543	NO

Intercept				Intercept	
Source	Estimate	t Ratio	Prob > |t|	t test	Significance
Intercept (β)	477.59	119.565	9.12E-24	2.131	YES